JOHANNES GUTENBERG
UNIVERSITÄT MAINZ

Screening and structure-based design of novel ligands for FabF and KPC-2 - first steps to counteract an antibiotic crisis

DOCTORAL THESIS

submitted in fulfillment of the requirements for the degree of

DR. RER. NAT.

at the Faculty of Chemistry, Pharmacy and Geoscience

Author:
Raphael KLEIN
born in [redacted]

Supervisors:
[redacted]

Mainz, 2018

Declaration of Authorship

I, Raphael KLEIN, declare that this thesis titled, "Screening and Structure-based design of novel ligands for FabF and KPC-2 - an approach to circumvent an antibiotic crisis" and the work presented in it are my own. I confirm that:

- This work was done wholly or mainly while in candidature for a research degree at this University.
- Where any part of this thesis has previously been submitted for a degree or any other qualification at this University or any other institution, this has been clearly stated.
- Where I have consulted the published work of others, this is always clearly attributed.
- Where I have quoted from the work of others, the source is always given. With the exception of such quotations, this thesis is entirely my own work.
- I have acknowledged all main sources of help.
- Where the thesis is based on work done by myself jointly with others, I have made clear exactly what was done by others and what I have contributed myself.

Signed:

Date:

JOHANNES GUTENBERG UNIVERSITY MAINZ

Abstract

Faculty of Chemistry, Pharmacy and Geoscience
Institute of Pharmacy and Biochemistry

Screening and structure-based design of novel ligands for FabF and KPC-2 - first steps to counteract an antibiotic crisis

by Raphael KLEIN

The number of infections with multidrug resitant bacteria is constantly increasing and thus, the need for new antibiotics is becoming more urgent. The World Health Organisation (WHO) recently published a list of 12 bacteria for which there is a critical, high or medium need for new antibiotics. In particular, Gram-negative bacteria like *Pseudomonas aeruginosa* are associated with a broad spectrum of infections. Attractive targets for drug design are the enzymes involved in cell membrane and wall synthesis.
In this thesis, the elongation condensing enzyme FabF of the fatty acid synthesis pathway was chosen as target for further studies. Fatty acids are essential for the formation of the inner and outer cellmembrane of Gram-negative bacteria. Using virtual screening, 2 compounds sharing a thiazolidine-4-carboxylic acid scaffold binding non-covalently to FabF were identified. Binding affinities of 278 μM and 321 μM were determined using biolayer interferometry. In addition, 1 compound binding covalently was identified using MALDI mass spectrometry. Further investigations of the active site regarding the binding mode of the natural product inhibitor platensimycin were carried out by introducing the point mutation for T271A using site directed mutagenesis and solving the structure of FabF T271A. A fragment library of 651 compounds was screened using biolayer interferometry (BLI). Due to a limited amount of publications using BLI in fragment screens, this gave new insights in the assessment of fragment binding profiles and responses. The false-positive rate was lowered by screening with FabF wild type with a closed binding site and FabF C164Q with an open binding site. Finally, 16 FabF C164Q specific hits were identified (hit rate: 2.5%) out of 67 hits found in the primary screening (10.3%).
Another approach of targeting the cell wall synthesis of bacteria is the inhibition of the glycopeptide transpeptidase by β-lactame antibiotics. However, this approach is limited due to the defence mechanism of bacteria, the production of β-lactamases, which can inactivate β-lactame antibiotics through hydrolysis. The carbapenemase KPC-2 was chosen as target enzyme for further studies. Using virtual screening, 10 ligands of KPC-2 were identified, the most potent with a K_I of 30 μM. In attempts to improve the binding affinity of this hit compound an amide linker was replaced by a sulfonamide in order to change the geometry of the ligand and to vary the attached group. This substitution targeted the side chains corresponding to amino acids Asn 132, Asn 170 and Leu 166. Finally, it was shown that the sulfonamide linker is not suitable for improving the binding affinity.

JOHANNES GUTENBERG UNIVERSITÄT MAINZ

Zusammenfassung

Fakultät für Chemie, Pharmazie und Geowissenschaften
Institut für Pharmacie und Biochemie

Screening und Strukturbasiertes Design neuer Liganden für FabF und KPC-2 - erste Schritte zur Verhinderung einer Antibiotika Krise

von Raphael KLEIN

Die Zahl mutiresitenter Bakterien ist stetig steigend und verstärkt somit die Notwendigkeit der Entwicklung neuer Antibiotika. Die Weltgesundheitsorganisation (WHO) veröffentlichte kürzlich eine Liste von 12 Bakterien für die die Entwicklung neuer Antibiotika besondere, hohe oder mittelfristige Priorität haben. Vor allem gramnegative Bakterien, wie *Pseudomonas aeruginosa* sind für ein breites Spektrum von Infektionen verantwortlich. Vielversprechende Angriffspunkte für rationales Wirkstoffdesign sind die für die Zellwandsynthese verantwortlichen Enzyme.
In dieser Arbeit wurde das Enzym FabF, welches Bestandteil des Fettsäuresynthesezyklus von Bakterien ist, als Zielprotein für weiterführende Studien ausgewählt. Zum besseren Verständnis der Bindetasche wurde der Bindungsmodus des Inhibitors Platensimycin untersuchts. Dazu wurde die Punktmutation T271A mittels Mutagenese eingefügt und die Struktur von FabF T271A gelöst. Mittels virtuellem screening wurden zwei Verbindungen, die ein gemeinsames Thiazolidin-4-Carboxylat Grundgerüst teilen als Liganden von FabF identifiziert (K_D= 278 und 321 μM). Außerdem wurde eine Verbindung mit kovalentem Bindungsmodus durch eine Acrylamidfunktion mittels MALDI Massenspektrometrie identifiziert.
Eine Fragment Bibliothek, bestehend aus 651 Verbindungen wurde mittels Bio-Layer-Interferometrie (BLI) gescreent. Die Erkenntnisse über das Bindundsprofil von Fragmenten ergänzen die bisher wenigen Publikationen bezüglich BLI zur Messung von Protein-Fragment Interaktionen. Das Screening wurde parallel mit der Variante FabF C164Q, mit einer offenen Bindetasche und dem Wildyp, mit geschlossener Bindetasche, durchgeführt. Dadurch konnte die falsch positiv rate gesenkt werden. Letztlich wurden 16 Fragmente (Trefferrate 2.5%) aus 67 Treffern des primären Screenings (Trefferrate: 10.3%) als FabF C164Q spezifisch indentifiziert.
Ein anderer Ansatz die Zellwandsynthese von Bakterien anzugreifen ist die Inhibierung von Glycopeptid-Transpeptidasen durch β-Lactam Antibiotika. Dieser Ansatz ist durch den Verteidigungsmechanismus von Bakterien, der Expression von β-Lactamasen, eingeschränkt. Die Carbapenemase KPC-2 wurde als Zielprotein für weiter Studien ausgewählt. Mittels virtuellem Screening konnten 10 Liganden der KPC-2 identifiziert werden, wobei der aussichtsreichste Ligand eine Inhibitionskonstante von 30 μM hatte. Zwecks Optimierung der Bindungsaffinität wurde der Amid-linker durch ein Sulfonamid ersetzt um die Geometrie des Liganden zu ändern un die angehängte Gruppe zu variieren. Diese Änderungen ermöglichen weitere Wasserstoffbrückenbindungen. Letztenendes führte die Variation des Linkers nicht zu einer Verbesserung der Bindungsaffinität.

JOHANNES GUTENBERG UNIVERSITETET I MAINZ

Sammendrag

Fakultet for Kjemi, Farmasi og Geovitenskap
Institutt for Farmasi og Biokjemi

Screening og Struktur-basert Design av nye Ligander for FabF og KPC-2 - første skritt for å Forebygg en Antibiotikakrise

fra Raphael KLEIN

Antallet infeksjoner som skyldes multiresistente bakterier øker stadig og behovet for nye typer antibiotika er presserende. Verdens Helseorganisasjon (WHO) har nylig publisert en liste over 12 bakterier hvor behovet for ny antibiotika er kritisk, høyt eller middels. Spesielt Gram-negative bakterier som *Pseudomonas aeruginosa* er ansvarlige for et vidt spekter av infeksjoner. Attraktive mål for struktur-basert medikament design av nye antibiotika er enzymer som deltar i celleveggsynthesen.
I denne avhandlingen fokuseres det på enzmyet FabF som deltar i fettsyresyntesesyklusen hos bakterier, som mål for dette studiet. To forbindelser som deler en 4-tiazolidin-4-karboksylsyrestruktur som binder ikke-kovalent til FabF, ble identifisert gjennom virtuell screening. Bindingsaffinitet på henholdsvis 278 og 321 μM ble bestemt gjennom biolayer interferometri. I tillegg ble en forbindelse med kovalent bindingsmekanisme identifisert som ligand gjennom MALDI massespektrometri. Undersøkelser av det aktive setet med hensyn til bindingmåten til platensimycin, en naturlig produkthemmer, ble gjennomført ved punktmutasjonen T271A med setestyrt mutagenese og ved å løse strukturen av FabF T271A. Et fragmentbibliotek bestående av 651 forbindelser ble screenet ved hjelp av BLI. På grunn av begrenset antall publikasjoner hvor BLI brukes som metode for fragmentscreening, ga dette ny kunnskap om vurderingen av bindingsprofiler og responser til fragmenter. Antallet falske positive ble minsket ved å screene med FabF villtype som har et lukket bindingssete of FabF C164Q som har et åpent bindingssete. Totalt ble 16 FabF C164Q spesifikke hits identifisert (hit rate: 2.5%) fra de 67 hit funnet i første screening (10.3%).
En annen tilnærmingen som retter seg mot celleveggsynthesen i bakterier, er hemming av glycopeptid-transpeptidasen med β-laktam-antibiotika. Denne tilnærmingen er begrenset på grunn av bakterienes forsvarsmekanisme gjennom produksjon av β-laktamaser. Carbapenemasen KPC-2 ble valgt for videre studier. Gjennom virtuell screening ble ti ligander av KPC-2 identifisert, hvor den mest potente forbindelsen ga en K_I= 30 μM. For å forbedre bindingsaffinitetet av denne hit forbindelsen, ble en amid linker erstattet med et sulfonamid for å endre geometrien av liganden og for å variere den tilstøtende gruppen. Disse endringer var siktet mot sidekjedene tilhørende aminosyrene Asn132, Asn170 og Leu166. Det ble vist at sulfonamidlinkeren ikke egnet seg for å forbedre bindingsaffiniteten.

Acknowledgements

First of all I would like to thank my supervisor [redacted] for giving me the opportunity to work in her group on an interesting project and the Deutsche Forschungsgemeinschaft (DFG) for funding the project. [redacted] had always an open door (or open Skype connection) for scientific discussions to forward the project. I am grateful for the opportunity to work at the institute of biomedicine in Bergen. Thanks for reading the manuscript of this thesis carefully to help improving it.
Also, I would like to thank [redacted] for admitting me into her group and for reviewing my thesis.
Likewise I would like to thank [redacted] for the opportunity to work in his laboratory at the institute of chemistry in Bergen and for the scientific expertise to help improving the results.
A special thanks goes to the Norsk Biokjemisk selskap (NBS) for funding my trip to the EuroQSAR conference in Verona and for organising social events at the university of Bergen. Also I would like to thank the Gesellschaft Deutscher Chemiker (GDCh) for partial funding my trip to the annual meeting of the DPhG.
I would like to thank my colleagues [redacted] and [redacted] for critical questions and constructive advices. Special thanks goes to [redacted], for his warm welcome in the [redacted] group at the institute of chemistry, his support for the fragment screening as new member of the [redacted] group and for providing me an accommodation for my last two stays in Bergen.
I would like to thank [redacted], University of Dundee / Newcastle) for measuring and analysing mass spectrometry data.
Our lab technicians [redacted] contributed assistance in the biochemistry lab and helped me for bureaucracy. [redacted] measured protein crystals and helped me with structure solution. [redacted] introduced me to the HPLC and helped me purifying the peptide. [redacted] performed mass spectrometry measurements. [redacted] performed NMR measurements as part of the Norwegian NMR Platform supported by the Research Council of Norway, the Bergen Research Foundation and Sparebankstifting Sogn of Fjordane. [redacted] supported me for CD-spectroscopy measurements.
I would like to thank the [redacted] group for including me into their group albeit my occasionally absence in Bergen. Special thanks deserve [redacted] for accompanying me on my way from Cologne to Mainz and for being a good interlocutor for scientifique and private problems.
Special thank goes to the Biorecognition group for their warm welcome upon my arrival in Bergen. Thanks to [redacted] for offering here apartment for the welcome evening and for pushing on Lønningspils evenings. Thanks to [redacted] for support in LaTeX and correcting my norwegian abstract. Also I would like to thank[redacted] for hints to find accommodations. Thanks to [redacted] for joining the norwegian language course with me and supporting me in writing python scripts. Thanks to [redacted] for his work on my project during my time in Mainz and for accompanying me for the 7-fjells-turen in Bergen.
Also, I would like to thank the students working on my projects. [redacted], [redacted], [redacted] and [redacted].
A special thank deserve my family, who always supported me on my path of live. Thanks to my wife [redacted] for accepting 4 years of long-distance relationship and for encouraging me in times of scientific setbacks.

Contents

List of Abbreviations

Å	Ångstrom (1 Å= 0.1 nm)
A_{280}	Absorption at 280 nm
ACN	ACetoNitrile
ACP	Acyl Carrier Protein
AcpS	Acyl Carrier Protein Synthase
APS	Ammoniumpersulfate
beta-ME	2-Mercaptoethanol
BLI	Bio-Layer-Interferometry
Bs	*Bacillus Subtilis*
c	concentration
CD	Circular dichroism
CoA	Coenzyme A
CPM	(7-Diethylamino-3-(4′-maleimidylphenyl)-4-methylcoumarin)
DCM	Dichloromethane
DHAP	2′,4′,-Dihydroxyacetophenone
DIC	N,N′-Diisopropylcarbodiimid
DMF	Dimethylformamide
DMSO	Dimethylsulfoxide
DTT	Dithiothreitol
ϵ	extinction coefficient
E. coli	*Escherichia coli*
EDT	ethanedithiol
EDTA	Ethylenediaminetetraacetic acid
FAS	Fatty Acid Synthesis
fmoc	Fluorenylmethyloxyarbonyl chloride
fw	forward
HEPES	4-(2-Hydroxyethyl)piperazine-1-ethanesulfonic acid
HPLC	High-performance liquid chromatography
IAA	iodoacetamide

ITC	Isothermal Titration Calorimetry
KAS	beta-Ketoacyl-ACP-Synthase
LB	Luria Bertani
MALDI	Matrix Assisted Laser Desorption Ionisation
MOE	Molecular Operating Environment
MR	Molecular Replacement
MW	Molecular Weight
NMT	N-myristoyl-transferase
NMR	Nuclear Magnetic Resonanz
Oxyma	Ethyl cyanohydroxyiminoacetate
PAGE	Polyacrylamide gel electrophoresis
PCP	Peptidyl Carrier Peptide
PCR	Polymerase Chain Reaction
PDB	Protein Data Base
PEG	Poly Ethylen Glycol
rev	reverse
rmsd	root mean square deviation
SDS	Sodium dodecyl sulfate
SEC	Size exclusion chromatography
SPPS	Solid Phase Peptide Synthesis
TEMED	N,N,N′,N′-Tetramethylethylen-1,2-diamin
TFA	Trifluoroacetic acid
TIS	Triisopropylsilane
Tris	Tris(hydroxymethyl)aminomethane
w. t.	wild type
WHO	World Health Organisation

Chapter 1

Introduction

1.1 Antibiotic crisis

There is an urgent need for new antibiotics as the number of multiple resistant bacteria is constantly increasing (French, 2010). The World Health Organisation (WHO) recently published a list of 12 bacteria for which new antibiotics are critically needed (priority 1), highly needed (priority 2) or medium needed (priority 3) (WHO, 2017; Figure 1.1). In particular, Gram-negative bacteria like *Pseudomonas aeruginosa* are associated with a broad spectrum of infections. As they are inherently resistant to many antimicrobials just a few antibiotics remain as therapeutic options (Gellatly and Hancock, 2013).

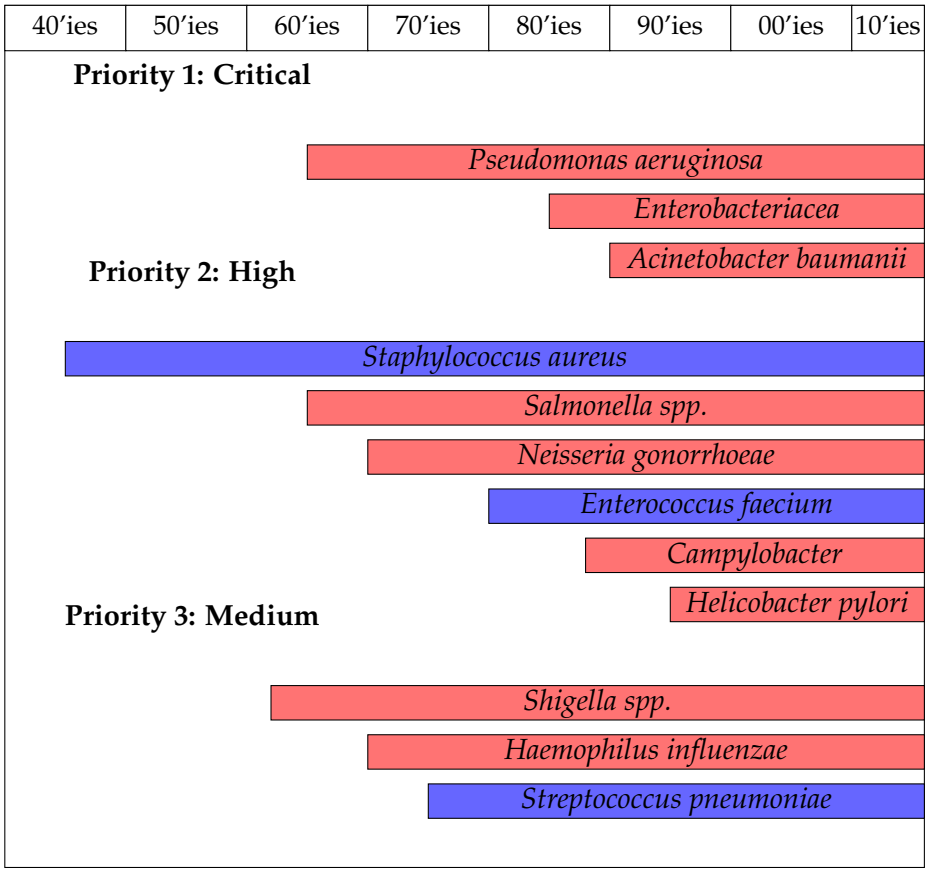

FIGURE 1.1: **Appearance of multiresistant bacteria** and the WHO rating for the critical, high or medium need of new antibiotics (red: Gram-negative bacteria, blue: Gram-positive bacteria) (WHO, 2017; Madigan et al., 2012; Cantón et al., 2012; Mégraud, 2012).

Infections of multiresistant bacteria are present in every country. In the winter of 2001/02 a contamination of mouth swabs, sold to several hospitals, caused a nationwide outbreak of *Pseudomonas aeruginosa* in Norway (Iversen et al., 2007). In spring 2015, an infection of 31 patients at the university hospital of Kiel in Germany led to 18 dead patients and an economic loss of around 6.5 million € (Grzegorek, 2015). Recently, a patient in Nevada (USA) died due to infection with the Gram-negative bacteria *Klebsiella pneumoniae* that was resistant against 26 approved antibiotics (Feldwisch-Drentrup, 2017).

1.2 Cell wall of bacteria

Gram-positive and negative bacteria differ by the anatomy of their cell wall. Both cell walls consist of a phospholipid bilayer and a peptidoglycan layer, whereas the latter is much thinner in Gram-negative bacteria and surrounded by a second phospholipid bilayer, the outer membrane (Figure 1.2, A).
The phospholipid bilayer (cell membrane) is built up of fatty acids forming ester bonds with two hydroxy groups of glycerol. The third hydroxy group of glycerol carries a phosphate ethanolamine residue (Figure 1.2, B).

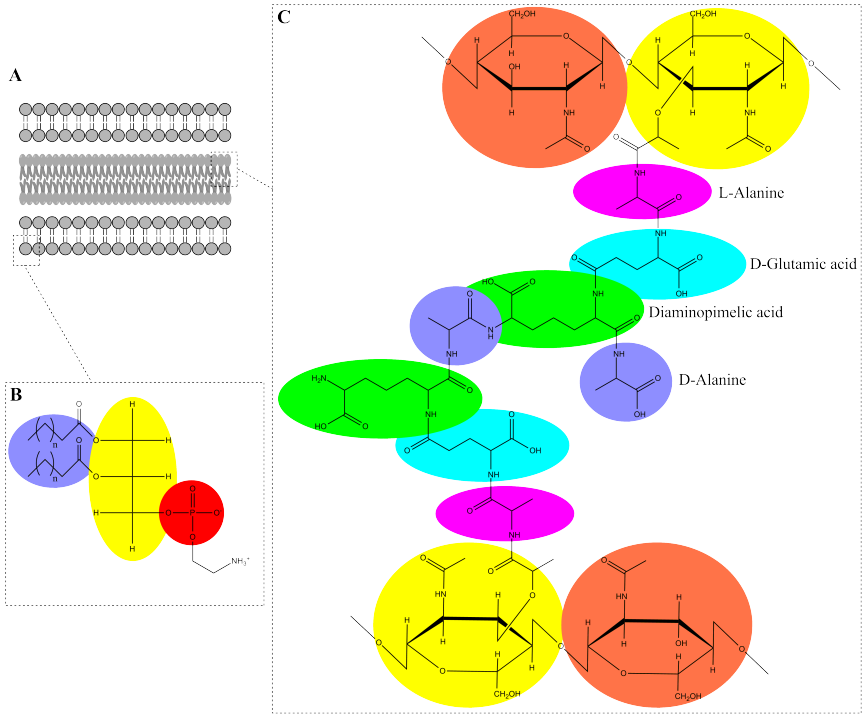

FIGURE 1.2: **Cell wall of Gram-negative bacteria.** A: Scheme of the cell wall. Two phospholipid bilayer surrounding the peptidoglycan layer. B: Phospholipid layer (blue: fatty acids, yellow: glycerol, red: phosphate), C: Peptidoglycan layer (orange: *N*-acetylglucosamine, yellow: *N*-acetylmuramic acid, blue: D-alanine, green: diaminopimelic acid, cyan: D-glutamic acid, purple: L-alanine). Figure adapted from Madigan et al., 2012.

The peptidoglycan layer consists of repeating sugar units of *N*-acetylglucosamine and *N*-acetylmuramic acid connected with β-1,4-glycosidic bonds. *N*-acteylmuramic acid forms a peptide bond at its lactic acid part to a tetrapeptide of L-alanine, D-glutamic acid, diaminopimelic acid and D-alanine. The latter is cross-connected with D-alanine of another strain, which results in a multilayer of peptidoglycans (Madigan et al., 2012; Figure 1.2, C).

1.3 Fatty acid synthesis cycle

Fatty acid synthesis in bacteria (FAS II, Figure 1.3) is performed by a series of monofunctional enzymes whereas in higher organisms one large multifunctional enzyme is used (FAS I, Zhang et al., 2006). FAS II starts with an initiation module, where acetyl-CoA is converted to malonyl-CoA by the four enzymes AccA-D and the 4'-phosphopantetheine prosthetic group is transferred to the Acyl Carrier Protein (ACP) by the ACP synthase (AcpS). The last step of the initiation module is the transfer of malonyl from malonyl-CoA to ACP by the transacylase FabD. The second module of FAS II is initiated by the condensation enzyme FabH that catalyse the formation of acetoacetyl-ACP from malonyl-ACP and acetyl-CoA. This reaction product enters the elongation cycle performed by four types of enzymes. FabG reduces β-ketoacyl-ACP to β-hydroxyacyl-ACP, that is dehydrated by FabA or FabZ. To complete the cycle FabI/K/L reduces the enoyl-ACP. Elongation of the fatty acid chain by two more carbon atoms is initiated by the condensing enzymes FabB or FabF (White et al., 2005).

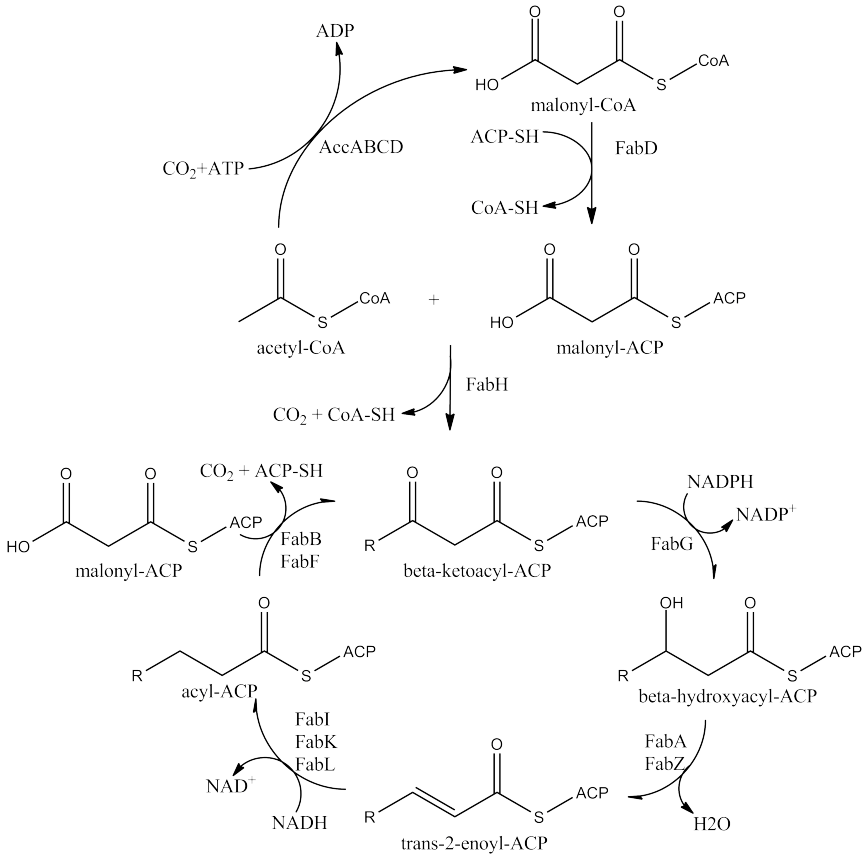

FIGURE 1.3: **Bacterial fatty acid synthesis pathway.** Figure adapted from Zhang et al., 2006.

1.3.1 β-ketoacyl-(ACP)-synthases

There are three β-ketoacyl-(ACP)-synthases in FAS II. Different terms are used for these enzymes, the most prevalent ones are FabB or KAS I, FabF or KAS II and FabH or KAS III (Zhang et al., 2006). In the following, the terms FabB, F and H, respectively, will be used. All the three enzymes elongate fatty acid chains via a Claisen condensation reaction. The catalytic triad of FabB and FabF consists of Cys-His-His whereas in FabH one histidine residue is replaced by asparagine. The substrates are the growing fatty acid chain, coupled to ACP and a malonyl group coupled to ACP (FabB/F) or CoA (FabH) (Heath and Rock, 2002). A structural alignment between *E. coli* FabB/F/H and *P. aeruginosa* FabF/H revealed that FabB/F and FabH are on a sequence level not related (identity 14%) while FabB and FabF are homologues (identity 37%). *E. coli* FabF and *P. aeruginosa* FabF share a sequence identity of 65.8%, confirming a conserved structure.
However, FabB and FabF differ in their substrate specificity. Both enzymes have an overlapping function for the elongation of saturated substrates. Their highest level of activity is for C6:0 up to C12:0 substrates. FabF elongates C14:0 substrates much more efficient than FabB. In addition it catalyzes the elongation of C16:1 unsaturated substrates, whereas FabB does not (Edwards et al., 1997).

1.3.2 FabF

FabF is an essential enzyme of the fatty acid biosynthesis pathway and has been validated as target for the natural products platensimycin and fasamycin A and B in Gram-positive bacteria (Wang et al., 2006; Feng et al., 2012). Platensimycin is inactive against wild type Gram-negative bacteria. However, it is active against efflux-negative *E. coli* (Wang et al., 2006). Similarly, the fasamycins are active against membrane permeabilized *E. coli* but not the unaltered strain (Feng et al., 2012). This suggests that the absence of activity in Gram-negative bacteria of the currently known FabF inhibitors is due to their inability to access their target. This issue could potentially be overcome by developing chemical matter based in different chemical scaffolds which are more easily taken-up by Gram-negative bacteria and that might also avoid efflux mechanism.
There are several crystal structures of FabF from ten different organisms available in the PDB (01.04.2018). The enzyme is a homodimer with a large interface area of hydrophobic residues. It contains a buried potassium binding site that has an octahedral coordination and forms hydrogen bonds to five amino acids (Asn302, Glu350, Ser395, Ala303, Asn396). The overall structure of the monomer consists of 14 β-sheets, 12 α-helices and four 3_{10}-helices. The arrangement results in two sets of five stranded β-sheets and a five layered structure α-β-α-β-α (Baum et al., 2015; Figure 1.4, left).
The active centre of FabF consists of two adjacent binding pockets. The first one accommodates the growing fatty acid chain and the second one binds malonyl-ACP. The fatty acid binding pocket is a channel formed by hydrophobic residues of both subunits of the homodimer. In contrast, the malonyl binding site consists of polar amino acids that allow several hydrogen bonding interactions.

In the wild type structure of FabF the binding site for malonyl-ACP is closed due to rotation of Phe400. Upon binding of a fatty acid or the covalent ligand cerulenin Phe400 turns into the open conformation and the malonyl-competitive binding site is accessible for ligand binding (Price et al., 2001). The variant FabF C164Q mimics the acyl-enzyme intermediate (Wang et al., 2006; Figure 1.4, right).

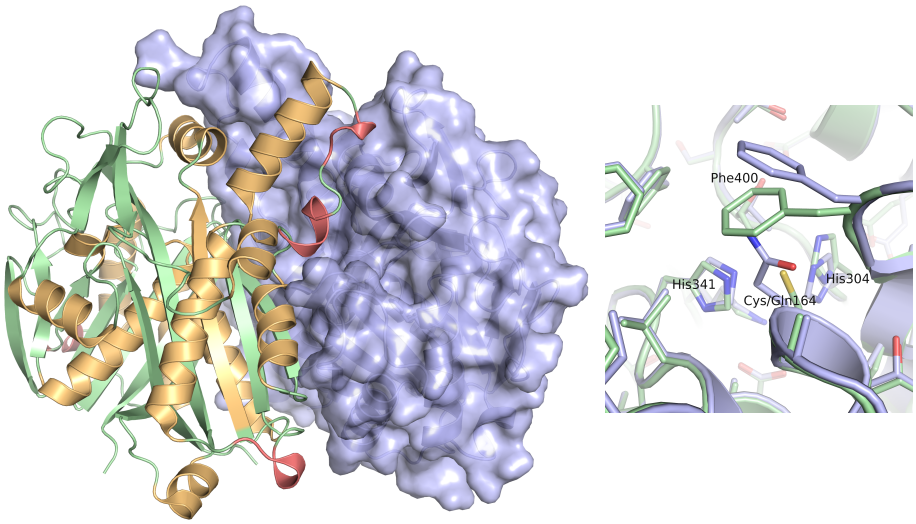

FIGURE 1.4: **Structure of FabF.** Left: The dimer of FabF (PDB code 4B7V). Chain B is colored in blue and secondary structure elements of chain A are shown (α-helices in orange, β-sheets and loops in green and 3_{10}-helices in red). Right: The structure of FabF w. t. (green, PDB code 4B7V) superposed with the structure of FabF C164Q (blue, PDB code 4JB6). The amino acid exchange C164Q leads to a rotation of Phe400.

1.3.3 Inhibition of FAS II

Due to significant differences in the fatty acid synthesis pathway of eukaryotes and prokaryotes accompanied with important structural differences almost all enzymes of the bacterial fatty acid synthesis pathway are interesting targets for drug design (Zhang et al., 2006).
Several inhibitors are known for the reductase FabI (isoniazid (Banerjee et al., 1994), triclosan (Sivaraman et al., 2003), diazoborin (Stewart et al., 1999), the dehydratase FabZ (NAS-91, NAS-21 (Sharma et al., 2003)), the isomerase FabA (allenic acid (Morisaki and Bloch, 1971), 3-decycoyl-NAC (Kass, 1968)) or the transacylase FabD (corytuberine (Liu et al., 2006)).
Three natural product inhibitors for the elongation condensing enzymes (FabB, FabF, FabH) are known, namely platensimycin, cerulenin and thiolactomycin. For three others, binding to FabF is suggested, namely BABX and fasamycin A and B.

Malonyl-competitive FabF inhibitors

Platensimycin, that has been isolated from *Streptomyces platensis*, is the most potent inhibitor of FabF known to date. An IC_{50} value of 48 nM for *S. aureus* FabF and 160 nM for *E.coli* FabF was determined. A direct binding assay with *E. coli* FabF wild type, preincubated with lauroyl-CoA resulted in a K_D value of 19 nM (Wang et al., 2006). The compound binds non-covalently to the acyl-enzyme intermediate and consists of three structural elements (Figure 1.5): a polar aromatic head that points deep into the pocket, an amide linker and a caged ring system. Every structural element forms two hydrogen bonds to the enzyme which might together with the good steric complementarity of the binding pocket explain the high affinity. The polar aromatic head forms hydrogen bonds to the catalytic histidines. In addition there is a water-bridged hydrogen bond to Asp266 (*P. aeruginosa* numbering). The amide linker interacts with Thr271 and Thr308 and the caged ring system forms two hydrogen bonds with Thr271 and Ala310 (Wang et al., 2006; Figure 1.5, left).

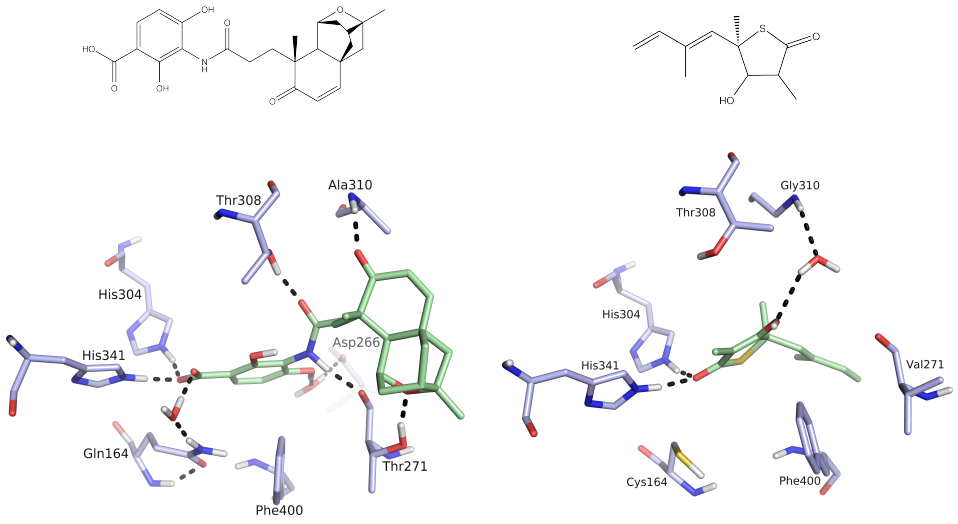

FIGURE 1.5: **Structures and binding modes of non-covalent FabF ligands.** Left: Structure and binding mode of platensimycin in *E. coli* FabF (PDB code 2GFX, *P. aeruginosa* numbering). Right: structure and binding mode of thiolactomycin in *E. coli* FabB (PDB code 2BV8, *P. aeruginosa* numbering). Ligands are colored in green and hydrogen bonds are indicated as black dots.

Thiolactomycin is an inhibitor that has been isolated from the culture filtrate of *Nocardia spp*. It also forms hydrogen bonds with the two catalytic histidines. The isoprenoid moiety forms stacking interactions with two peptide bonds (399-400 and 272-273, *P. aeruginosa* numbering). The hydroxyl group forms water mediated hydrogen bonds with the backbone of Gly310. The sulfur atom does not make any specific interactions (Price et al., 2001; Figure 1.5, right). Thiolactomycin was determined to be most active for *E. coli* FabF (IC_{50}= 6 μM) and slightly less active for *E. coli* FabB (IC_{50}= 25 μM) using a radiochemical assay with [^{14}C]malonyl-CoA. Activity against *E. coli* FabH was specified using a filter disc assay with [^{14}C]acetyl-CoA and is relatively low (IC_{50}= 110 μM) (Price et al., 2001).

Acyl-competitive FabF inhibitors

Cerulenin, a natural product isolated from *Cephalosporium caerulens*, is an irreversible acyl-ACP competitive inhibitor that binds covalently to the side chain of Cys164 (Figure 1.6). Two crystal structures in the PDB contain cerulenin covalently bound to *E. coli* FabF via the C2 carbon atom (PDB codes 1FJ8, 1B3N) and one crystal structure contains cerulenin covalently bound to *Bacillus subtilis* FabF via the C3 carbon atom (PDB code 4LS8). The carboxamide group forms a hydrogen bond to the catalytic histidines and occludes the malonyl-ACP binding site. The former epoxide oxygen lies in an oxyanion hole formed by the Cys164 backbone NH and Phe400 backbone NH (*P. aeruginosa* numbering). The hydrophobic tail of cerulenin containing two double bonds with trans-conformation is accommodated in the hydrophobic pocket that is formed by amino acids from both subunits of the FabF homodimer.

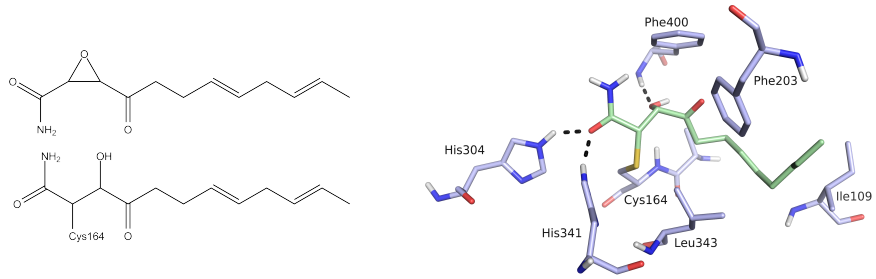

FIGURE 1.6: **Structure and binding mode of cerulenin.** Left: Structure of cerulenin in the unbound (epoxide) and bound state. Right: Binding mode of cerulenin (green) in *E. coli* FabF (PDB code 1B3N, *P. aeruginosa* numbering). Hydrogen bonds are indicated as black dots.

Drug discovery for FabF

In the course of time drug discovery for FabF has been attempted by using several screening and synthetic approaches.
A natural product named platencin has been explored by screening natural product extracts. Platencin is related to platensimycin with the caged ring system replaced by another one. It targets FabF with an IC_{50} of 113 nM and FabH with an IC_{50} of 16.2 nM (Wang et al., 2007). Inspired by these findings novel FabF inhibitors were discovered by using de novo structure-based ligand design. The caged ring system of platensimycin/platencin was replaced by a series of analogs. For the most active inhibitor a K_D value of 50 μM was determined using a waterLOGSY competition assay (Fisher et al., 2014).
A novel class of inhibitors was identified by virtual screening of large compound libraries. This class is based on a benzoxazolinon scaffold with different substituents. The most active inhibitor showed an IC_{50} of 260 μM in a radiochemical enzymatic assay (Zheng et al., 2014).
Some other inhibitors for the fatty acid elongation enzymes were found by high throughput screening of bacterial culture broth extracts. These inhibitors, namely BABX (Kodali et al., 2005) and Fasamycin A and B (Feng et al., 2012) share a common anthracene-substructure. Inhibition was measured using a fatty acid synthesis pathway assay. IC_{50} values of 11.4 μg/ml

in the *S. aureus* assay and 35.3 μg/ml in the *E. coli* assay were determined for BABX. Fasamycin A and B inhibit the fatty acid elongation of *S. aureus* with IC_{50} values of 50 and 80 μg/ml, respectively. The authors suggested inhibition of the condensation enzyme FabF (Kodali et al., 2005; Feng et al., 2012).
Also phomallenic acid A, B and C were discovered to have activity against FabF and FabH in a screen for natural product inhibitors. The compounds inhibit the fatty acid pathway of *S. aureus* with IC_{50} values of 22, 3.4 and 0.77 μg/ml, respectively (Ondeyka et al., 2006).

1.3.4 Enzymatic FabF assay

In order to determine the binding strength of FabF ligands several binding assays have been used (Fisher et al., 2014; Zheng et al., 2014; Wang et al., 2006). However, enzymatic assays are needed to measure the inhibitory effect. A general problem is the need of substrates coupled to the Acyl Carrier Protein (ACP). All enzymes of the elongation cycle use substrates coupled to ACP. A K_M value of 600 μM for malonyl-CoA and 8.2 μM for malonyl-ACP in the condensing reaction catalyzed by FabF reveals the importance of this protein (Borgaro et al., 2011; Table 1.1). Thus, FabD that catalyze the transfer of malonyl from CoA to ACP and ACP itself are needed to be prepared in advance. Further, the FabF reaction product is not easily detectable. Thus, the reaction has to be coupled to another enzyme which includes the risk of interaction of the ligand with the coupled enzyme. Alternatively, the use of radioactive substrates leads to toxic waste.

TABLE 1.1: **Substrates of FabF**. Natural substrates and sequences of peptide substrates are listed with their corresponding K_M value for *E. coli* FabF. K_M values of MalPPant substrates and malonyl-CoA were determined at a constant lauroyl-CoA concentration of 75 μM, for malonyl-ACP at a concentration of 10 μM lauroyl-ACP and for lauroyl-CoA at a constant concentration of 500 μM malonyl-CoA. The K_M value for lauroyl-CoA was determined at a constant concentration of 2 mM malonyl-CoA and the K_M for malonyl-CoA at a constant concentration of 100 μM lauroyl-CoA. Values taken from Borgaro et al., 2011 and Machutta et al., 2010.

	peptide sequence	**K_M [μM]**	**kcat / K_M [μM / min^{-1}]**	**activity [%]**
Borgaro et al., 2011				
lauroyl-CoA	-	25	0.05	-
malonyl-CoA	-	600	-	-
MalPPant	-	590	0.0022	1
MalPant-8mer	DSLDMLEI-NH_2	23.7	0.05	22
MalPPant-14mer	DSLSLMLEIAVQTED-NH_2	6.1	0.25	108
MalPPant-16mer	DPDSLSMLEIAVQTED-NH_2	6.2	0.23	100
malonyl-ACP	-	8.2	0.23	100
Machutta et al., 2010				
malonyl-CoA	-	510	0.005	2
lauroyl-CoA	-	53.7	0.06	25

The enzymatic assays used in literature so far are on the one hand a FabD-coupled radioactive assay and on the other hand a FabG-coupled assay.
The most prevalent assay is based on radioactive labeled substrates (Edwards et al., 1997; Price et al., 2001; Wang et al., 2007; Zhang et al., 2006; Zheng et al., 2014) first published by Garwin et al., 1980. This assay uses [^{14}C]-malonyl-CoA and tetradecanoyl-, myristoyl- or lauroyl-ACP as substrates. In a first step, malonyl is transferred from CoA to ACP using FabD. In the next step, FabF is added and the Claisen condensation of both ACP-substrates takes place. EDTA and DTT are added to reduce FabD and ACP for a maximum activity and the reaction is terminated with a reducing agent. Wang et al., 2007 introduced the use of lauroyl-CoA as substrate instead of lauroyl-ACP.
Beside the counting of radioactive labeled products the consecutive reaction in the fatty acid synthesis cycle (FabG) could be used for detection of FabF activity (Machutta et al., 2010; Schaeffer et al., 2001). FabG reduces β-ketoacyl-ACP under oxidation of NADPH to $NADP^+$, which can be measured at 340 nm. This assay was performed with lauroyl- and malonyl-ACP as well as with lauroyl- and malonyl-CoA as substrates and K_M-values were determined (Table 1.1). Using this assay, the recognition site of the ACP was determined (Borgaro et al., 2011). For that purpose, three different peptides were synthesized and malonyl-phosphopantetheine was coupled to a serine residue of these peptides in order to mimic the natural substrate malonyl-ACP. K_M-values of all malonyl-substrates were determined and revealed that the MalPPant-14mer (further called malonyl-PCP) represented best the ACP-recognition site.

1.4 β-Lactamases

The last step in the cell wall synthesis of bacteria is the cross-linking of peptidoglycan layers catalysed by the glycopeptide transpeptidase (Figure 1.2; Klebe, 2009). This enzyme is inhibited by β-lactam antibiotics like penicillins, cephalosporines or carbapenems (Figure 1.7). In the course of time bacteria have developed a defence mechanism by producing extended spectrum β-lactamases (ESBL) that hydrolyze the lactam ring of penicillins and cephalosporines and therefore inactivate these antibiotics.

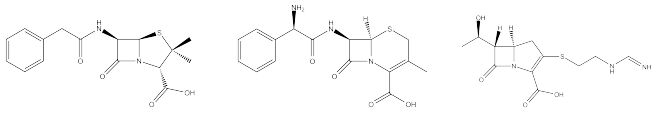

Benzylpenicillin Cefalexin Imipenem

FIGURE 1.7: **Structure of β-lactam antibiotics.** The first discovered penicillin Ppenicillin G (left), the cephalosporine cefalexin and the carbapenem imipenem.

Based on their amino acid sequence, β-lactamases are classified into the classes A to D (Ambler, 1980; Jaurin and Grundström, 1981; Huovinen et al., 1988). Classes A, C and D are serine dependent β-lactamases, whereas class B includes metalloenzymes. Selection pressure by combination of β-lactam antibiotics with lactamase inhibitors, like clavulanic acid, led to inhibitor-resistant β-lactamase (IR) producing bacteria. After time, only carbapenems remained as therapeutic option against multiresistant bacteria (Papp-Wallace et al., 2011). However, shortly after introducing carbapenems in clinical therapy, a new type of β-lactamases, namely carbapenemases evolved. These enzymes were able to inactivate carbapenems by hydrolyzing the lactam ring (Drekonja et al., 2014).
The mechanism of β-lactam hydrolysis is a two step reaction. In the acylation step the β-lactam antibiotic binds covalently to Ser70 (Ambler numbering for class A β-lactamases) leading to ring opening of the lactam. This step is followed by deacylation, activated by a water molecule and release of the hydrolyzed and therefore inactive antibiotic. Carbapenems are deactivated following the same mechanism, but with a slower turnover rate. In contrast, with carbapenemases this turnover rate is increased by several fold (Papp-Wallace et al., 2011).

1.4.1 Carbapenemases

Carbapenem antibiotics used to have the broadest range of activity against Gram-negative and Gram-positive bacteria in respect to all classes of β-lactams. Their unique role of resisting hydrolysis by most of the β-lactamases was limited when carbapenemases appeared. This type of lactamases was able to hydrolyse the lactam ring of carbapenems and occurred in serine-dependent β-lactmases as well as in metalloenzymes (Papp-Wallace et al., 2011).
Carapenemases within class A β-lactamases can be distinguished into several groups: *Serratia marcescens* enzymes (SME), non-metallo carbapenemases (NMC), imipenemases (IMI), *Serratia fonticola* carbapenemases (SFC1),

Klebsiella pneumoniae carbapenemases (KPC) and Guyana extended spectrum carbapenemases (GES). The latter two are plasmid mediated and widely distributed in clinical bacterial pathogens, whereas the others are chromosomally encoded and clinically relatively inconspicuous (Tondi et al., 2016).
All of these carbapenemases share common structural features of group A β-lactamases (Figure 1.8). A tetrad, formed by Ser70 (Ambler numbering), two variable amino acids and Lys73 (SXXK), a triad of Ser130, Asp131 and Asn132 (SDN) and a triad of Lys234, Thr/Ser235 and Gly236. Furthermore, Glu166 is a higly conserved residue. Two water molecules are conserved in the binding site. The first one is placed in an oxyanion hole formed by Ser70 and Thr237, the second one, responsible for deacylation, is coordinated between Glu166 and Asn170 (Walther-Rasmussen and Høiby, 2007).
Carbapenemase activity is caused by only a few point mutations leading to aminoacid changes in the active site of β-lactamases as structural analysis indicates. However, the mechanism of carbapenemase activity is still not clear.

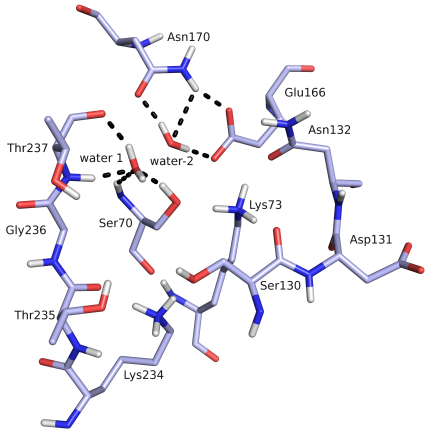

FIGURE 1.8: **Structural features of carbapenemases binding sites.** Hydrogen bond interaction patterns of the conserved water molecules are indicated as black dots.

1.4.2 KPCs

The KPC group covers 23 variants with KPC-2 and KPC-3 being the dominant isoforms. The name is attributed to *Klebsiella pneumoniae* being the predominant host but the plasmid has spread among several Gram-negative bacteria like for instance *Pseudomonas aeruginosa* (Tondi et al., 2016).
On a structural basis just a few amino acids in the active site differ from class A β-lactamases. Within the class A β-lactamases position 69 is usually occupied by a methionine. In carbapenemases it is a cysteine leading to a common feature of carbapenemases, a disulfide bond formed between Cys69 and Cys238. Coming along with the formation of the disulfide bond and the insertion of Gly239 the carbonyl group of Cys238 is reoriented. Other amino acid exchanges with respect to class A β-lactamases are Arg220, Thr237 and His274. This leads to a reduction of the active site volume. Asn132 is shifted in opposite directions to Asn170 and the positions

of the hydroxyl groups of Ser130, Thr216 and Thr235 are reoriented (Tondi et al., 2016).
Two structures of the hydrolyzed β-lactam antibiotics cefotaxime and faropenem(PDB codes 5UJ3, 5UJ4; Figure 1.9; Pemberton et al., 2017) in complex with KPC-2 were recently solved. Both ligands form hydrogen bond interactions with their C4-carboxyl group to Ser130, Thr235 or Thr237. The dihydrothiazine moiety of cefotaxim and the dihydrothiazole moiety of faropenem form π-π-stacking interactions with Trp105. In the apo-enzyme this side chain adopts two rotamers, upon binding of a ligand only one. Mutagenesis studies have shown the importance of Trp105 in substrate recognition (Papp-Wallace et al., 2010). The faropenem ring nitrogen forms a hydrogen bond interaction to Ser130, the ring nitrogen of cefotaxim a hydrogen bond to Ser70. The aminothiazole ring of cefotaxime forms van der Waals contacts to Leu167, Asn170, Cys238 and Gly239, while the oxyimino group and the hydroxyethyl group of faropenem are solvent exposed (Pemberton et al., 2017; Figure 1.9).

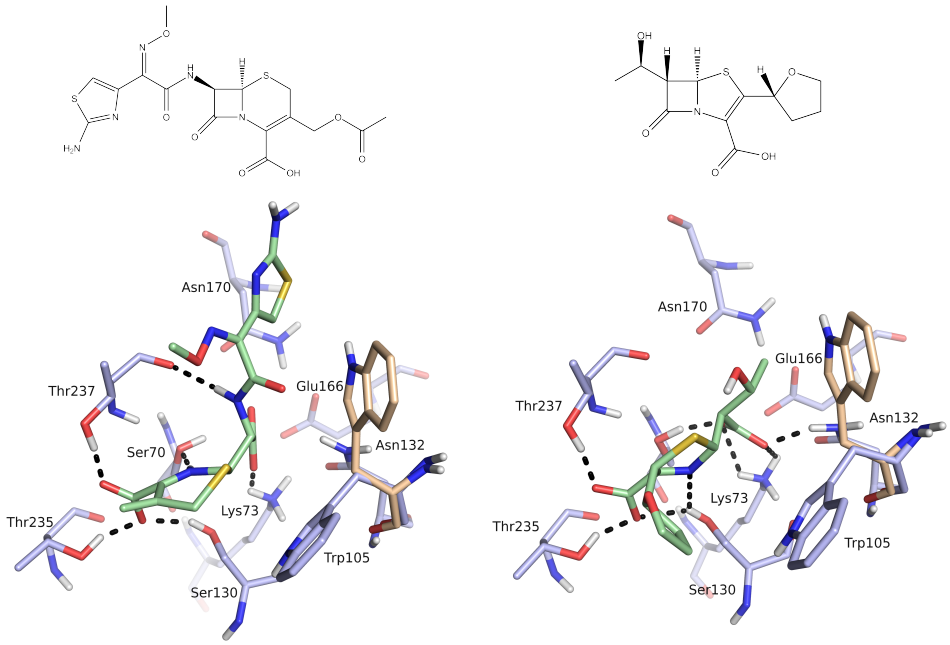

FIGURE 1.9: **Structures and binding modes of hydrolysed β-lactam antibiotics in the KPC-2 binding site.** Left: Binding mode of hydrolyzed cefotaxim. Right: Binding mode of hydrolyzed faropenem. The second rotamer of Trp105 adopted in the apo-enzyme is colored in beige, protein side chains in blue and ligands in green. Hydrogen bonds are indicated as black dots.

1.4.3 KPC-2 inhibitors in drug discovery

In the last decade new inhibitors for β-lactamases were investigated, including inhibitors for carbapenemases like KPC-2. For some of them crystal structures were determined. The binding modes were analysed in order to set the basis for structure-based inhibitor design.
The β-lactamase inhibitor protein (BLIP) was isolated from the soil bacterium *Streptomyces clavuligeris*. It has a subnanomolar affinity to KPC-2 (K_I= 84 $\pm$ 69 pM). The protein binds with two loops to KPC-2, which occlude the binding site. Asp49 of BLIP forms hydrogen bond interactions with Ser130, Lys234 and Thr237 as well as a salt bridge to Lys234. Trp105 of KPC-2 favors the closed conformation also found upon binding of cefotaxim and faropenem. (PDB code 3E2K; Doran et al., 1990; Hanes et al., 2009).
Several boronic acid transition state analogs (BATSI) were designed to inhibit serine β-lactamases such as KPC-2. For instance, 3-nitrophenyl boronic acid (3-NPBA, PDB code 3RXX) with a K_M value of 1 $\pm$ 0.1 μM (determined in a competition assay with the substrate nitrocefin) or S02030 (PDB code 5EEC) with an IC_{50} of 80 $\pm$ 2 nM. Both ligands bind covalently to Ser70 with their boronic acid. In both structures, a boron oxygen points into an oxyanion hole formed by the backbone nitrogen of Ser70 and Thr237. The other boron oxygen forms hydrogen bond interactions with Asn170 and Glu166 that usually coordinates the deacylating water (Ke et al., 2012; Powers et al., 2014; Nguyen et al., 2016).
The penam sulfone PSR3-226 inhibits KPC-2 with a K_M of 3.8 $\pm$ 0.4 μM (determined in a competition assay with the substrate nitrocefin). The rational design of this class of inhibitors is based on a *trans*-enamine transition state formed by tazobactam found in a deacylation deficient variant of a SHV β-lactamase variant. The penam sulfones form a more stable intermediate (Padayatti et al., 2006; Ke et al., 2012; Rodkey et al., 2014). Aside from the covalent bond to Ser70 all other groups of the molecule are flexible (PDB code 3RXW).
A class of non-β-lactam β-lactamase inhibitors, the diazabicyclooctanes includes avibactam, a KPC-2 inhibitor that was approved by the European Medicines Agency (EMA, www.ema.europa.eu). Avibactam is a covalent reversible inhibitor and binds to KPC-2 with a K_D of 11 nM (Coleman, 2011; Krishnan et al., 2015). Its carbonyl oxygen points into the oxyanion hole formed by Ser70 and Thr237. The amide forms hydrogen bond interactions with Asn132 and the sulfate moiety forms hydrogen bond interactions to Ser130, Thr235 and Thr237. Avibactam undergoes van der Waals interactions with Trp105 and therefore favors the closed conformation (PDB code 4ZBE).

1.5 Screening approaches for drug discovery

As there is a constant increase of infections caused by multiresistant bacteria new starting points for the design of novel antibiotics are needed. Identification of this hit compounds is the first step of a drug discovery process, which often starts with *in silico* methods. Virtual screening of large compound libraries has become a standard method (Kitchen et al., 2004). In the recent years also fragment screening became a valuable tool for hit identification (Keseru et al., 2016). The basic principles of both techniques will be elucidated in the following paragraphs.

1.5.1 Virtual screening

Molecular docking is a computational approach to predict the binding modes of small molecules to e.g. a protein binding site. This approach can be divided in a search algorithm, that is fitting the ligand into the binding site (posing) and a scoring function, that is ranking the poses by estimating the free energy of binding (scoring) (Kitchen et al., 2004). Molecular flexibility is the most challenging part of posing. Many proteins differ in their apo and their holo structure due to conformational changes of side chains, helices or domains (Antunes et al., 2015). Albeit some search algorithms have been developed to handle protein flexibility in molecular docking, most docking programs keep the protein structure rigid and focus on ligand flexibility (Guedes et al., 2014). Different docking programs use different search algorithms: a systematic search, which includes as examples the exhaustive (Glide; Friesner et al., 2004), incremental construction (FlexX; Rarey et al., 1996; Kramer et al., 1999) or conformational ensemble (DOCK; Shoichet et al., 1992; Meng et al., 1992; Nicholls and Honig, 1991; Mysinger and Shoichet, 2010) search or a stochastic search, which can also be divided into several algorithms (Guedes et al., 2014). With all algorithms a large number of poses are generated for each ligand. A scoring function now selects the ”best” pose of each ligand which should be the most nearnative pose and ranks the best poses of different ligands. These scoring functions can be divided into three groups: physics-based scoring functions (DOCK), empirical scoring functions (FlexX, Glide) and knowledge-based scoring functions (Bello et al., 2013).
Physics-based functions are based on a force field which consists of a sum of energy terms such as van der Waals interactions, electrostatic interactions and hydrogen bond energies. Empirical scoring functions use a sum of selected terms describing interactions, which are supposed to determine the binding affinity. These terms are weighted with a factor, determined with a training set of protein-ligand complexes with known 3D structure and binding affinities. Knowledge-based functions use available 3D structures to determine the strength of interacting atom pairs in a statistical manner (Huang et al., 2010).
All these functions have their limitations in accuracy and speed. Consensus scoring combines different scoring functions in order to mitigate these disadvantages (Huang et al., 2010).

FlexX

FlexX is a docking program that treats the protein structure as rigid and generates poses by using a systematic search algorithm to predict binding poses of ligands in protein binding sites. In more detail, it uses an incremental fragment based method, which cuts the ligand at each rotateable acyclic bond (Rarey et al., 1996; Kramer et al., 1999).
In the first step, a fragment is selected as starting point for docking (”base selection”). Next, the fragment is docked into the binding site using ”pose clustering” (”base placement”) (Linnanmaa et al., 1988). The final step is the reconstruction of the ligand. Remaining fragments are added one by one to the base fragment (”complex construction”). In each step, a large number of conformations are generated based on the conformational search programs MIMUMBA (Klebe and Mietzner, 1994) and SCA (Hoflack et al., 1989). However, these programs are based on the bond lengths and angles in the input file. Therefore, molecules have to be energy minimized before docking.
Protein-ligand interactions are calculated and the poses are ranked based on an empirical scoring function initially developed by Böhm, 1994 that considers hydrogen bonds, ionic interactions, lipophilic protein-ligand contact surfaces, number of rotatable bonds and the loss of entropy due to translational and rotational hindrance. In addition, aromatic interactions are taken into account (Kramer et al., 1999; Equation 11-15).

$$\Delta G = \Delta G_0 + \Delta G_{rot} \times N_{rot} \tag{11}$$

$$+\Delta G_{hb} + \sum_{neutral H-bonds} f(\Delta R, \Delta\alpha) \tag{12}$$

$$+\Delta G_{io} + \sum_{ionic int.} f(\Delta R, \Delta\alpha) \tag{13}$$

$$+\Delta G_{aro} + \sum_{aro.int.} f(\Delta R, \Delta\alpha) \tag{14}$$

$$+\Delta G_{lipo} + \sum_{lipo.cont.} f^{*}(\Delta R) \tag{15}$$

FlexX contains also a covalent docking batch mode. For that purpose, the search algorithm is modified. The user defines the covalent bond and the base placement algorithm is exchanged by an algorithm that superimposes the parts of the fragment and the protein that contain the covalent bond in the complex. This fragment is then the starting point for the incremental complex construction (BiosolveIT GmbH, www.biosolveit.de).

DOCK3.6

DOCK3.6 places ligands into the binding site by matching spheres that represent receptor and ligand atoms. Several programs are used to calculate receptor spheres and grids that characterize the binding pocket.
First, polar hydrogen atoms are added and the protein is converted into the Amber charge format (Cornell et al., 1993). "SPHGEN" (Kuntz et al., 1982) calculates spheres around ligand atoms to describe the shape of the molecular surface.
Further programs calculate three dimensional cubic grids to score protein-ligand complexes. "DISTMAP" (Shoichet et al., 1992) calculates grids for contact scoring, "CHEMGRID" (Meng et al., 1992) calculates van der Waals and electrostatic terms based on the Amber potential function for force-field scoring, "DelPhi" (Nicholls and Honig, 1991) calculates grids for electrostatic scoring and "SOLVMAP" (Mysinger and Shoichet, 2010) calculates a grid to score the influence of ligand desolvation.
DOCK3.6 uses a systematic search in which both protein and ligand are kept rigid. However, a conformational ensemble of each compound to be docked is precalculated to consider ligand flexibility. Finally, the program "AMSOL" (Hawkins et al., 2003) calculates partial charges and desolvation energies of the small molecules.
The calculated sphere set is reduced by applying critical distance between ligand and receptor spheres, as well as between two ligand spheres. The resulting spheres are then used as receptor matching positions for docking molecules in the binding site.
The evaluation of protein-ligand complexes is performed with a physics-based scoring function (Mysinger and Shoichet, 2010). This function includes a van der Waals term, an electrostatic term and a term for ligand desolvation (Equation 16).

$$E_{score} = E_{vdw} + E_{elec} + \Delta G^{L}_{desolv} \tag{16}$$

The ligand desolvation is calculated using the Generalized Born theory, that models atoms as charged spheres. The free energy contribution of desolvating each ligand atom as well as the fractional desolvation for positions in the protein binding site are precalculated. Finally, a fractional desolvation free energy is calculated depending on how much the ligand is engulfed by the protein (Mysinger and Shoichet, 2010).

1.5.2 Fragment screening

Fragment Based Drug Discovery (FBDD) was established as a useful method to find hit structures as starting points for the development of new drug candidates. Fragments, once validated as binding to the target molecule, opens a broad chemical space accessible by fragment growing, linking or merging. The resulting lead-like compounds usually have a high ligand efficiency. Fragments are small molecules fulfilling the rules of three (Congreve et al., 2003) with a molecular weight not more than 300 g/mol, a cLogP ≤ 3, the number of hydrogen bond acceptors ≤ 3 and the number of hydrogen bond donors ≤ 3. This small molecules can be used for efficient exploration of chemical space. In a second step, fragment growing or merging can be used to develop a new lead structure. Due to the size of fragments, the affinity to the target molecule is very low. Therefore, sensitive biophysical techniques are necessaryto detect the binding event (Keseru et al., 2016; Wartchow et al., 2011). One option is Bio-Layer-Interferometry (BLI).
BLI is an optical method that uses the interference of white light reflected from two surfaces to detect a binding event (Figure 1.10). The surface, an internal reference layer and a biocompatible layer with immobilized ligand (e.g. protein) are located on a biosensor. Reflection of light leads to constructive or destructive interference of the light waves, resulting in an interference pattern detected at the CCD array detector. Upon dipping the biosensor into a solution of an analyte, binding to the immobilized molecule occurs. Therefore, a shift in the interference pattern is observed and reported as a change of wavelength (nm) on a sensorgram. The shift of wavelength depends on the reflection properties of the molecule, respectively the density of the formed layer and the thickness. Also, the association rate constant (k_{on}) is influencing the observed rate constant. A higher k_{on} leads to a higher response if the analyte concentration is constant (Kumaraswamy and Tobias, 2015).

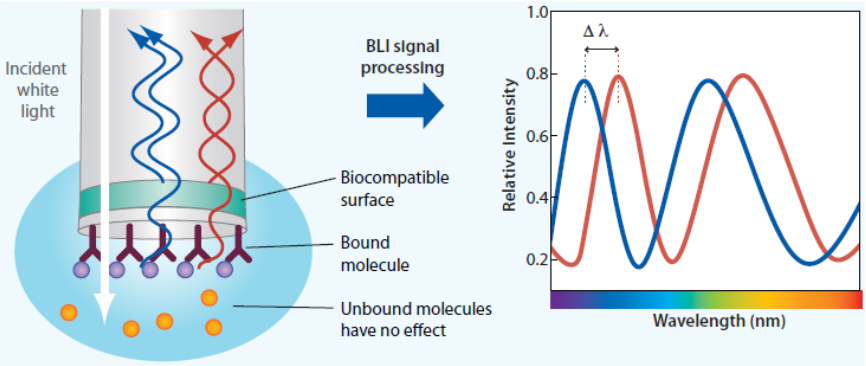

FIGURE 1.10: **Scheme of Bio-Layer-Interferometry.** Left: Structure of a biosensor tip and reflection of light on both surfaces. Right: The signal is processed into a shift of the interference pattern. Figure taken from FortéBio, application note 14.

1.6 Objectives

The number of infections with multidrug resitant bacteria is constantly increasing and thus, the need for new antibiotics is becoming more urgent. As pointed out in the previous paragraphs enzymes involved in cell wall and cell membrane synthesis of bacteria are attractive targets for drug design. In this thesis, the elongation condensing enzyme FabF of the fatty acid synthesis pathway was chosen as target for further studies. New starting points for structure-based drug design of FabF inhibitors are needed. These should be obtained by using covalent and non-covalent virtual screening and fragment screening methods. Thus, a fragment screening assay need to be developed. Obtained virtual hits should be validated using biophysical techniques and an enzymatic assay. The latter requires the development of a suitable test setup under the aspect of green chemistry and avoidance of coupled enzymes. As a basic principle of structure-based drug design a high knowledge of the binding site is essential. Therefore, mutagenesis studies should be carried out to obtain more detailed information about the importance of interactions between FabF and its natural product inhibitor platensimycin.
Another approach of targeting the cell wall synthesis of bacteria is the inhibition of the glycopeptide transpeptidase by β-lactam antibiotics. This approach is limited due to the defence mechanism of bacteria, the production of β-lactamases. For the β-lactamase KPC-2 a new starting point for the design of inhibitors should be identified using virtual screening methods. Subsequently, the obtained hits should be optimised guided by structure-based design principles.

Chapter 2

Materials and Methods

2.1 Materials

Chemicals

Chemicals were purchased from Sigma Aldrich, Roth, Merck and Santa Cruz Biotech. The enzyme ACP synthase was obtained from New England Biolab. Screening hits of the fragment screen were ordered from Otava chemicals. Hits from virtual screenings were purchased from Apollo Chemical, Asinex, Chembridge, Chemdiv, Enamine, Interbioscreen, Key Organics, LifeChemicals, Otava, Sigma Aldrich, Specs, Timtec and Vitas-M.

Oligonucleotides, vectors and *E. coli* strains

Sequences for oligonucleotides for the variant FabF T271A were generated using the Quik Change Primer Design online tool of Agilent (Novoradovsky et al., 2005) and ordered from Sigma Aldrich. In order to insert the point mutation C164Q the primers as described previously (Baum et al., 2015) were ordered from Eurofins Genomics.

TABLE 2.1: **Oligonucleotides including point mutations coding for amino acid exchanges C164Q and T271A.** The base triplet responsible for the point mutation is printed in bold.

mutation	primer
fwd(C164Q)	5′-GCCCTCACCACCGCC **CAG** ACCACCGGTACCCAC-3′
rev(C164Q)	5′-GTGGGTACCGGTGGT **CTG** GGCGGTGGTGAGGGC-3′
fwd(T271A)	5′-CCTTCCACATG **GCC** GCGCCGCCG-3′
rev(T271A)	5′-CGGCGGCGC **GGC** CATGTGGAAGG-3′

The vector pNIC28-Bsa4 (Stols et al., 2002, GenBankID: EF198106) was used for the expression of FabF and its variants. It contained a gene sequence for a 6x histidine tag, a TEV (Tobacco Etch Virus) cleavage site and a kanamycin resistance gene. The sequence of *Pa* FabF was included between the 5′-ligation site at 135 bp and 3′-ligation site at 2084 bp.
The *S. pneumoniae* acyl carrier protein synthase cloned in the vector pET-15b between the restriction site of NdeI and BamHI was a gift from Michael Johnson (Addgene pasmid # 63687).
The *E. coli* acyl carrier protein synthase gene was synthesised by GenScript

USA Inc. and cloned in the vector pET-15b between the restriction site of NdeI and XhoI. The vector contains a 6x histidine tag, an ampicillin resistance gene and a thrombine cleavage site. In addition the TEV protease cleavage site was cloned between the thrombine site and the AcpS gene sequence.
Three different *E. coli* strains were used for vector amplification or recombinant protein expression (Table 2.2).

TABLE 2.2: ***E. coli* strains.** Origin, genotype and application of used *E.coli* strains.

Name	Application	Genotype	Supplier
E. coli XL-10 GOLD	Vector amplification	endA1 glnV44 recA1 thi-1 gyrA96 relA1 lac Hte δ(mcrA)183 δ(mcrCB-hsd SMR-mrr)173tet^R F'[proAB lacl^{q}ZδM15 Tn10(Tet^R Amy Cm^R)]	Agilent Technologies
E. coli Rosetta (DE3) pLysS	Expression	F$^-$ ompT hsdS$_B$($R_B^-m_B^-$) gal dcm λ(DE3)pLysS[lacl lacUV5-T7 gene 1 ind1 sam7 nin5]) pLys SRARE (Cam^R)	Novagen
*E. coli*Arctic Express (DE3)	Expression	B F$^-$ ompT hsdS($r_B^-m_B^-$) dcm+ Tet^r gal λ(DE3) endA Hte [cpn10 cpn60 Gent^r]	Agilent Technologies

2.2 Molecular Biological Methods

Site-directed mutagenesis

Point mutations were introduced using the QuikChange II Site-Directed Mutagenesis Kit from Agilent Technologies. The polymerase chain reaction was performed according to the instruction manual of the kit. Afterwards the parental DNA was digested using DpnI. Subsequently, *E.coli* XL-10 GOLD competent cells were transformed with the plasmid as described in the instruction manual of the QuikChange kit.
Plasmid DNA was isolated out of 5 ml of overnight culture using the peqGOLD Plasmid Miniprep Kit I (peqlab) or the QIAprep Spin Miniprep Kit (QIAGEN) following exactly the protocol of the supplier. DNA was eluted using 50 μl water.
Accurate insertion of point mutations was verified using the sanger sequencing service of GATC Biotech. The T7 and pET-RP primer were used. Sequencing results were analysed using the program Serial Cloner 2.6.
Finally, *E. coli* Rosetta (DE3) pLysS cells (Novagen) or *E. coli* Arctic Express (DE3) cells (Agilent Technologies) were transformed with the plasmid as described in the instruction manual of the supplier.

2.3 Biochemical Methods

Expression and Purification of recombinant FabF

Purification of recombinant FabF and its variants was performed as described previously (Baum et al., 2015). Media and buffers are listed in appendix A.1. *E. coli* Rosetta (DE3) pLysS cells (Novagen) were used as expression system for all enzymes used in this work. In addition, *E. coli* Arctic express (DE3) cells were used for the expression of FabF C164Q:T271A. LB-Medium supplemented with kanamycin (50 μg/ml) and gentamycin (20 μg/ml) was inocculated with 5 ml of an 100ml overnight culture of FabF C164Q:T271A. Expression was induced with 1 mM IPTG after reaching an optical density of 0.7 and run for 48 hours at 10°C. Purification was performed as described earlier for FabF C164Q (Baum et al., 2015).

Expression and Purification of recombinant AcpS

S. pneumoniae AcpS was expressed in *E. coli* Rosetta (DE3) pLysS cells (Novagen) using autoinduction medium supplemented with ampicillin (20 μg/ml). Therefore, an overnight culture with 5 ml LB-medium was added to 1000 ml of autoinduction medium. After shaking at 20°C the cells were harvested by centrifugation (10 minutes, 6000 rpm, 4°C). The buffers chosen for purification were based on the buffer used by New England Biolab for the storage of *E. coli* AcpS (Appendix A.1). Cell pellets were resuspended in buffer A containing a *cOmplete*^{TM}EDTA-free protease inhibitor cocktail tablet (Roche) and 0.1 μg·ml^{-1} DNaseI (Sigma) and lysed by sonification. The suspension was centrifugated twice for 30 minutes at 20.000 rpm and subsequently purified using a Ni^{2+} charged HisTrap column (GE Healthcare). AcpS was eluted with a linear gradient of 0-100% buffer B.
E. coli AcpS was expressed in *E. coli* Rosetta (DE3) pLysS cells using LB-medium supplemented with ampicillin (20 μg/ml) and chloramphenicol (30 μg/ml). The expression was induced by adding 1 mM IPTG after reaching an optical density of 0.7 and carried out for 4 hours.
Buffers used for purification are listed in appendix A.1. The cells were harvested by centrifugation for 10 minutes at 6000 rpm at 4°C, resuspension in 0.9% NaCl solution and another centrifugation for 10 minutes at 4000 rpm. Cell pellets were resuspended in buffer A containing a *cOmplete*^{TM}EDTA-free protease inhibitor cocktail tablet (Roche) and 0.1 μg·ml^{-1} DNaseI (Sigma) and lysed by sonification. The suspension was centrifugated twice for 30 minutes at 20.000 rpm and subsequently purified using a Ni^{2+} charged HisTrap column (GE Healthcare). AcpS was eluted using a step gradient with 5 column volumes (cv) 0% and 5 cv 5% buffer B, 10 cv 20% and 10 cv 100% buffer B. Pooled protein fractions were treated overnight with TEV protease (ratio 1:10) at 4°C to cleave off the 6x-histidine tag. TEV protease was removed by running another HisTrap affinity chromatography. The pooled protein was then purified with size exclusion chromatography on a Superdex 75 HiLoad 26/600 prep grade column (GE Healthcare) using buffer C.

Determination of protein concentration

Concentration of the purified proteins was measured at a wavelength of 280 nm using a Nanodrop 1000 (Thermo Fisher Scientific). The correlation of concentration and absorbance was given by the Lambert-Beer law (Equation 1).

$$c = \frac{A_{280} \cdot MW}{\epsilon \cdot d} \quad (1)$$

Molecular weights and extinction coefficients (ϵ) were calculated using the Molecular Operating Environment (MOE, Chemical Computing Group, Montreal, QC, Canada). The calculated extinction coefficient of FabF was 21430 $M^{-1} \cdot cm^{-1}$. The molecular weights without His-tag were 43497 $g \cdot mol^{-1}$ (FabF w. t.), 43522 $g \cdot mol^{-1}$ (FabF C164Q), 43442 $g \cdot mol^{-1}$ (FabF T271A) and 43467 $g \cdot mol^{-1}$ (FabF C164Q:T271A). For *E. coli* ACPS an extinction coefficient of 17990 $M^{-1} \cdot cm^{-1}$ and a molecular weight of 14052$g \cdot mol^{-1}$ without His-tag and 17459 $g \cdot mol^{-1}$ with His tag was calculated.

Solid Phase Peptide Synthesis (SPPS)

SPPS was carried out with a Biotage-peptide synthesizer using an orthogonal Fmoc/Boc-protecting group strategy (Table 2.4). The peptide was synthesized on a 150 μmol scale using a rink amid resin (loading density = 0.47 mmol/g). The synthesized peptide was a 14-mer with the following sequence: DSLSMLEIAVQTED-NH_2 with a molecular weight of 1549.7 $g \cdot mol^{-1}$.

TABLE 2.4: **Synthesis cycle of SPPS**

	step	minutes	repetition
1	swelling of the resin in DMF	5	1
2	Fmoc-deprotection	2	1
3	Washing with DMF	5	3
4	Coupling of respective amino acid	20	1
5	Washing with DMF	5	3
6	repetition of steps 2-5	-	13
7	Washing with DMF, DCM	5	1

1% formic acid was added to the Fmoc-deprotection agent (20% piperidin in DMF) in order to avoid aspartimid formation (Michels and Rudolf, 2012). Oxyma (ethylcyano hydroxyimino acetate) and DIC (N,N′-diisopropylcarbodiimid) were used as coupling agents. The peptide was cleaved of the resin using 94% TFA (trifluoroacetic acid) and a scavanger of 1% TIS (triisopropylsilane), 2.5% EDT (ethanedithiol) and 2.5% H_2O. The cleaved peptide was precipitated in ice-cold diethylether and washed three times.

Modification of Peptide

The peptidyl carrier peptide (PCP) was modified according to Borgaro et al., 2011 and the ACP Synthase protocol (New England BioLabs Inc.). In one batch, 1.55 mg peptide (0.1 μmol) were modified. A solution of 1 mM PCP was mixed with 800 μl of malonyl-CoA (2.5 mM), 150 μl of ACP-synthase (6 μM) and 50 μl of reaction-buffer (appendix A.1). All reaction participants were previously dissolved in or diluted with reaction buffer. Each reaction was carried out for 2.5 hours at 37°C and 220 rpm. The reaction mixture was lyophylised and purified using preparative HPLC.

Purification and Analysis of Peptide

PCP was dissolved in 0.5 % NH_4OH solution with a final concentration of 20 mg/ml and purified using reversed-phase HPLC with a linear gradient of 25-40% ACN (+0.1% TFA) in 20 minutes. In each HPLC run 0.5 ml of peptide-solution were purified using a Xbridge^{TM}Prep C18, 5 μm, OBDTM column. The eluting peptide was detected at a wavelength of 220 nm.
Purity of PCP was analyzed with analytical HPLC using a Xbridge^{TM}C18, 5 μm, OBDTM column. A gradient of 25-40% ACN in 20 minutes was used. Absorption was measured at wavelength of 220 nm.
Analyses with ESI-MS was performed with peptide samples dissolved in DMSO at a concentration of 30-100 μM. The samples were measured in negative mode with a fragmentor of 225 and a range of 600 to 1600 g/mol as well as with a fragmentor of 50 and a range of 800 to 2000 g/mol.

Biotinylation of FabF

FabF and its variants were biotinylated using the EZ-Link NHS-PEG_4-Biotin kit of Thermo Scientific. The linker binds to primary amines of lysine or the *N*-terminus of the protein by forming an amide bond and releasing the N-hydroxysuccinimide group. The linker has a net mass addition of 473.22 g/mol and a length of 29 Å (Figure 2.1).

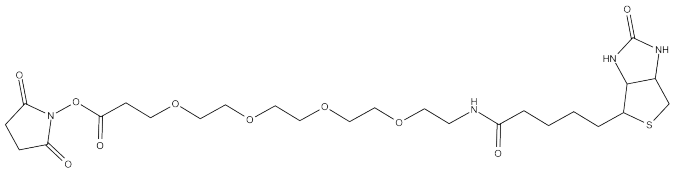

FIGURE 2.1: **EZ-NHS-PEG_4-Biotin-linker.**

A 2 mg aliquot of NHS-PEG4-biotin was dissolved in 170 μl of DMSO to give a 20 mM solution. Subsequently, the solution was diluted with MilliQ water to reach a concentration of 2 mM. A protein solution with a concentration of 0.5 mg·ml^{-1} and a volume of 400 μl was prepared and a 1.5 molar equivalent of NHS-PEG4-biotin solution was added as calculated (Equation 2). After 30 minutes incubation free biotin was removed using Zebra size exclusion columns (2000 rpm, 10 minutes).

$$\mathrm{n_{biotin}(mmol)} = \frac{V_{\mathrm{protein}}(ml) \cdot c_{\mathrm{protein}}(mg \cdot ml^{-1})}{MW(mg \cdot mmol^{-1})}\ 1.5\ \mathrm{mmol} \qquad (2)$$

2.4 Analytical Methods

2.4.1 ^{1}H NMR spectroscopy

^{1}H NMR spectroscopy spectra were recorded on a Bruker BioSpin 850 MHz Ascend or a Bruker BioSpin NEO 600 MHz spectrometer. Chemical shifts (δ ppm) were reported relative to TMS as an internal standard. Coupling constants (J) were reported in hertz (Hz).

2.4.2 Gel electrophoresis

Purity of protein samples was checked after each purification step via SDS PAGE using Mini-PROTEAN® TGX Precast Gels (BioRad) with 10% acryl amide or with a gradient of 4-20% acryl amide. Electrophoresis was run for 30 minutes at 200 V. The size of protein bands were assigned using the BLUEeye Prestained Protein Ladder (Sigma Aldrich). Gels were stained using EZBlue^{TM}gel staining reagent (Sigma Aldrich) and destained with water.

2.4.3 Enzymatic assay for FabF

The assay is based on the FabG coupled enzymatic assay described earlier (Machutta et al., 2010; Schaeffer et al., 2001). As substrates served lauroyl-CoA and malonyl-PCP or malonyl-CoA. In contrast to the known assays for FabF, 7-diethylamino-3-(4'-maleimidylphenyl)-4-methylcoumarin (CPM) was used to detect the curve of the reaction as it was described for other CoA releasing enzymatic reactions like FabD and FabH (Marcella and Barb, 2016) and NMT (Goncalves et al., 2012). CPM is a profluorescent dye that contains a maleinimid group, which reacts with free thiol groups.
Concentrations were chosen according to the concentrations used before in the FabD and FabG coupled enzymatic assays (Table 2.7). The assay was performed with a BioTek-Synergi-H1-Hybrid-Reader in Greiner 96 flat bottom well plates with an excitation wavelength of 380 nm and an emission wavelength of 470 nm at a constant temperature of 30°C. The fluorescence was measured every 30 seconds over a period of 30 minutes.
The K_M values for lauroyl-CoA and malonyl-CoA were calculated by plotting the initial slope against the concentration. The curve was fitted using the Michaelis-Menten equation (Equation 3) with the reaction velocity (v), substrate concentration ([S]). The K_M value of lauroyl-CoA was measured at a constant concentration of 20 μM of mal-PCP, the K_M value for malonyl-CoA with a constant concentration of 75 μM of lauroyl-CoA.

$$v = \frac{v_{max} \cdot [S]}{K_M + [S]} F \tag{3}$$

TABLE 2.7: **Concentration of FabF assay components.** Concentrations of stock solutions, final concentrations in the assay and volume of all assay components.

component	c (stock)	c (assay)	volume (assay)
lauroyl-CoA	375 μM	75 μM	20 μl
malonyl-PCP	40 μM	8 μM	20 μl
CPM	100 μM (10% DMSO)	20 μM (1% DMSO)	20 μl
inhibitor	varying (10% DMSO)	varying (1% DMSO)	10 μl
FabF w.t.	1.665 μM	500 nM	30 μl
total	-	(2% DMSO)	100 μl

2.4.4 MALDI mass spectrometry

30 μl of FabF wild type (15 mg/ml) dissolved in buffer C were incubated with 3 μl of the ligand (10 mM in DMSO) for 30 minutes at room temperature. Not reacted ligand was removed by centrifugation with VIVACON Spin tubes (2 kDa cutoff). The protein solution was desalted using Spin-OUT^{TM}GT-1200 columns (GBiosciences).
MALDI mass spectrometry measurements were performed by Rachel Heap (Trost group, Newcastle University).
FabF with a mass of 45831.5 Da was used for calibration. Therefore, the sample was diluted with 25 mM Tris buffer to 5 different concentrations, mixed 1:1 with the matrix 2', 4', -dihydroxy aceto phenone (DHAP; 75% EtOH) and spotted in triplicate on a 1536 anchorchip target. Subsequently, the samples were analysed with a RapifleX mass spectrometer (Bruker Daltonics) in the range of 30-55 kDa. The protein ligand samples were mixed in a ration of 1:1 with the matrix DHAP (75% EtOH, 14 mM ammonium citrate) and spotted in a quadruplet on a 1536 Anchorchip target. Subsequently, the samples were analysed in the same way as the FabF sample.

2.4.5 ESI-MS

Protein digestion with trypsin and chymotrypsin

FabF was incubated with the ligand and desalted in the same way as described for the MALDI measurements. Around 100 μg of FabF was mixed with 2.5 μg of chymotrypsin in a 50 mM Tris buffer, pH 7.9. After 4h resp. 8h half of the reaction mixture was supplemented with trypsin. The reaction was stopped after 4h resp. 8h by adding formic acid to a final concentration of 1%.
Samples were analysed by the Proteomics Unit of University of Bergen (PROBE).

Protein digestion with thermolysin

30 μl of FabF wild type (15 mg/ml) were incubated with 3 μl of potential covalent ligands (10 mM in DMSO) and incubated 30 minutes at 30°C while shaking. Afterwards the remaining cysteine thiol groups were reduced by adding DTT (5 mM) and shaking 1 h at 56°C. The reduced thiol groups were alkylated by adding IAA (iodoacetamide) (15 mM) and shaked 30 minutes at room temperature. The excess of IAA was quenched with DTT (10 mM). Subsequently, 100 μl of the protein ligand mixture was digested with thermolysin in a ratio of 1:50 or 1:100.
Samples were analysed by the mass spectrometry core facility of University of Mainz (Tenzer group).

2.4.6 Isotermal titration calorimetrie

ITC experiments were performed using a Microcal VP-ITC instrument at 20°C. The protein sample was dialyzed over night with buffer containing 0.5% DMSO. The final concentration of FabF C164Q in the measuring cell was 6 μM. The concentration of the ligand platensimycin was 50 μM. In a first experiment the signal of 24 injections of 10 μl ligand solution was measured. The following experiments were measured with 5 injections of 10 μl, followed by 10 injections of 5 μl, 10 injections of 10 μl ligand solution and 3 injections of 20 μl ligand solution. The final concentration of platensimycin in the protein solution was 7.32 μM in the first experiment and 7.93 μM in the follow up experiments.
Results were analyzed using Origin® 7 (OriginLab, Northampton, MA). Curves were fitted with the one set of sites model. The model included the parameters stoichiometry (N), enthalpy (ΔH) and binding affinity (K_A). These parameters allowed to determine the dissociation constant (K_D), the entropy (ΔS) and the free energy (ΔG) (Equation 4, 5, 6; Du et al., 2016), with R as universal gas constant (1.987 J·mol^{-1}·K^{-1}) and T as temperature (K).

$$\Delta G = \Delta H - T\Delta S \tag{4}$$

$$\Delta G = RT \cdot \ln K_D \tag{5}$$

$$K_D = \frac{1}{K_A} \tag{6}$$

2.4.7 Bio-layer-interferometry

Bio-Layer-Interferometry measurements including the fragment screening were performed using an Octet RED96 instrument (FortéBIO) in 96 well micro-plates (Greiner bio-one, black, PP, flat-bottom). All measurements were run at a constant temperature of 30°C. Super Streptavidin (SSA) biosensors were used to immobilize the biotinylated ligand (FabF w. t. resp. FabF C164Q). These sensors have a very high density of biotin binding sites that is necessary for measuring the weak protein-fragment interaction. The sensors were hydrated for at least 10 minutes in the loading buffer (1 x PBS pH 7.2, 0.01% TritonX, 5 mM DTT) prior to use. Biotinylated FabF as well

as biocytin (10 μg/ml) were diluted in loading buffer and each was loaded to a row of eight biosensors (Figure 2.2).
Loading of biosensors with protein resp. biocytin was performed in four steps. An initial baseline step in loading buffer for 300 seconds (s) followed by immobilization of the ligand for 900 s until a response of around 5-6 nm was reached. Thereafter a baseline step of 60 s in loading buffer was used to wash the sensors to prepare them for the last step. In this step, not occupied streptavidin positions were quenched with biocytin for 300 s.
Binding of compounds to FabF w. t. resp. FabF C164Q was measured in general within four steps: Baseline, association, dissociation, baseline. Depending on the experiment the association and dissociation steps were of different length. The baseline step was in general performed for 60 s. The association step ranged from 30 to 180 s, the dissociation step from 120 to 600 s. The obtained curves were analyzed using the FortéBio software. Association and dissociation curves were fitted (Equation 7, 8) with Y (level of binding), A (asymptote), k_{obs} (observed rate constant), k_{off} (dissociation rate constant) and t (time). The overall rate constant of the combined association and dissociation is described as k_{obs}. The dissociation constant (K_D) was calculated using the determined association (k_{on}) and dissociation rate constants (Equation 9, 10).

$$Y = Y_0 + A \cdot (1 - e^{-k_{obs} \cdot t}) \tag{7}$$

$$Y = Y_0 + A \cdot e^{-k_{off} \cdot t} \tag{8}$$

$$k_{on} = \frac{k_{obs} - k_{off}}{c_{analyte}} \tag{9}$$

$$K_D = \frac{k_{off}}{k_{on}} \tag{10}$$

Validation of virtual screening hits

The ligands were dissolved at a concentration of 400 μM in BLI assay buffer and added to a 96 well plate. The plate was screened for compounds binding to FabF C164Q immobilised on SSA-biosensors. The association time was set to 60 seconds followed by 180 seconds of dissociation. In order to exclude effects of the neighbouring wells the plate was screened forwards and backwards.

2.4.8 Fragment screening

A fragment library of 651 compounds was screened for hits specific for FabF w. t. and FabF C164Q. The library fulfilled the "rules of three" criteria for fragment-like compounds and was dissolved with a concentration of 200 mM in d_6-DMSO and stored on 96 deep well plates. The compounds were diluted to 20 mM in DMSO (daughter plates) and further to 10 mM in DMSO (screening stock plates) using a Bravo Automated Liquid Handling Platform (Agilent Technologies). The compounds were screened using library analysis plates that were prepared directly before measuring by diluting the screening stock plates using a mosquito HV liquid handling robot (TTP Labtech). The compounds were finally diluted to 500 μM in 1x PBS pH 7.2, 0.01% TritonX, 5 mM DTT, 5 % DMSO.
Concentration series of the initial screening hits were prepared to validate specific binding to FabF (Figure 2.2). Concentration dependency of the response and shape of the curves served as indicator for specific binding.

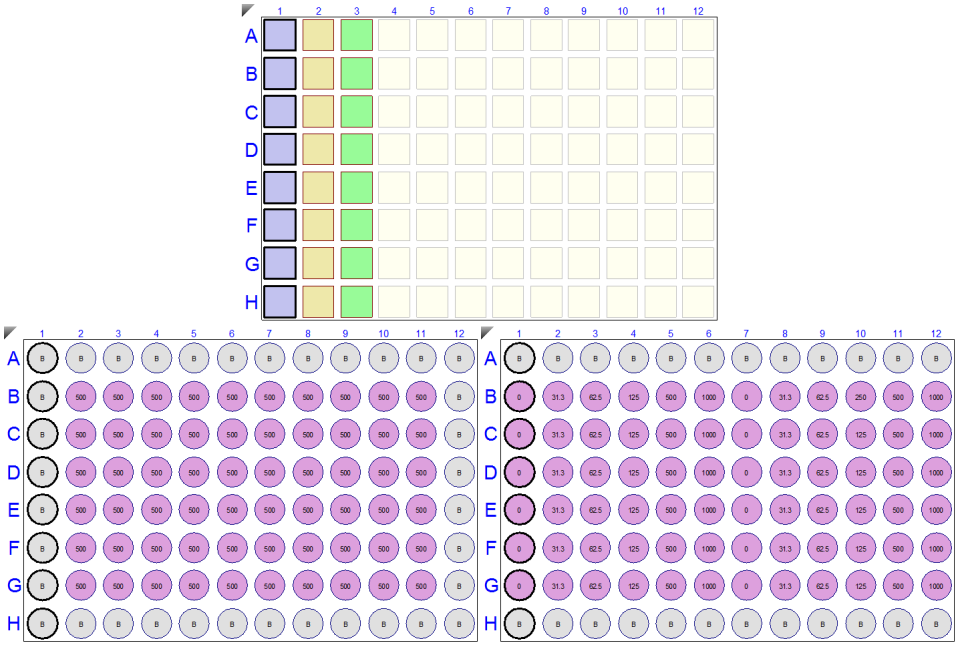

FIGURE 2.2: **Design of plates for fragment screening.** Plate of biosensors immobilized with FabF C164Q in column (col) 1, FabF w. t. in col 2 and biocytin in col 3 (top). Plate design for initial fragment screening (left) and hit picking (right). The baseline was measured in col 1 (left) or 1 and 7 (right), association in col 2-11 (left) or 2-6 and 8-12 (right) and dissociation in col 12 (left) or 1 and 7 (right) (grey: wells filled with buffer; purple: wells filled with fragments).

2.5 Computational Methods

2.5.1 Receptor preparation

The Protein Data Bank (PDB; Berman et al., 2000) contains around 136.272 biological macromolecular structures (22.12.2017). The bulk of it, especially with molecular weights higher than 20 kDa, has been solved by X-ray crystallography (89%). The final 3D-structure is therefore an interpretation of the electron density map that is in turn calculated by a Fourier transformation out of the diffraction pattern. Caused by flexible regions like the *N*- or *C*-terminus, different rotamers of amino acid chains or loops, this electron density map is often not distinct. Also hydrogen atoms cannot be resolved due to a lack of electron density and bond orders are not defined. In order to use PDB structures for virtual screening these issues have to be corrected first (Sastry Madhavi et al., 2013; Labute, 2009).
In this work the "Structure Preparation" tool of the Molecular Operating Environment (MOE, Chemical Computing Group, Montreal, QC, Canada) was used. The included "Protonate3D" method is useful for the prediction of correct protonation states as it considers the flipping of rotamers and tautomers as well as different ionization states (Labute, 2009). Partial charges were set using the AMBER force field parameters (Weiner et al., 1984). The same force field was used afterwards to minimize the position of added hydrogen atoms. In addition, water molecules, that are not conserved, ions, and chains not necessary for docking were deleted.

FlexX

The crystal structure of FabF C164Q (PDB code 4JB6) was prepared as described above but using formal charges. The coordinates of the ligand platensimycin (PDB code 2GFX) were transferred to the FabF structure, by aligning both structures using MOE, and loaded in the program LeadIT. The receptor was specified within a 10 Å radius around the ligand platensimycin (Figure 2.3).

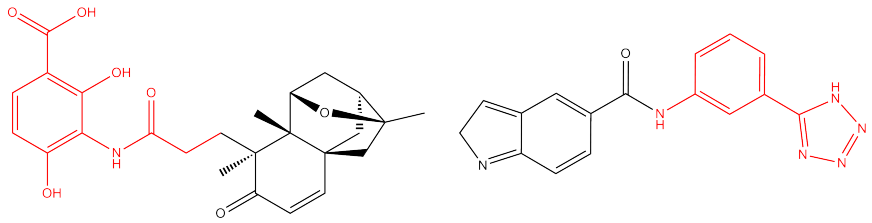

FIGURE 2.3: **Reference ligands.** Platensimycin (left) and 0J6 (right), the atoms used as reference ligands for receptor preparation are colored in red.

DOCK3.6

The crystal structures of FabF C164Q (PDB code 4JB6) and KPC-2 (PDB code 3RXW) were prepared as described above. Finally also non polar hydrogens were removed. The coordinates of the ligands platensimycin (PDB code 2GFX) for FabF and 0J6 (PDB code 4DE1) for KPC-2 were transferred into the particular protein structures by aligning the structures using MOE. The aromatic polar head of platensimycin including the amide linker and

the phenyl tetrazole part of 0J6 (Figure 2.3) were used to define spheres as matching points for docking. Grid-based excluded volumes, van der Waals potentials and electrostatic potentials as well as a solvent occlusion maps were calculated as described earlier (Brenk et al., 2005).
Each receptor was tested with a training set of compounds. For FabF, the ligand platensimycin (PDB code 2GFX) was used. The receptors of KPC-2 was tested with a training set consisting of the ligands GF4 (PDB code 3G2Y), F13 (3G35), 0JB (4DE0) and DN3 (4DE2).
The initial receptor of FabF was modified after testing the prediction of the binding mode of platensimycin. The partial charges of His304 and His341 that form obligatory hydrogen bonds with platensimycin were adapted to generate a stronger hydrogen bond interaction. The partial charge of NE2 was reduced by 0.3, whereas the partial charge of HNE was increased by 0.3, keeping the net charge constant.

2.5.2 Database for virtual screening

An in-house MySQL database of around 5 million commercially available compounds (origin, see chapter 2.1) was prepared. Starting with a SMILES code of the compounds (Weininger, 1988), physicochemical parameters were calculated and unwanted reactive or toxic groups were determined using in-house python scripts based on OpenEye's OEChem toolkit (Openeye, Santa Fe, US).
The database was filtered for molecules fulfilling lead-like criteria with limited complexity (Brenk et al., 2008) listed in table 2.10. Compounds containing unwanted reactive or toxic groups were excluded.

TABLE 2.10: **Summary of selection criteria.**

	FabF (DOCK)	FabF (FlexX)	KPC-2 (DOCK)
heavy atoms	10-30	10-27	10-25
h-bond acceptors	1-7	1-6	1-6
h-bond donors	1-3	1-3	1-3
clogP	$\geq 3, < 3$	$\geq 3, < 3$	$\geq 3, < 3$
rotatable bonds	< 8	< 8	< 7
ring systems	1-3	1-4	1-3
number of nitril groups	< 2	< 2	< 2

In order to screen for covalent ligands of FabF the following reactive groups were taken into account: epoxides, michael acceptors, alkyl halides, acid halides, cumarine, chinone and aldehydes.
For the optimization of compound 78 the database was screened for sulfonyl halides with 6-20 heavy atoms and 1 or 2 ring systems.

Input for DOCK3.6

In-house python scripts based on OpenEye's OEChem toolkit (Openeye, Santa Fe, US) were used to generate protonation states assuming a pH of 7.0 +/- 2 as well as tautomers and steroisomers of the selected compounds. Low energy conformers were generated using OpenEye's OMEGA tool (Openeye, Santa Fe, US). The dataset of conformers was filtered with a pharmacophore query using MOE (Chemical Computing Group, Montreal, QC, Canada)(Figure 3.15).

Partial charges were assigned to the resulting molecules using AMSOL (Li et al., 1999). Again low energy conformers were generated using OMEGA and stored in a hierarchical database for docking (Lorber and Shoichet, 2005).

Input for FlexX

The molecules were obtained as a list of SMILES codes from the MySQL in-house database. A list of SMIRKS codes (Daylight Chemical Information Systems, Inc.), a reaction transform language, described the reaction of electrophilic warheads with the side chain of cysteine. The electrophilic warheads were expressed as SMARTS, a code that characterize a molecular pattern. A script based on OEChem used the SMIRKS codes to identify the chosen electrophilic warheads and generated the reacted molecules, assigned formal charges and calculated stereoisomers. Finally 3D structures of the molecules were generated using OMEGA.

2.5.3 Molecular docking

DOCK3.6

Screening the database for potential non-covalent binding partners of FabF and KPC-2 was performed using DOCK3.6. The parameters were set as follows: ligand and receptor bins were set to 0.4 Å, overlap bins to 0.2 Å and distance tolerance for matching ligand atoms to receptor matching sites was set to 1.5 Å. Compounds that passed a filter for steric fit were scored for electrostatic and van der Waals interactions and their score was corrected based on their estimated partial desolvation energy. For each compound the best scored representative was stored in the docking hit list.

FlexX

The receptor setup was tested by prediction of the binding mode of cerulenin.
A virtual screening for potential covalent ligands of FabF was performed using FlexX2.0.2 with the following settings: The correction of valences and bonds, preprocessing and localizing molecules, assigning of default protonation, assigning of formal charges and assigning of atom-types was set to off. Aromaticity check and assigning of delocalized systems was set to on. The base fragment was manually placed by positioning the atoms of ligand and receptor onto each other.

Optimization of compound 78

Our in-house database of commercially available compounds was screened for building blocks carrying a sulfonyl halide function with 1 or 2 ring systems and 6-20 heavy atoms. The reaction between the fragment of compound 78 and the building blocks was performed with an in-house python script based on OEChem using a SMIRKS code (Figure 2.4). Protonation states assuming a pH of 7.0 +/- 2 as well as tautomers and stereoisomers of the reaction products were calculated and low energy conformers were generated using OMEGA.
The resulting database of sulfonamide derivates of compound 78 was docked using DOCK3.6 with the same settings as for the virtual screening.

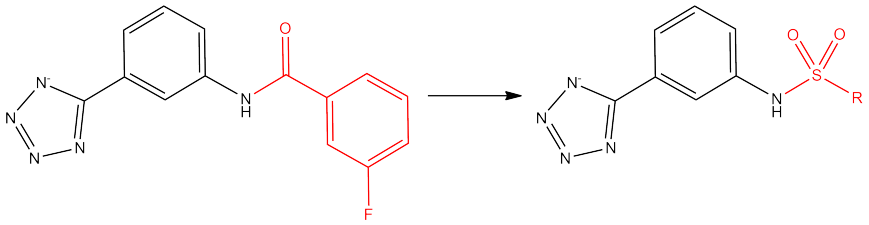

FIGURE 2.4: **Optimization of compound 78.** Virtual screening hit compound 78 (left), amine 1 (black) and the optimized part of the molecule (red).

Evaluation of docking hit list

The docking hit list was analysed using MOE (Chemical Computing Group, Montreal, QC, Canada). The number of heavy atoms ($N_{\text{heavy atoms}}$) was determined and the ligand efficiency (LE, Equation 17) calculated (Hopkins et al., 2004). The list was filtered with a pharmacophore using rigid docking poses. Finally the ligands were ranked according to their ligand efficiency and the best 1000 poses were inspected by eye.

$$\text{LE} = \frac{score}{N_{\text{heavy atoms}}} \tag{17}$$

The docking hit list obtained after screening for derivatives of compound 78 was divided into diverse subsets of compounds. Therefore, BCUT descriptors were calculated (Pearlman and Smith, 1998) using MOE. A principal component analysis was used to generate clusters. The top 5 poses of each cluster, in terms of ligand efficiency, were inspected by eye.

2.6 Structural Methods

Protein crystallisation

The bulk of available protein structures in the PDB is based on X-ray diffraction (Berman et al., 2000). Therefore, the protein need to form highly ordered crystals. Two steps are necessary, formation of a crystal nucleus followed by crystal growth. Altering the protein environment brings it into the supersaturated phase and nuclei are formed. As a consequence, the protein concentration is lowered and the crystals grow in the metastable phase (Figure 2.5, left).
Supersaturation of proteins can be achieved by altering physical parameters like pH or temperature, chemical parameters like addition of salt, ions or polymers or by evaporation (García-Ruiz, 2003; McPherson, 2004). Usually, a precise matching of these parameters lead to the desired crystal formation. Several methods have been investigated whereas the most commons are vapour diffusion with sitting or hanging drops (Figure 2.5, right). The drops are mixtures of protein solution and reservoir solution, facing a much larger reservoir volume. Due to mixing the reservoir with the protein solution in the drop the concentration of additives in the reservoir is higher. Over time water evaporates from the drop into the reservoir and the concentration of additives and protein slightly increases. Therefore, the additives and the protein compete for water molecules of their hydration shells. As a consequence, protein-protein interactions are formed leading to crystal formation (McPherson, 1990).

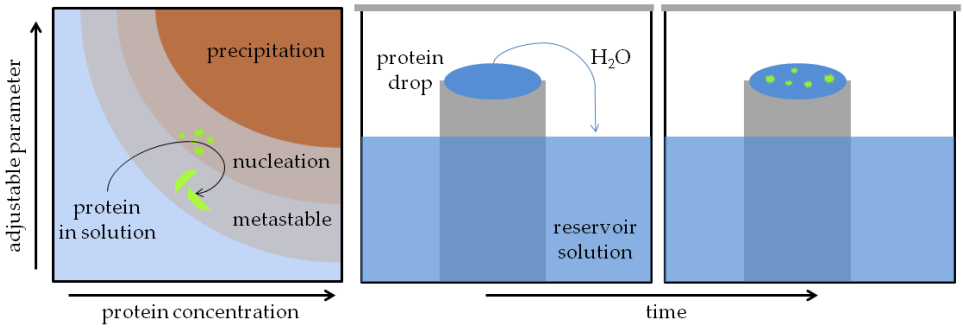

FIGURE 2.5: **Schematic illustration of protein crystallisation.** Phase diagram of protein crystallisation (left). Due to diffusion of water, protein concentration increases and reaches supersaturation. Upon nucleation, the protein concentration decreases and crystals grow in the metastable phase. Sitting drop vapour diffusion method (right). Protein solution and reservoir are mixed in the protein drop. Incubation leads to diffusion of water and the protein reaches supersaturation. Figure adapted from Chayen, 2004.

In this thesis the sitting drop vapour diffusion method was used. Crystallisation was performed either in 24-well plates (Greiner bio-one) with a reservoir volume of 750 μl and a drop volume of 4 μl or in 96-well MRC 2-drop plates (Molecular Dimensions) with a reservoir volume of 60 μl and a drop volume of 2 μl. Protein and reservoir were mixed in a ratio of 1:1.

Crystallisation conditions obtained in a previous work (Lecker and Hunter, 2012) are listed in table 2.12. The protein concentration ranged from 15 - 25 mg/ml respectively 7.5 - 12.5 mg/ml in the crystallisation drop. Plates were stored at 20°C and regularly inspected under the microscope. For all crystallisation experiments FabF without His-tag was used.

TABLE 2.12: **Crystallisation conditions for FabF with cleaved His-tag.** Reservoir II was used for obtaining FabF C164Q (PDB code 4JB6), reservoir V was used for obtaining the structures of FabF w. t. (PDB code 4B7V) and FabF C164Q in complex with a ligand (PDB code 4PF).

reservoir	components	concentration	protein
I	Tris/HCl, pH 7.4	0.1 M	FabF w. t.
	PEG8000	22%	
	β-ME	0.01 M	
II	NH_4HCO_2	0.2 M	FabF C164Q
	PEG3350	26%	
III	NaCl	0.2 M	FabF w. t.
	PEG3350	20%	
IV	$NaNO_3$	0.2 M	FabF w. t.
	PEG3350	20%	
V	Tris/HCl, pH 7.0	0.1 M	-
	$MgCl_2$	0.2 M	
	PEG8000	10%	
VI	NaHEPES, pH 7.5	0.1 M	FabF w. t.
	PEG3000	25%	

Crystallisation to obtain protein-ligand complexes

In structure-aided drug design (SADD) determination of ligand-protein binding modes is essential. Formation of co-crystal complexes is the basis. Albeit crystallisation conditions for a protein can be well established, generation of a co-crystal structure with a small molecule is still challenging. Routes to co-crystal complexes are either co-crystallisation or soaking (Danley, 2006).
In a co-crystallisation experiment ligand and protein are incubated prior to crystallisation whereas in soaking experiments the preformed apo crystal of a protein is incubated with a ligand.
There are several pitfalls for both methods. Due to a low affinity of small molecules to their target relatively high concentrations in the milimolar range are needed, which leads to solubility problems. Most of the small molecules need DMSO to increase solubility but the concentration of DMSO can have a bad influence on crystal formation and growth. Conditions

resulting in crystallisation are sometimes outside the usual physiological range. For instance, the pH can have a major effect on the binding affinity, if certain protonation state is obligatory for binding. Also conformational changes induced by the ligand can result in crystal cracking or dissolution if they are not compatible with the crystal lattice packing. It can go to such an extent that the conformation or solubility of a protein-ligand complex can differ from the apo-enzyme in a way that another crystallisation condition has to be used for successful co-crystallisation (Danley, 2006).

A DMSO-free co-crystallisation approach was established by Christopeit et al., 2016 and used for co-crystallisation of the fragment screening hits with FabF C164Q. 1.5 μl of each ligand dissolved in DMSO (200 mM) was added to a reservoir well of a 96-well 2-drop plate. The plate was placed open in a fume hood over 24 h for evaporation of DMSO. Subsequently 60 μl of the reservoir solution (II, Table 2.12) was added and the plate was placed on a shaker over 24 h for dissolvation of the ligand. Finally the reservoir solution was mixed with the protein in a ratio of 1:1 with a drop size of 1 and 2 μl.
A screening for conditions to obtain co-crystals of FabF w. t. and the covalent ligand FC-4 was carried out using the JCSG-plus^{TM}(MD1-37) and PACT premier^{TM}(MD1-29) screens. The protein (15 mg/ml) was mixed in a ratio of 10:1 with the ligand (10 mM in DMSO) and incubated for 30 minutes shaking at room temperature. A 96-well 3-drop plate was filled with 60 μl of the reservoir. Reservoir solution and the protein/ligand-mixture were mixed in a ratio of 1:2, 1:1 and 2:1 with a drop size of 300 nl.

Cryoprotection

Collection of diffraction data is done at low temperatures around 100 K in order to minimize radiation damage due to formation of radicals. Cryogenic cooling of crystals requires protection to avoid crystal damage due to ice formation. This is done by adding cryoprotective agents. Several compounds have been identified as cryoprotective, like organic solvents or sugars. The most common ones are glycerol or ethylene glycol. The latter is often present in the reservoir condition used for crystallisation. Protein crystals may therefore grow directly in the cryoprotecting solution if the poly-ethylene-glycol concentration is high enough. Otherwise the crystal has to be transferred into the cryoprotective solution previously to freezing (Farley and Juers, 2014).
In this work glycerol was added as cryoprotectant to the reservoir conditions. A concentration of 15% was necessary for condition I and 17.5% for condition III. Condition II was enriched with 20% of glycerol. The crystals were picked in cryo loops, quick dipped into the cryoprotective solution and frozen in liquid nitrogen.

Twinning

Twinning is the association of different domains in one crystal, in which the orientation of the domains to each other is described by a symmetry operation (Nespolo, 2015). The obtained diffraction patterns of a twinned crystal are rotated, reflected or inverted to each other, described by the twin operator. The repetition of unit cells in the crystal is not continuous leading to

a heterogeneous crystal. Thus, the space group cannot properly be determined. Twinning is distinguished into holohedral structures, if the symmetry is equal to its Bravais lattice or merohedral structures, if the symmetry is lower.

Diffraction data processing, model building and refinement

Diffraction pattern images obtained from the X-ray diffraction experiments were indexed, scaled and integrated using XDS and XSCALE (Evans, 2006; Kabsch, 2010). As the crystals were twinned ,the obtained cell constants were used as input to reindex, rescale and reintegrate the X-ray diffraction intensities with spacegroup P1. The quality of the data set was assessed with the population and the quality of fit given after indexing. The population expresses how many of the 3000 strongest reflections can be indexed with a single lattice. The quality of fit has always the best solution for triclinic spacegroups (P1, P-1) as there are no restrictions and the data fit easy to the reduced cell. For the correct solution the quality of fit should be in the range below 10 (Kabsch, 2010). Moreover, the values $I/\sigma(I)$, R_{meas} and $CC_{1/2}$ as function of resolution served as measures for the quality of the dataset after integration (Karplus and Diederichs, 2015). The $I/\sigma(I)$ value expresses the signal-to-noise ratio base on the intensities in a resolution shell (Diederichs, 2010). The R_{meas} is a redundancy independent R-factor, that expresses the precision of individual intensity measurements. The Pearson correlation coefficient of two random half data sets ($CC_{1/2}$) links data accuracy with the agreement of crystallographic model and data quality. The measure is near 1 for highly precise data and near 0 for very imprecise data (Karplus and Diederichs, 2012; Karplus and Diederichs, 2015). Cell content analysis to determine the Matthews coefficient (Equation 18) and solvent content of the asymmetric unit was performed using the CCP4 software package. The Matthews coefficient (V_m) describes a relation between the volume of the asymmetric unit (V_{ASU}) and the molecular weight of the protein (MW), respectively the number of protein molecules per asymmetric unit (n) (Matthews, 1968; Matthews, 1974; Kantardjieff and Rupp, 2003).

$$V_m = \frac{V_{ASU}}{n \cdot MW} \tag{18}$$

A three dimensional model of the protein structure was built by molecular replacement using PhaserMR (McCoy et al., 2007). The structure of the FabF dimer (PDB code 4B7V) served as matrix and the number of molecules per asymetric unit was set based on the cell content analysis suggestion. Space group assignment was performed using the program Zanuda (Lebedev and Isupov, 2014. The diffraction intensities were reindexed, rescaled and reintegrated using the suggested space group and cell constants. Real-space refinement was performed using Coot-0.8.3 (Emsley et al., 2010), phenix.refine (Afonine et al., 2012) and the PDB-REDO server (Joosten et al., 2014). Criteria for successful refinement were the R-values, R_{work} and R_{free} (Equation 19). These values resemble a correlation between measured and calculated structure factor amplitudes ($|F_{obs}|$ and $|F_{calc}|$). A low value indicates a good match between the calculated and the observed diffraction pattern (Brünger, 1992). However, during the refinement the data can

be overfited. Therefore, a test set of 10% of the reflections was removed from the data before refinement started. The R_{free} value is calculated analogue to R_{work} using this test set. Thus, R_{free} is a measure how well the diffraction pattern calculated from the refined model is in agreement with the diffraction data omitted from refinement.

$$R_{work} = \frac{\sum_{hkl} ||F_{obs}(hkl)| - |F_{calc}(hkl)||}{\sum_{hkl} |F_{obs}(hkl)|} \tag{19}$$

The *electronic Ligand Builder and Optimization Workbench* (eLBOW; Moriarty et al., 2009) was used to generate coordinates for the ligands. Ligand placement was performed using Coot-0.8.3 by screening the $2F_o$-F_c and the F_o-F_c electron density difference maps.

Chapter 3

Results and Discussion

3.1 FabF

3.1.1 Binding site analysis

Platensimycin, the most potent inhibitor of FabF, is a malonyl-competitive ligand. Binding to the wild type enzyme is blocked by Phe400, that adopts another rotamer upon binding of the fatty acid. The variant C164Q mimics this intermediate state with an open malonyl binding site (Figure 1.4, right). A major part of platensimycin, a bulk ring system is not binding in the binding site but on top (Chapter 1.3.3). In order to explore the importance of the hydrogen-bond interaction of Thr271 to this ring system the amino acid T271 was replaced by alanin for further measurement of enzymatic activity. Measuring the dissociation constant of platensimycin for the variant T271A is only possible with an open binding site. Thus, the amino acid exchange T271A was also introduced to the variant C164Q. This was successfully done by site-directed mutagenesis. The variants were expressed and purified for crystallisation experiments and to determine thermodynamic and kinetic parameters.

Recombinant protein FabF T271A

The point mutation to coding for A271 was inserted using Qick Change site-directed mutagenesis. Sequencing the plasmid confirmed the success of mutagenesis. The plasmid was transformed into *E. coli* Rosetta(DE3) pLysS cells. Overexpression and purification of FabF T271A was carried out as described previously for *Pa* FabF wild type (Baum et al., 2015). Finally, 190 mg of pure FabF T271A were obtained out of 3 liter of autoinduction medium. Expression of the variant FabF C164Q:T271A in *E. coli* Rosetta(DE3) pLysS cells resulted in insoluble protein. Thus, the plasmid was transformed into *E. coli* Arctic Express cells in order to slow down protein folding using an expression temperature of 10°C. Finally, a low amount of FabF C164Q:T271A was obtained. Correct folding of the protein was confirmed using circulardichroism spectroscopy (data not shown). Nevertheless, cleavage of the His-tag using TEV protease led to precipitation of the protein.

FabF-platensimycin interaction

The binding affinity of platensimycin to FabF C164Q was measured using isothermal titration calorimetry (ITC) as well as biolayer interferometry (BLI). Based on ITC experiments a dissociation constant (K_D) of 8.9 ± 5.7 nM

was determined. BLI experiments gave a K_D of 25 $\pm$ 6 nM. These values were in agreement with previously published data (Wang et al., 2006). The molar ratio of all ITC experiments was around 0.5. During four independent ITC experiments over a time of three month a slight increase of K_D was observed which might be due to hydrolysis of the amide linker. In ESI mass spectrometry measurements an amide hydrolysis fragment containing the bulky ring system was detected (m/z_{calcd}= 273.2 , m/z_{found}= 273.2).
Thermodynamic characterization of the platensimycin FabF C164Q interaction revealed a free enthalpy (ΔG) of -45.5 kJ/mol. The enthalpic contribution (ΔH) was determined to-20.0 kJ/mol and the entropic contribution (-TΔS) to -25.5 kJ/mol (Figure 3.1). ITC measurements with FabF C164Q:T271A could not be carried out as no soluble protein was obtained.

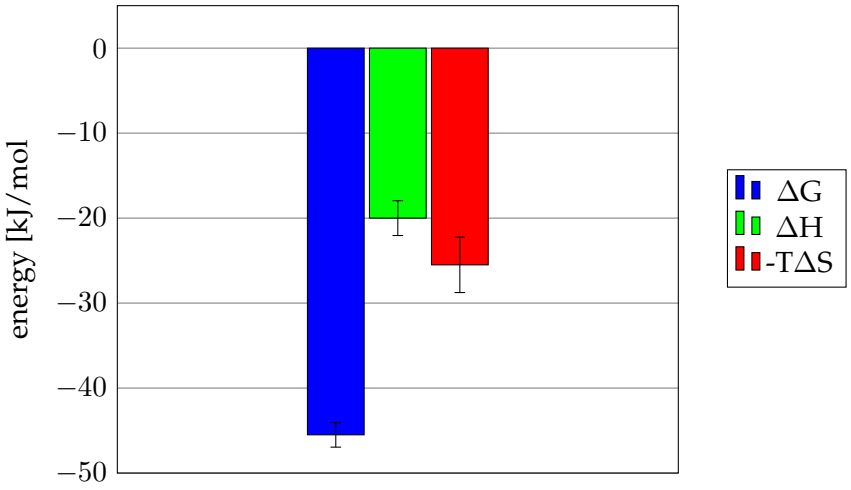

FIGURE 3.1: **Thermodynamic profile of the platensimycin-FabF interaction.** A free enthalpy of -45.5 $\pm$ 1.46 kJ/mol was calculated, consisting of an enthalpic contribution of -20.0 kJ/mol $\pm$ 2.05 kJ/mol and an entropic contribution of -25.5 $\pm$ 3.26 kJ/mol.

Crystallisation and structure solution of FabF T271A

FabF T271A with cleaved His-tag was successfully crystallised using reservoir condition IV (0.2 M $NaNO_3$, 20% PEG3350) as done before with FabF wild type. Crystals in form of thin plates growing out of one origin were obtained. A crystal was picked, quick dipped into the cryo condition (reservoir condition IV containing 20% glycerole) and measured at the ID30A-1 beamline at ESRF synchrotron. The obtained diffraction data were indexed, integrated and scaled using XDS. The program suggested the orthorhombic space group P222. However, due to twinning the correct monoclinic space group was determined using Zanuda. Therefore, space group P1 was set manually. A cell content analysis suggested 8 FabF T271A molecules in the asymmetric unit with a Matthew coefficient of 2.13 $Å^3 \cdot Da^{-1}$ and a solvent content of 42.4%. 4 copies of the *Pa* FabF wild type dimer (PDB code 4B7V) were used as matrix for molecular replacement. A symmetry analysis using Zanuda revealed space group $P12_11$ with 2 copies of the dimer in the asymmetric unit as the best solution (Figure 3.2; top). The twinning

fraction was calculated using Xtriage and one pseudo-merohedral twin operator was found (h,-k,-l). The twin law was included in the last refinement step. Finally, the structure was solved with a resolution of 1.55 Å (Table 3.1).

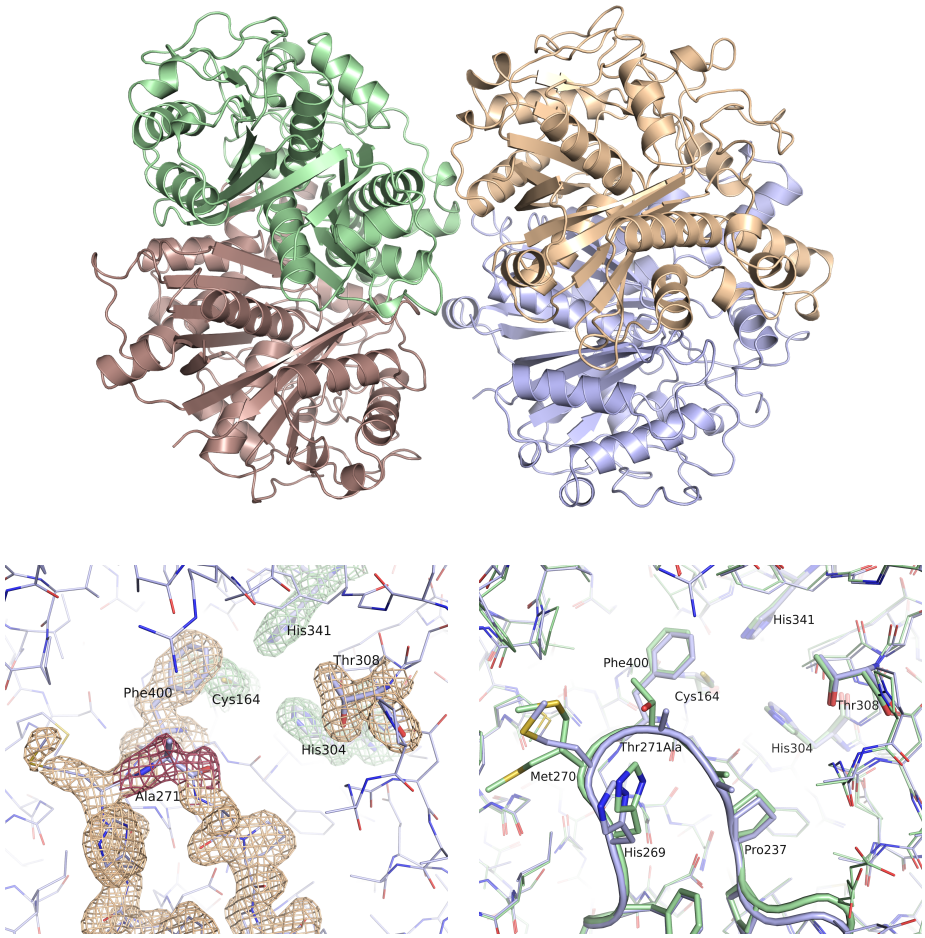

FIGURE 3.2: **Structure of FabF T271A.** Top: Asymmetric unit consisting of two biological assemblies, with chain A (beige), chain B (blue), chain C (red) and chain D (green). Left: Active site of FabF T271A with the $2F_o$-F_c electron density map at σ level 1. The catalytic triad is highlighted in green, the exchanged amino acid at position 271 in red and other amino acids in beige. Right: Alignment of FabF wild type (PDB code 4B7V, green) with FabF T271A (blue).

After alignment with the wild type structure (PDB code 4B7V) an rmsd value of 0.2 Å for the Cα atoms was calculated using MOE. Considering only the binding site residues the rmsd was determined to be 0.31 Å. Thus, no significant conformational changes in the structure were observed (Figure 3.2, bottom). The side chains of the catalytic triad were in the exact same position as in the wild type structure. Also Phe400 adopts the closed conformation. In the loop that includes A271 occurred slight changes in the conformation of the side chains of His269 and Met270. The latter adopts two different rotamers in the wild type but only one in the structure of FabF T271A. This conformation of the active site was observed in all four chains of the asymmetric unit.

TABLE 3.1: **Data collection and refinement statistics for *Pa* FabF T271A.**

Data collection and processing	
Spacegroup	$P12_11$
a, b, c [Å]	65.2, 134.2, 84.73
α, β, γ [°]	90.0, 90.0, 90.0
Diffraction data	
Resolution range [Å]	46.76 - 1.55 (1.605 - 1.55)
Total reflections	685047 (66555)
Unique reflections	203675 (20947)
Multiplicity	3.4 (3.3)
R_{merge}	0.1063 (1.362)
R_{meas}	0.1264 (1.622)
Wilson B-factor [Å^2]	14.91
Completeness [%]	99.31 (97.90)
Mean I/σ(I)	6.71 (0.78)
$CC_{1/2}$	0.992 (0.266)
CC*	0.998 (0.649)
Refinement	
R_{work}	0.1873 (0.1686)
R_{free}	0.2161 (0.2600)
Protein residues	1640
Water molecules	503
RMS	
bonds	0.006
angles	1.15
Ramachandran plot [%]	
favored	97.37
allowed	2.63
outliers	0.00
Rotamer outliers [%]	0.08
Clashscore	2.93
Mean B factors [Å^2]	
Overall	22.51
Protein atoms	22.06
Water molecules	33.28

Discussion

A basic requirement for successful structure-based drug design is a detailed knowledge about the binding site of FabF and the binding modes of the ligands. Three natural product inhibitors for the elongation condensing enzymes FabB, FabF and FabH are described in literature. IC_{50} or K_D values are reported for thiolactomycin and cerulenin for all three enzymes. For platensimycin only values for FabF are known so far. The K_D value determined for *E. coli* FabF was 19 nM (Wang et al., 2006). Using ITC and BLI K_D values in the same order of magnitude could be determined. Nevertheless, hydrolysis of the amide bond in platensimycin was observed during the ITC measurements and verified by ESI-MS (m/z_{calcd}= 273.2 , m/z_{found}= 273.2). This finding underlined the need of new stable ligands.
The bulky ring system of platensimycin forms two hydrogen bond interactions with side chains distant from the catalytic triad (Figure 1.5). On the one hand to the backbone nitrogen of Ala310, on the other hand to the side chain hydroxy group of Thr271. An exchange of the bulky ring system with other groups led to a strong decrease of affinity to FabF (Chapter 1.3.3).
These findings led to the question about the contribution of this interaction to the binding affinity of platensimycin to its target protein FabF. The variants FabF T271A and FabF C164Q:T271A prepared in this work should be used to determine IC_{50} and K_D values in order to answer this question.
Expression and purification of the FabF T271A variant was successfully done with the conditions and buffers described in literature for FabF wild type. Expression of the FabF C164Q:T271A variant led to insoluble protein. This might be due to the formation of inclusion bodies or degradation of the protein. Precipitation was also observed for the variant FabF C164Q. As the variant FabF T271A is soluble, the precipitation of FabF C164Q:T271A is likely caused by the change C164Q. Hence, the buffer was adopted to keep the protein in solution. The HEPES buffer used for the wild type was changed to a phosphate buffer. Also 10% of glycerol and 0.5 mM of DTT were added. The pH was 7.8 for purification and 7.4 for the storage. Nevertheless, upon cleavage of the His-tag the variant FabF C164Q:T271A precipitated again. Thus, for future experiments a screening might help to find an appropriate buffer. Due to the very little yield obtained in one batch of expression and the susceptibility to precipitation upon buffer exchange, that is necessary for ITC measurements, the K_D of platensimycin could not be determined. Also the variant FabF T271A could not be used for determining an IC_{50} value as the development of an enzymatic assay is not yet finished (Chapter 3.1.2). Finally, the influence of the hydrogen-bond interaction between the bulk ring system of platensimycin and the hydroxy group of side chain T271 could not be determined. However, once a robust assay system is established, FabF T271A can be used to follow up this question.

3.1.2 Development of an enzymatic assay

Enzymatic assays of FabF used so far in literature were coupled with several enzymes and radio labeled malonyl-CoA was used for detection of the reaction progress. Additional work for protein purification is necessary. Also the coupled enzymes might interact with the ligands and falsify the results. Finally, radio labeled detection produces toxic waste.
Thus, an improved enzymatic assay was developed (Figure 3.3). This assay used a peptide substrate that mimics the recognition site of ACP (Table 1.1). After the transfer of lauroyl from CoA to Cys164 the acyl-en-zyme intermediate reacts with the peptide substrate leading to the release of an elongated chain. Upon the transfer of lauroyl, CoA is released with a free thiol group. This group is detected by the profluorescent dye CPM, that carries a reactive maleimide group.

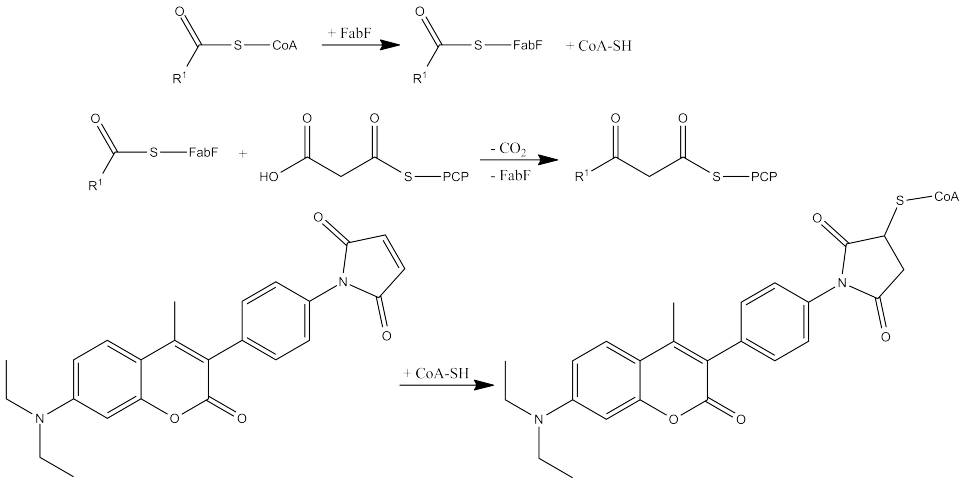

FIGURE 3.3: **Scheme of the enzymatic assay.** In a first step FabF reacts with lauroyl-CoA, forming the acyl-enzyme intermediate and releasing CoA with a free thiol group. Subsequently malonyl-PCP reacts with a Claisen condensation under release of CO_2 and an elongated fatty acid chain. The first reaction is monitored by an increase of fluorescence due to the reaction of the profluorescent dye CPM with CoA-SH.

Synthesis of PCP

The peptide MalPPant-14mer (further called malonyl-PCP) was identified to resemble the recognition site of ACP. Thus, a batch of 0.15 mmol PCP (232.46 mg) was synthesized using solid phase peptide synthesis. After cleavage of the resin and washing with diethyl ether 148.2 mg of PCP (yield: 63.8%) were obtained. The raw PCP was analyzed by ESI-MS and analytical HPLC. The mass spectra showed the double charged molecule peak $[M-2H]^{-2}$ (m/z_{calcd}= 773.9, m/z_{found}= 773.9). The analytical HPLC chromatogram showed the major peak at 34% ACN with a retention time of 12 minutes. Purification of the raw PCP was performed in batches of 0.5 ml with a concentration of 20 mg/ml. The peptide eluted as expected with a retention

time of 12.7 minutes at a concentration of 34.5% ACN (Figure 3.4, left). Albeit 10 mg of PCP were purified in one batch, the absorption at 220 nm was relatively low with a maximum of 22 mAU.

Expression and purification of AcpS

Overexpresssion of *S. pneumoniae* AcpS was proved by SDS-gel electrophoresis. Elution of the His-trap column using a linear gradient of imidazole occurred at a concentration of 15% buffer B (Table A.1). Out of 3 liter of autoinduction medium 51 mg of protein were obtained. During concentration of the protein a significant amount precipitated.
Overexpression of *E. coli* AcpS was proved by SDS-gel electrophoresis. After cell lysis no protein could be detected on the lysate indicating the formation of inclusion bodies during expression or the degradation of the protein in the chosen buffer.

Peptide modification

PCP was modified enzymatically with malonyl-phosphopantetheine using *E. coli* AcpS in order to obtain malonyl-PCP. Modification of PCP led to a shift of the retention time from 12 minutes for PCP to 6 minutes for malonyl-PCP (Figure 3.4, right). In the chromatogram a second much smaller peak with a retention time of 7 minutes occurred (30% ACN). This might be due to the light-sensitive thioester. Malonyl is bound with a thioester to phosphopantetheine, which is bound to the peptide. The cleavage of malonyl would lead to a less hydrophilic molecule and shift to a higher retention time. However, in a mass spectrum this theory could not be confirmed. Also the modified peptide could not be detected in ESI-MS measurements. Performing the modification reaction with *S. pneumoniae* AcpS led to a shift of the retention time from 6 to 4.7 minutes (28.5% ACN). Again, the peptide could not be identified with ESI-MS.

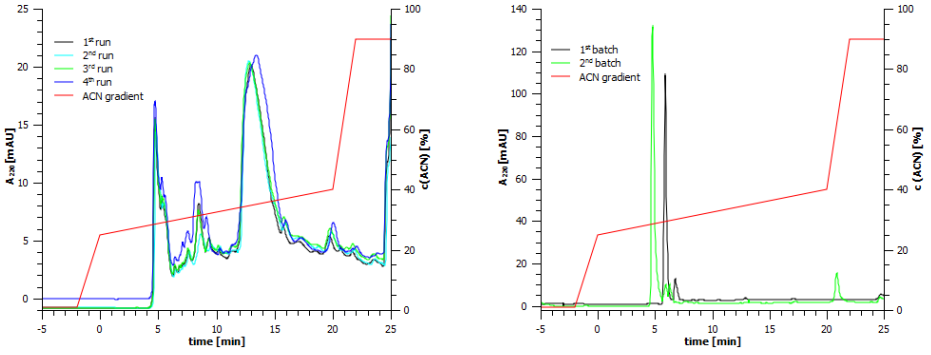

FIGURE 3.4: **Peptide synthesis and modification.** The absorption at 220 nm and the corresponding concentration of ACN are plotted against the time. Left: Purification of raw peptide. The peptide eluted with a concentration of 34% ACN after 25 minutes. Right: Purification of the peptide modified at the serine side chain with malonyl-phosphopantetheine. The peptide eluted with a concentration of 29.5% ACN with a retention time of 6 minutes.

Basic measurements

In order to establish the assay, feasible concentrations of all compounds had to be chosen. For the initial measurements this was done according to similar assays described in the literature (Chapter 1.3.4). Using FabF concentrations ranging from 0 to 2 μM resulted in a stronger increase of the fluorescence signal (higher conversion of substrate) relative to the enzyme concentration (Figure 3.5, top).
The K_M-value of lauroyl-CoA was determined to 35 ± 12 μM. This fits well with the literature values that range from 25 to 53 μM (Machutta et al., 2010; Borgaro et al., 2011). The K_M-value of malonyl-CoA was determined to 255 ± 58.4 μM, which is lower than the literature value in the range from 510 μM (Machutta et al., 2010) to 600 μM (Borgaro et al., 2011), but still in the same order of magnitude.
All basic measurements were performed with peptide from the first batch, modified using *E. coli* AcpS ordered from New England Biolab. The second batch of peptide purified with *S. pneumoniae* AcpS resulted in curves independent of FabF concentration, assuming that the modification reaction did not work properly.

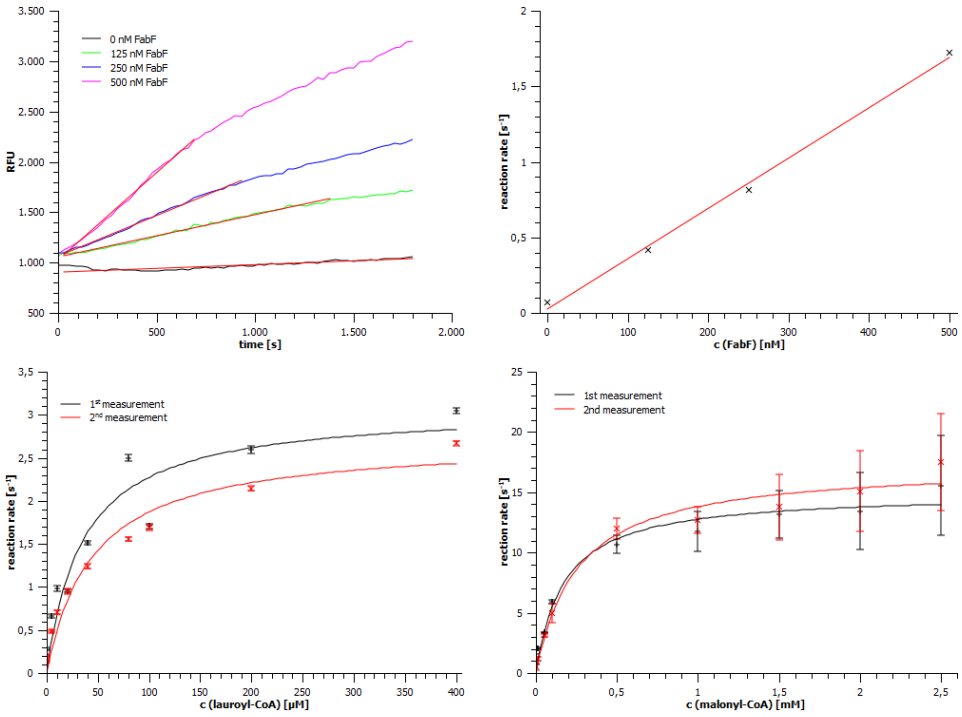

FIGURE 3.5: **Basic measurements of enzymatic assay.** Fluorescence signal at different enzyme concentrations was measured (top, left). The initial reaction rate was plotted against the enzyme concentration (R^2= 0.996; top right). Determination of K_M for lauroyl-CoA (bottom left) and malonyl-CoA (bottom right).

Discussion

Compounds discovered in screening approaches need to be tested for their inhibitory activity. Thus, enzymatic assays for the target proteins to measure the enzymatic activity are necessary. The assays used so far for FabF were coupled assays with several enzymes. Beside the additional work for protein purification, the compounds might interact with these enzymes and falsify the results. Also radio labeled malonyl-CoA was used to detect the reaction product which is not in agreement with nowadays requirements of avoidance of problematic waste.
A peptide substrate that mimics the recognition site of ACP was synthesised and modified with malonyl-phosphopantetheine. Thus, two enzymes necessary so far were replaced. Solid phase peptide synthesis is an established method and was used to successfully synthesize the 14-mer. Modification of the peptide was performed enzymatically using *E. coli* AcpS (New England Biolab). In order to lower the costs and due to discontinuing of AcpS by New England Biolab, the enzyme should be expressed and purified as well. Purification failed, as only insoluble protein was obtained. This might be due to degradation or the formation of inclusion bodies. The chosen expression system in *E. coli* cells using the vector pET-15b is well established. *E. coli* is the most convenient host and the pET-family of expression vectors is widely used (Doyle, 2005). Thus, insolubility might be due to unfavourable expression conditions.
Basic measurements with different concentrations of FabF revealed the suitability of the assay. An increase of the FabF concentration gave an increase in the reaction rate in a linear manner. Without FabF the fluorescence did not increase. Also the K_M values of lauroyl-CoA and malonyl-CoA fitted well with the literature values. Thus, the assay might be useful as well for measuring IC_{50} and K_I values of hit compounds.

Conclusion and future perspectives

In a proof of concept study, the feasibility of a simplified assay system was shown (Figure 3.3). The number of proteins involved could be minimized and the enzymatic reaction could be measured with a profluorescent dye. Nevertheless, transferring malonyl from CoA to the peptide substrate remains challenging. The enzyme AcpS, catalysing the reaction could not be expressed soluble and hence not be purified. First, a screening for feasible expression conditions for *E. coli* AcpS should be performed. Once the enzyme is ready to use, modification of the peptide should be verified using mass spectrometry. The K_M of malonyl-PCP should be determined and compared with the literature value of Borgaro et al., 2011. Preliminary K_M values of lauroyl-CoA and malonyl-CoA were in agreement with the literature values. In addition, the IC_{50} value of platensimycin should be determined in order to prove the applicability for use in drug discovery.

3.1.3 Fragment screening

A fragment screening was carried out using the Bio Layer Interferometry (BLI) technology. For this purpose it is necessary to immobilize the analyte (protein) on biosensors. In the case of protein-fragment interactions the expected binding affinity is in the high micromolar or low milimolar range (Keseru et al., 2016). Therefore, a high immobilization density is crucial for detecting a binding event. Thus, super streptavidin biosensors, with a high density of biotin binding sites were chosen. Straight after the biotinylation reaction the analyte was immobilized on the biosensor surface. Immobilisation of FabF w. t. and FabF C164Q over 900 seconds gave a response of around 6 nm for the wild type and around 5 nm for the mutant FabF. Not occupied streptavidin positions on the biosensor were quenched with biocytin. Quenching for 360 seconds did not change the response, suggesting that almost all binding sites were occupied by the analyte (Figure 3.6; A, B).

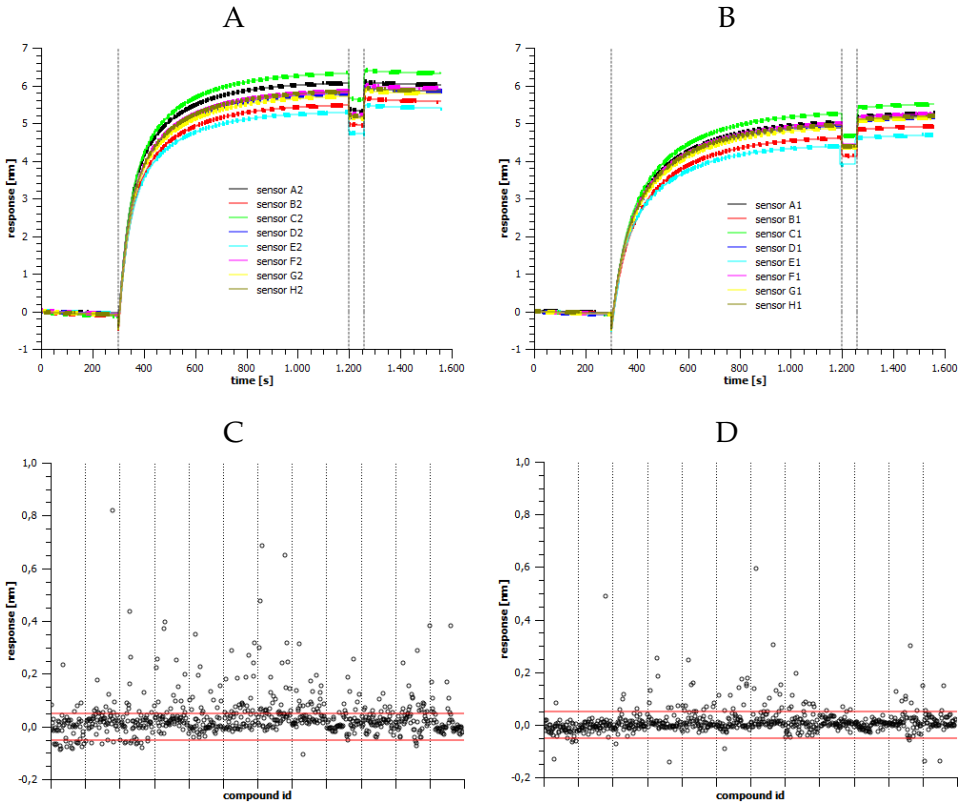

FIGURE 3.6: **Immobilisation, quenching and results of primary fragment screening.** FabF w. t. (A) and FabF C164Q (B) were immobilized on each of 8 SSA-Biosensors over a time of 900 seconds followed by a 30 seconds baseline step. Subsequently not occupied binding sites were quenched with biocytin. Responses of the variant C164Q substracted with responses of biocytinylated sensors (C) and response of the variant C164Q substracted with the responses of the wild type sensors (D). A threshold of 0.055 nm was set, in order to determine hits (red lines).

Screening of fragment database

The fragment database was screened to obtain hits specific for FabF w. t. and specific for FabF C164Q. Specificity was calculated by substracting the response of the wild type from the response obtained from the variant C164Q. Positive values indicated binding to the variant, negative values binding to the wild type enzyme. A value close to zero indicated unspecific or no binding of the fragments. A reference sensor was loaded with biocytin (N^{ϵ}-biotinyl-L-Lysin), resembling a natural protein surface. Substracting the responses of biocytinylated sensors from the responses of sensors loaded with protein eliminated as well unspecific protein-fragment interactions.
The responses of FabF C164Q immobilized biosensors substracted with the response of biocytin sensors had a median of 0.026 nm, substracted with the wild type sensor responses a median of 0.012 nm. The response of the majority of the compounds was lower than the response measured for platensimycin (0.055 nm), demonstrating that hits differentiate from non-binding compounds. Substracted responses were plotted and a threshold of 0.05 nm was set based on inspection by eye. Only wild type substracted responses (Figure 3.6, D) were used for hit picking. By substraction of the wild type signal from the variant signal a much smaller deviation was obtained. Finally, 67 out of 651 compounds (10.3%) were selected as FabF C164Q specific hits (Table C.1). 11 fragments (1.7%) were specific for the wild type enzyme (Table C.1 and C.3).

TABLE 3.2: **Structures of validated fragment screening hits, specific for FabF C164Q.**

3-F3	4-B5	4-G6	5-B2
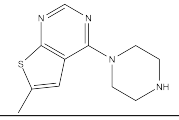	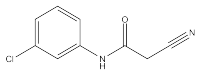	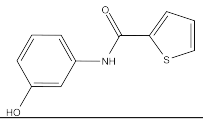	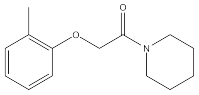
5-C7	5-D5	5-D10	6-C5
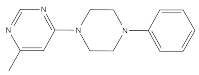	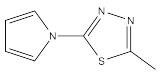	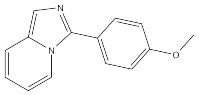	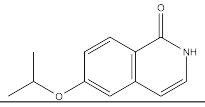
6-G6	7-G5	8-B8	8-C2
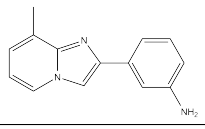	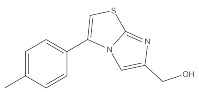	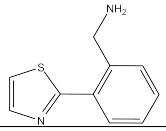	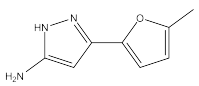
8-C11	8-E3	8-F3	8-G3
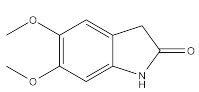	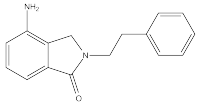	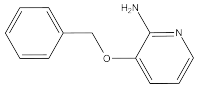	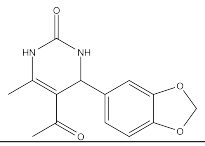

Hit validation

Binding events between the 67 hits and FabF C164Q were validated by measuring concentration series with 6 different concentrations ranging from 0 μM to 1000 μM. The curves were inspected by eye. Fragments that resulted in curves at zero level for all concentrations and curves that had an atypical shape were excluded (Figure 3.7, A, B, E). For the remaining curves the dependency between concentration and response was inspected and those with concentration independent responses were excluded (Figure 3.7, C). In addition, fragments with non-stoichiometric binding behavior (Figure 3.7, D) and those with incomplete dissociation within the time of the experiment (Figure 3.7, F) were excluded.

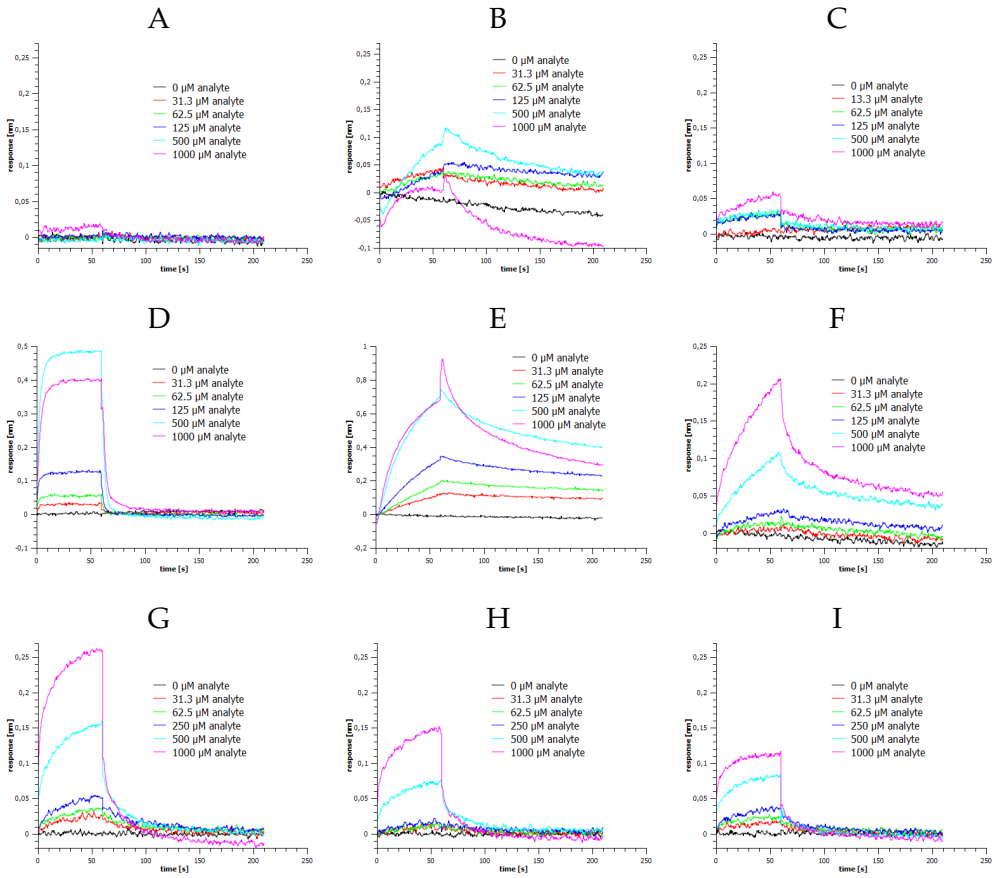

FIGURE 3.7: **Evaluation of fragment screening hits.** Compounds were excluded from the hit list if all concentrations had zero responses (A), if the curves had an atypical shape (B, E), if the responses were not dependent on the concentration (C), if the responses indicated non-stoichiometric binding (D) or if dissociation was incomplete (F). Compound HP6-H-E3 was evaluated as a hit. The wild type substracted response of FabF C164Q (G), the biocytin substracted response of FabF C164Q (H) and the biocytin substracted response of FabF w. t. (I) for the same compound (8-E3) indicated a specific binding event.

FabF C164Q specific fragments were expected to bind to FabF C164Q but not to FabF w. t. or the biocytin blocked sensors. Thus, for these fragments a high response when substracting the FabF C164Q response from the biocytin response and also when substracting the FabF C164Q response from the wild type FabF response was expected. Further, the response of the wild type FabF substracted with the biocytin response had to be lower or close to zero compared to the variant FabF C164Q (Figure 3.7, G-I). Finally, 16 compounds (2.5%) were validated as binding specific to FabF C164Q (Table 3.2 and C.2).

Discussion

Fragment-based drug discovery has become a successful tool for identification of new drug leads. However, using BLI as technology to determine binding events is quite new (Keseru et al., 2016). To our knowledge, only two screens of a fragment database using BLI were published so far (Wartchow et al., 2011; Robinson, 2016). These publications served as guidelines to develop the binding assay and to identify hits.

Development of binding assay

BLI requires immobilization of the protein. After biotinylation of FabF on the biosensors a high loading density, necessary for fragment - protein interactions, could be reached. Precipitation of the protein could not be observed. We used platensimycin as a reference ligand to validate the method. The inhibitor (K_D= 19 nM; Wang et al., 2006) is a large molecule with a bulky branched ring system binding outside the binding site (Figure 1.5). As described in chapter 1.5.2 the increase of BLI response is due to the reflection properties of the molecule, the density of the formed layer and an increase of the biolayer upon ligand binding. Also k_{on} is impacting the height of the response. Thus, different than for SPR measurement the response does not correlate with the size or the affinity of the ligand. A bulky ligand like platensimycin might have a lower response level at saturation as fragments and vice versa. In any case, the response of platensimycin and fragments that bind to the analyte (FabF) should differ from fragments that do not bind to the analyte. The saturation response (R_{max}) measured with platensimycin was 0.055 nm. A value that stands out from the medians obtained for screening compounds 1-18 (median: 0.0135) and compounds 36-67 (median: 0.0125). Binding of platensimycin is characterized by a moderate on-rate and a slow off-rate resulting in a K_D of 25 $\pm$ 6 nM (Chapter 3.1.1). The measured value agrees well with the literature value of 19 nM (Wang et al., 2006). Thus, identification of binding events using BLI was validated.
For screening the fragment library each plate was measured with FabF w. t., FabF C164Q and biocytin immobilized on biosensors. Three plates per day were measured in a time period of 9 hours. During this time denaturation of the proteins could not be observed. Only one plate was measured with an unreasonably high hit rate. When measured again, with a new diluted plate and a new set of immobilized proteins the hit rate was lowered and in the same range as determined for the other plates. Finally, BLI could be used as a hightroughput method for measuring the fragment library. Preliminary hits in the screening of Wartchow et al., 2011 and the positive control (K_D= 450 μM) had responses around 0.08 nm. Robinson, 2016 obtained hits with responses ranging from 0.04 to 0.1 nm. These values are in agreement with the ones obtained in the FabF screening.

Finding hits in the bulk of data

In the FabF fragment screening unspecific binding should be detected by using the wild type protein and the C164Q variant (Chapter 1.3.2). Assuming that unspecific binding occurs on the protein surface in the same way on both proteins only fragments binding specificly in the active site remain. An alternative way is to use the response of FabF C164Q substracted with the response of biocytin. In fact, the hit rate of FabF C164Q specific hits could be lowered from 25.1% (170 hits), if substracted with the biocytin responses to 10.3% (67 hits), if substracted with the wild type responses. In addition, the median response and the standard deviation (std) were lowered from 0.0258 nm (std: 0.066 nm) to 0.0118 nm (std: 0.045 nm). Still, these values were quite high compared to the results of Wartchow et al., 2011 and Robinson, 2016. The latter calculated a median response of 0.0026 nm. This might be explained by the concentration of the fragments. It was shown that the concentration has an influence on the obtained responses (Robinson, 2016). These were 200 μM (Wartchow et al., 2011), 400 μM in the FabF screening and 500 μM (Robinson, 2016). Wartchow et al., 2011 calculated the average plus three standard deviations as threshold for hit determination. The same calculation for FabF gave a threshold of 0.0114 nm if substracted with the wild type (average: 0.0009 nm, std: 0.0035 nm) or 0.0192 nm if substracted with biocytin (average: 0.0031 nm, std: 0.0054 nm). Both thresholds would yield in a tremendous hit rate with more than the half of the library. Due to these inconsistencies in determining a threshold in a statistical manner the primary hit determination limit was set to 0.05 nm after inspection by eye. Due to the higher median also the threshold was higher compared to previous screenings (0.03 nm and 0.0225 nm)
These previous fragment screenings revealed a target dependency of the hit rate (Wartchow et al., 2011). For the different targets hit rates of 3.5%, 6.6%, 21% and 24% were obtained. The FabF screening hit rate of 10.3% for FabF C164Q specific and 1.7% for FabF wild type specific fragments fitted well to this range.

Validation of screening hits

The major challenge is to differentiate hits from fragments that bind unspecific. Albeit the difference in binding to the wild type and the variant FabF C164Q helped to exclude unspecific binding fragments, still a broad spectrum of different binding curves was observed. Wartchow et al., 2011 used the results of SPR measurements as evidence to identify hits. Together with the interpretation of SPR sensorgrams (Rich and Myszka, 2008; Elinder et al., 2011) and the previous BLI fragment screen of Robinson, 2016 the following exclusion criteria were used for hit validation:

- nonstoichiometric and superstoichiometric binding behavior
- unreasonably slow on- and off-rates
- atypical binding curves

In addition, concentration dependent binding was required for validated hits.

Nonstoichiometric binding behavior is indicated by a significantly higher response than R_{max} determined with a control compound (Giannetti et al., 2008). If the response is more than five times higher than R_{max} the compound is a superstoichiometric binder. The reference compound platensimycin used in the FabF fragment screening had a maximum response of 0.055 nm. Thus, fragments with responses higher than 0.275 nm (5 x R_{max}) are supposed to bind in a superstoichiometric manner. In the primary hit list four compounds exceeded this threshold (2-F9, 7-B9, 7-F11, 7-H10). In the follow-up experiment with a concentration series these four compounds showed a concentration independent behavior and were excluded. Compound 4-C7 revealed a significant higher response (0.4835 nm) as in the primary screening (0.2523 nm) and was for that reason excluded as well. Nevertheless, 15 of 16 validated hit compounds had a response higher than the reference. A median response of 0.0791 nm (std: 0.0417 nm) for the validated hits was calculated compared to a median response of 0.0845 nm (std: 0.0956 nm) for the primary hits. A maximum response of 0.1785 nm (compound 6-G6) is still 3.2 times the reference R_{max}, which might indicate a nonstoichiometric behavior (Giannetti et al., 2008, Wartchow et al., 2011). However, the response is not only dependent on the number of molecules that bind to the protein. Compared to the results of previous screening the highest responses of hits were in the range of 1.2 nm (Robinson, 2016; Wartchow et al., 2011). Thus, due to the lack of experience with BLI a nonstoichiometric binding behavior of some fragments cannot be excluded.

Unreasonably slow on- and off-rates suggest non-specific binding of the fragments (Wartchow et al., 2011; Elinder et al., 2011; Robinson, 2016). The definition of slow off-rates is different in literature. Wartchow et al., 2011 defined slow off-rate as an incomplete dissociation of the fragments within the dissociation time given in the experiment (90 s). Elinder et al., 2011 defined two report points, the first one 5 seconds after dissociation started (SE), the second (SL) 5 seconds before the end of the dissociation time in the experiment (60 s). A dissociation ratio (DR) was calculated by the quotient of SL and SE. Fragments with values above 0.8 were kept as hits. Fragments that dissociated very fast, i. e. already leveled out after 5 seconds, were excluded due to unspecific binding. Robinson, 2016 defined two types of fragments. On the one hand 'excellent' fragments with fast on-rates and moderate off-rates, on the other hand 'typical' fragments with fast on-rates and fast off-rates. Two examples of 'excellent' fragments leveled out after 60 to 70 seconds. The two examples of 'typical' fragments leveled out after 5 to 10 seconds. In addition, curves of 'excellent' and 'typical' fragments should have good or at least reasonable fits ($R^2 > 0.8$, X^2 tending to 0).
In the FabF fragment screening a dissociation time of 150 seconds was chosen. Seven fragments with very fast off-rates were identified (2-H5, 5-D2, 6-G10, 7-A11, 7-H11, 8-A11, 8-G11). Dissociation leveled out already after the first two seconds of dissociation. Three of them had maximum responses of 0.04 nm with the highest concentration. These fragments were excluded due to likely unspecific binding. Three fragments were excluded as false positives (3-C3, 7-D5, 9-C3). For these no association was observed. The responses were ± 0.01 nm for all concentrations and therefore within the noise.

Dissociation and association rates and the resulting dissociation constant were calculated using the Octet software. The association rates were in a range of 10^1 to 10^2 $M^{-1} \cdot s^{-1}$ for all fragments. Dissociation rates ranged from 10^{-1} to 10^{-2} s^{-1}. Whereas the dissociation range was in agreement with the rates Robinson, 2016 observed, the association range disagreed with the reported rates that were in the range of 10^3 to 10^4 $M^{-1} \cdot s^{-1}$. Also, the goodness of fit (R^2 and X^2) was bad for the majority of the recorded data. Thus, identification of hits based on kinetic rate constants was not possible. However, inspection by eye revealed many fragments with association curves not ending up in saturation combined with an incomplete dissociation within 150 seconds. Those fragments were excluded from the hit list, if the goodness of the fit was bad as well (1-D2, 2-A2, 4-B3, 4-C9, 5-B5, 5-B7, 5-C2, 5-D5, 5-F10, 6-A4, 6-B4, 6-D6, 7-A10, 7-B6, 7-E3, 7-G6, 8-B8, 8-C9, 8-C11).

Concentration dependency of the responses should fulfill the requirements for a typical saturation curve (Rich and Myszka, 2008; Wartchow et al., 2011). If saturation is reached for a fragment concentration 10 times the K_D, the response equals the maximum response (R_{max}). For concentrations below, the response at equilibrium is directly proportional to the fragment concentration (Rich and Myszka, 2008). The expected dissociation constant for fragments is roughly around 0 μM and 1 mM. Therefore, the top concentration of 1 mM is unlikely to reach saturation. The top concentrations (0.5 and 1 mM) should result in response that are proportional. Fragments resulting in an inconsistent response pattern were excluded (3-F3, 4-E8, 4-F3, 5-B2, 5-F4, 6-F6, 6-G4, 6-F10, 7-G10, 8-E6, 8-H5, 8-H10). Those fragments had for instance no responses for the three lowest concentrations and a response more than twice as much for the 1 mM concentration relative to the response at 500 μM.

Atypical binding curves were identified for 13 fragments. For seven of these fragments, the association and dissociation curves were not smooth and the responses decreased or even got negative independent of the fragment concentration (3-C8,5-G6, 5-G8, 6-E11, 6-G5, 7-H10, 7-H11). This behavior might indicate aggregation (Rich and Myszka, 2008). The dissociation responses of six other fragments started on a much higher level than the final response of the association (2-F9, 3-C7, 3-C9, 6-B4, 6-H4, 7-F6). This phenomenon was always in combination with an incomplete dissociation in the time of the experiment.

Conclusion and future perspectives

Finally, BLI is a straightforward method for identification of protein - fragment interactions. 16 primary hits were validated as FabF C164Q specific fragments (2-H5, 4-B5, 4-G6, 5-C7, 5-D10, 6-C5, 6-G6, 6-G10, 7-G3, 7-G5, 8-A11, 8-C2, 8-E3, 8-F3, 8-G11, 8-G3). The overall hit rate is in the same range as the hit rates obtained in previous works (Wartchow et al., 2011: 2.5%; Robinson, 2016: 0.23%). However, the selection of validated hits should be considered carefully. A shape of the curve that is typical for specific binding events is described different in literature. Thus, another biophysical method should be used to confirm the binding event. In addition, an enzymatic assay will clarify if the binding affects the fatty acid elongation activity. Structure activity relationship by ordering derivatives of the hits can help to improve binding affinity. Co-crystal structures were not obtained within this work. Addition of fragments influenced the crystal growth and only non-uniform branched crystals were obtained. Still, some could be used for data collection but the structures did not contain a fragment. In the future, co-crystal structures should be solved in order to determine the binding mode. Based on these findings fragments could be merged or grown to give lead structures for further design of new antibiotics.

3.1.4 Virtual screening

New starting points for the design of novel antibiotics targeting FabF should be identified using virtual screening. The basis, for the success of virtual screening approaches is the detailed knowledge about the binding site of the target protein and the binding mode of substrates and inhibitors. Based on the hydrogen bond interaction pattern a pharmacophore model was generated in oder to filter the library.
First, the binding site of FabF was analysed. Alignment of all 10 available crystal structures in the PDB (01.01.2018) revealed a rigid binding site. Only Phe400 (*Pa*FabF numbering) is adopting two different rotamers. In the apo FabF w. t. structure Phe400 blocks the binding site with its closed conformation. Upon binding of a fatty acid or a covalent ligands like cerulenin it turns into the open conformation and the malonyl-competitive binding site is accessible for ligand binding. The open conformation is also present in the variant C164Q that mimics the acyl-enzyme intermediate (Figure 1.4, right). Thus, for virtual screening a structure carrying the mutation C164Q was selected (*Pseudomoas aeruginosa* FabF (PDB code 4JB6), 2.4 Å resolution). The side chain of Glu164 was virtually modeled to cysteine. Thus, a structure with an open malonyl-competitive binding site and a native catalytical triad was obtained.

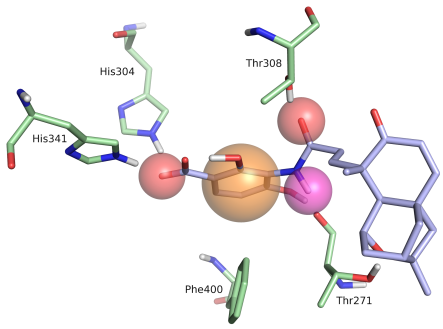

FIGURE 3.8: **Pharmacophore model for FabF.** The pharmacophore model of the malonyl-competitive binding site of FabF based on the binding mode of platensimycin (blue). It contained an essential hydrogen bond acceptor feature for the interaction with His304 and His341 (red). Other features are a hydrogen bond acceptor to interact with Thr308 (red), a hydrogen bond donor to interact with Thr271 (magenta) and an aromatic feature for the interaction with Phe400 (orange).

A pharmacophore hypothesis was generated based on the binding modes of FabF ligands. Platensimycin and its derivatives are contained in 7 of 11 FabF structures in complex with ligands. Three further structures contain cerulenin and one a covalent complex with the natural substrate dodecanoic acid. In addition, the structures of thiolactomycin in complex with FabB were taken into account. FabB and FabF are homologues proteins with a conserved binding site. The ligand thiolactomycin binds to both enzymes with a significant binding strength (Chapter1.3.3). Analysis of these structures suggested that a hydrogen-bond interaction to His304 and His341 is crucial for binding. It is formed by the lauroyl-competitive

inhibitor cerulenin as well as by the malonyl-competitive inhibitors thiolactomycin and platensimycin (Figure 1.6, 1.5). Furthermore, the backbone amide of Thr271 and the side chain of Thr308 formed hydrogen-bond interactions with platensimycin and its derivates. Phe400 formed edge-to-face interactions with the phenyl ring in platensimycin. These interactions were also included in the pharmacophore hypothesis. In addition, no atoms were allowed to be placed inside the protein volume. Only the interactions to His304 and His341 were set to be essential as they were found in all binding modes. In addition, two more pharmacophore hypothesis conditions of the described interactions had to be fulfilled to satisfy the pharmacophore hypothesis (Figure 3.15).

Validation of docking setup for DOCK3.6

A sphere set for the placement of ligand atoms was generated. This sphere set was validated by predicting the binding mode of platensimycin. In a first approach the ligand was placed incorrect (PDB code 2GFX; Figure 3.9, left). Thus, the partial charges of His304 and His341 were adjusted (by 0.3 units for the ϵ nitrogen and hydrogen) in order to favor the hydrogen-bond interaction with the polar aromatic head group of platensimycin. Thereafter, the binding mode was successfully predicted with a total score of -27.95 kJ/mol and a rmsd to the pose in *E. coli* FabF of 6.14 Å (Figure 3.9).

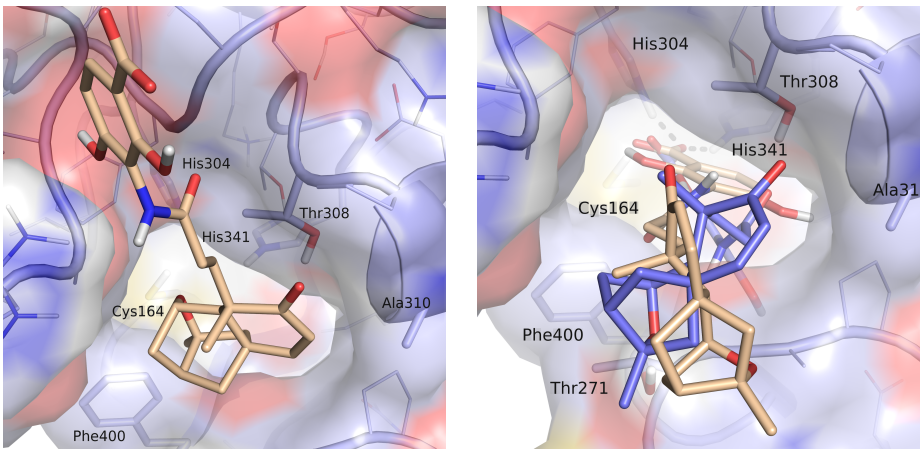

FIGURE 3.9: **Validation of docking setup.** Left: Platensimycin (beige) docked into the receptor of *Pa* FabF with partial charges as set by the amber force field parameters (total score: -22.35 kJ/mol). Right: Platensimycin (beige) docked in the receptor with adjusted partial charges of His304 and His341 (total score: -27.95 kJ/mol).

Virtual screening for non-covalent ligands

A hierarchical approach was adopted for virtual screening. First, our in-house database of around 5 million commercially available compounds was filtered for lead-like molecules (Brenk et al., 2008). Subsequently, the obtained hits were screened with the above described pharmacophore resulting in 66053 compounds. Out of these 48064 compounds could be docked into the *Pa*FabF binding site. Filtering these rigid binding poses again with

a pharmacophore containing just the important hydrogen-bond interaction to His304 and His341 resulted in 13244 compounds. These were ranked in respect to their calculated ligand efficiency (Kuntz et al., 1999; Hopkins et al., 2004) and inspected by eye. Finally, 18 compounds were selected for hit validation (Table B.1).

Validation of non-covalent virtual screening hits

Validation of binding events of the virtual screening hits was carried out using BLI. The response of the wild type enzyme, the response of FabF C164Q and the response of biocytin immobilized on SSA-biosensors were recorded. For analysis, the response of the wild type was substracted from the response of the variant FabF C164Q. Compound 6 reached a maximum response of around 0.8 nm. The dissociation curve levels out at around -0.4. This and the very high amplitude might indicate non-specific binding. Compound 8 had a maximum response of 0.15 nm.

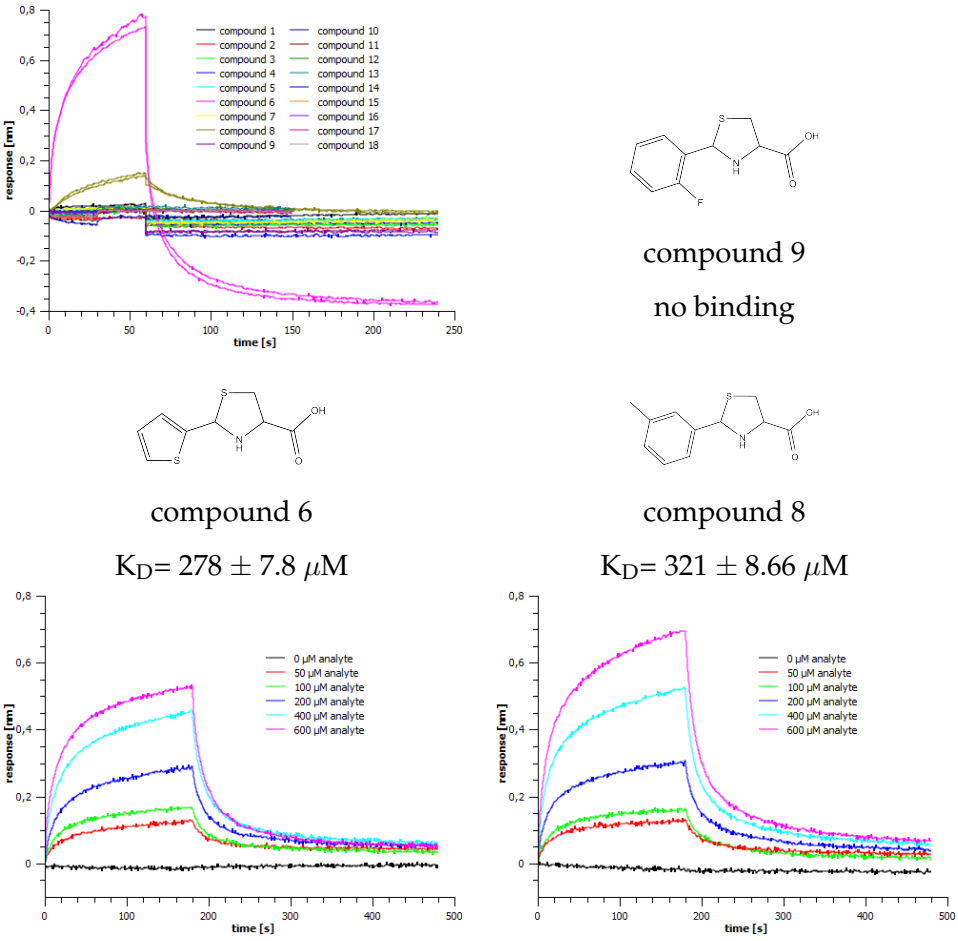

FIGURE 3.10: **Validation of non-covalent virtual screening hits.** The raw signal of biocytin was substracted from the raw signal of FabF C164Q. Association and dissociation of compound 1-18 at a constant concentration of 400 μM (top left). Structures of compound 6, 8 and 9 with their K_D-values and curves of the follow up experiments with a concentration series for compound 6 (bottom left) and compound 8 (bottom right).

All remaining compounds gave responses around ± 0.1 nm (Figure 3.10, top). Follow-up experiments with a concentration series ranging from 0 to 600 μM were performed for compound 6 and 8. Specific binding of the compounds will lead to proportionality between concentration and response at low concentrations in the BLI experiment. For high concentrations saturation will be reached and the level of response will be constant. Compounds 6 and 8 gave these proportional responses. The highest concentrations did not have the same response level, indicating that saturation did not occur. However, based on the steady state a K_D (Equation 10) value was calculated. The K_D of compound 6 was determined to 278± 7.8 μM, of compound 8 to 321± 8.66 μM. K_D determination when plotting the response at equilibrium against the compound concentration resulted in a dissociation constant of 384.6± 70.07 μM for compound 6 and 943.6± 267.2 μM for compound 8.
Both ligands share a 1,3-thiazolidine-4-carboxylic acid substructure with a varying group at position 2. Unfortunately, co-crystallisation as well as soaking approaches were not successful. However, in the predicted binding mode both ligands form hydrogen-bond interactions with their carboxylate groups to the histidines of the catalytic triad (His304, His341). The secondary amine of the thiazolidine is predicted to form a hydrogen bond to Phe398. The major difference in the binding modes is the orientation of the aromatic ring. The five-membered ring in compound 6 points deep into the pocket. Thus, sulfur-hydrogen bond interactions to Thr306 and Thr308 are postulated to be formed by the thiazolidine ring. The 6-membered ring of compound 8 is located between Phe398 and Pro273. Thus, the orientation of the thiazolidine ring is not in an ideal position to form the sulfur-hydrogen bond interactions. This interaction is only predicted to be formed to Thr308 (Figure 3.11).

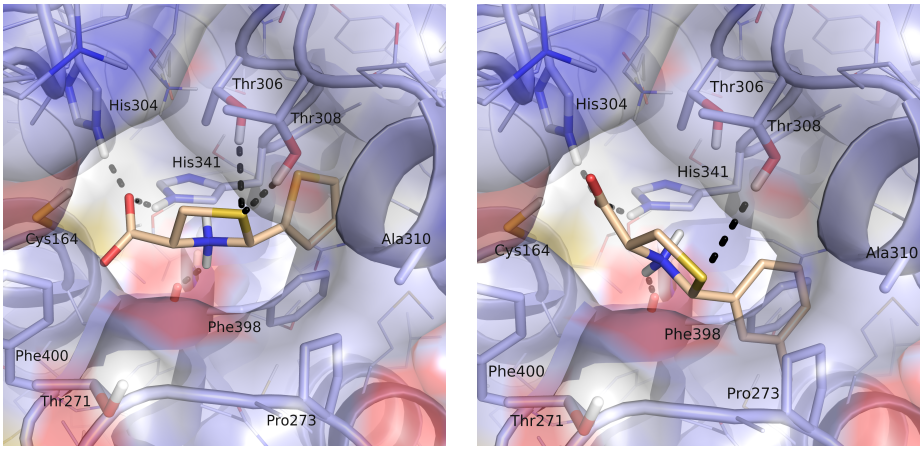

FIGURE 3.11: **Predicted binding modes of virtual screening hits.** Binding mode of compound 6 (left) and compound 8 (right) in the binding site of *Pa* FabF (DOCK3.6).

Compound 9, also containing the thiazolidine-4-carboxylic acid substructure with a six-membered ring at position 2 is not binding to FabF as determined by the BLI measurements. In the predicted binding mode the distance between sulfur atom of the thiazolidine ring and the hydroxyl groups of Thr306 and Thr308 is too long for hydrogen-bond interactions, which might explain the results of the BLI experiments.

Discussion

In the past, a benzoxazolinon scaffold was identified by virtual screening as a class of new FabF inhibitors (Zheng et al., 2014). All other FabF inhibitors were found by screening natural product extracts or by derivatising natural inhibitors. The most active designed inhibitor, a derivative of platensimycin had a K_D of 50 μM (Fisher et al., 2014). Platensimycin by itself is prone to hydrolysis and synthetic availability is limited due to the branched ring system. This reveals the need of new scaffolds for structure-based drug design.
Using virtual screening, two ligands binding to FabF C164Q were identified. Both ligands share a 1,3-thiazolidine-4-carboxylic acid substructure with varying groups at the second position (compound 6 and 8). The thiazolidine heterocycle is a subgroup in several biologically active substances. The most prevalent substructure are thiazolidine-one and thiazolidine-dione, which are associated with antibacterial, antiviral, anticancer and antifungal activity (Andres et al., 2000; Verma and Saraf, 2008; Da Silva et al., 2014). But also the thiazolidine-4-carboxylic acid substructure is described in association with biological activity. The most famous representative is the group of penicillin antibiotics (Kong et al., 2010). Beside antibacterial activity also anticancer and antiviral activity is described (Gududuru et al., 2005; Liu et al., 2011).
The synthesis of thiazolidine-4-carboxylic acid derivatives is well established (Skvortsov et al., 2010; Liu et al., 2011; Credico et al., 2011; Amino et al., 2016). It is a simple condensation reaction of cysteine with an aldehyde leading to a diastereomeric mixture. Susceptibility of the thiazolidine ring to hydrolysis seems to be insignificant in view of the broad application in biologically active compound. Some compounds had been discussed as cysteine releasing molecules, but enzymes were necessary for hydrolysis (Bjelton and Fransson, 1990).
Compound 9 has the same thiazolidine scaffold, but binding to FabF C164Q could not be confirmed. Based on the predicted binding modes, the major difference between compound 6, 8 and 9 is the orientation of the aromatic ring. The 6-membered ring of compound 8 and 9 leads to an not ideal position of the thiazolidine ring for the formation of the postulated sulfur-hydrogen bond interactions with Thr306 and Thr308. Preference of a 5-membered ring is also reflected in the measured K_D values (Figure 3.11), although the goodness of fit was not optimal with X^2 around 3. Nevertheless, structure activity relationship based on three compounds remains tentative. Also, information about stereochemistry are missing as the compounds were purchased as diastereomeric mixture.
In addition, the results of BLI should be considered carefully. The response measured in the primary screen was 0.8 nm for compound 6. In the follow-up experiment the same concentration (400 μM) resulted in a response of 0.4 nm. For compound 8 this phenomena was observed the other way round (primary: 0.15 nm, follow-up: 0.5 nm). As discussed in the foregoing section (Chapter 3.1.3) this might indicate nonstoichiometric binding. Kinetic binding parameters were in the same range as those determined for the fragment screening hits.

Virtual screening for covalent ligands

The natural product inhibitor cerulenin binds covalently to FabF. Thus, also covalently bidning ligands were considered as possible starting points for new lead-structures. Virtual screening was carried out using the covalent docking mode of FlexX with its incremental construction approach. The receptor setup was validated by predicting the binding mode of the covalent inhibitor cerulenin. The binding mode of cerulenin in the lauroyl-CoA binding site could not be predicted as it was found in the structure of *B. subtilis* FabF (PDB code 4LS8; Figure 3.12, left). Thus, a receptor with the structure of *B. subtilits* FabF was prepared in the same way and the ligand was docked into the binding site. Here, the binding mode was successfully predicted (Figure 3.12, right). Slight differences in the structures of *Pa* FabF and *B. subtilits* FabF presumably led to the different binding mode predictions. Nevertheless, in both poses the important hydrogen-bond interaction to His304 and His341 were formed. Only the flexible aliphatic tail was placed in a wrong position. Therefore, the receptor of *Pa* FabF was considered to be suitable for virtual screening.

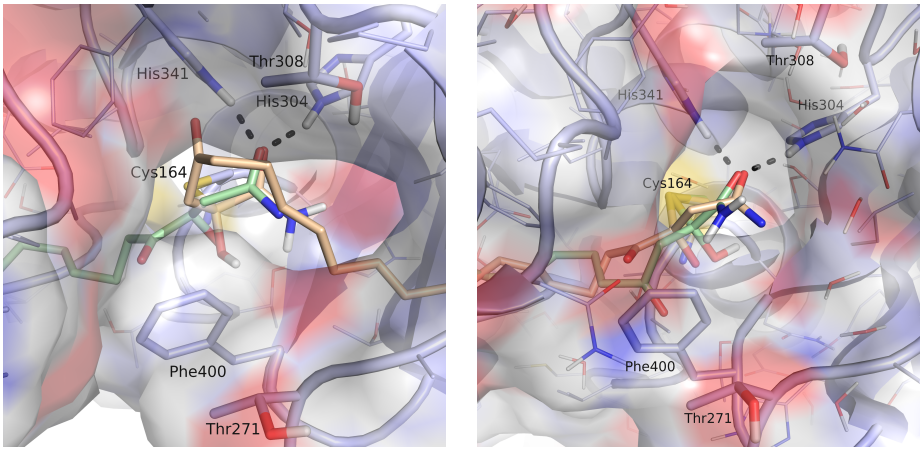

FIGURE 3.12: **Validation of receptor for docking.** Crystallographically determined binding mode of cerulenin in complex with *B. subtilis* FabF (beige) superimposed with cerulenin docked into the receptor of *Pa* FabF (total score: -9.039 kJ/mol, green, left) or cerulenin docked into the receptor of *B. subtilits* FabF (total score: -13.185 kJ/mol, green, right). The hydrogen-bonds to His304 and His341 (*Pa*FabF numbering) are indicated as black dots.

The validated receptor was used for virtual screening. First, our in-house library of around 5 million purchasable compounds was filtered for lead-like molecules containing electrophilic warheads, e.g. epoxides or michael acceptors. In a second step, the molecules were transformed into their reacted state resulting in 166882 compounds. Out of these 14282 could be docked into the *Pa*FabF binding site. Filtering these rigid binding poses with a pharmacophore containing just the crucial hydrogenbond interactions to His304 and His341 resulted in 5243 compounds. These were ranked according to their calculated ligand efficiencies and inspected by eye. Finally, 20 compounds were selected for hit validation (Table B.2).

Validation of covalent virtual screening hits

Virtual screening hits containing electrophilic warheads were validated using MALDI mass spectrometry. This method allowed to measure the hole protein mass. Attachment of the covalent bound ligand was indicated by a shift of the mass-to-charge ratio (m/z). Specific binding to Cys164 in the active site was validated in a follow-up experiment using ESI-MS after digestion of the protein.
FabF w. t. and FabF w. t. in complex with the natural compound inhibitor cerulenin were measured with 5 different concentrations to establish the method. The protein was detectable down to 77.9 fmol on the anchorchip. In complex with cerulenin the detection limit went up to 1026 fmol on the chip. In protein samples preincubated with cerulenin no native FabF was detected. After optimizing the method all compounds were spotted with 30 to 70 pmol on the anchorchip.
A shoulder was detected for compound 22 (MW: 190.2 g/mol). Substracting the signal of FabF w. t. resulted in a molecular weight addition of 162.26 g/mol. Several peaks shifted by masses that differed significantly from the molecular weights of the compounds. A shift of around 12 was detected for three compounds (compound 21, 25, 35), a shift of 15.9 for compound 24, 18.39 for compound 20, 42.21 for compound 27 and 50.83 for compound 34 (Table 3.3).
Compound 23 contained an acryl amide substructure that is able to form a covalent bond with cysteine side chains. The binding pose predicted by FlexX placed the amide in the same position as found in the binding mode of platensimycin. It formed hydrogen-bond interactions to Thr306 and Thr308 with its carbonyl group as well as to Thr271 with its amine hydrogen. In addition, the crucial hydrogen-bond to His304 and His341 was formed by the carbonyl group of the acryl amide substructure (Figure 3.13). Based on these findings 6 derivatives of compound 22 were purchased (compounds 22.1 - 22.6). Binding to FabF was measured again using MALDI mass spectrometry but results are still outstanding (Table B.2).

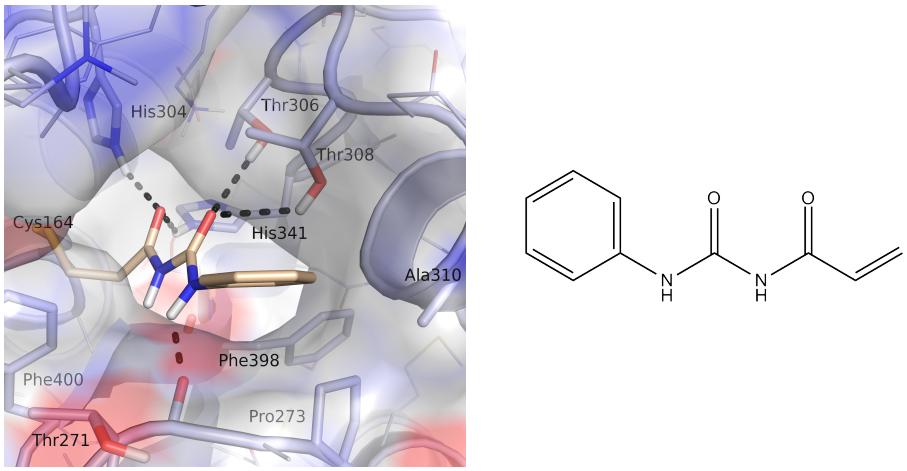

FIGURE 3.13: **Predicted binding mode and structure of compound 22.** Compound 22 (beige) covalent attached to Cys164. Hydrogen bond interactions are indicated as black dots.

TABLE 3.3: **Validation of covalent virtual screening hits using MALDI mass spectrometry.** Molecular weights of the compounds, expected and measured m/z values and the calculated mass addition are listed. Compound 28 was not measured due to solubility problems.

compound	MW [g/mol]	$m/z_{exp.}$	$m/z_{meas.}$	$m/z_{meas.}$ - m/z_{FabF}
FabF w. t.	45832.50	45832.50	45832.89	0.39
cerulenin	223.3	46054.77	46058.21	225.32
20	206.6	46038.10	45851.28	18.39
21	172.2	46003.70	45845.24	12.35
22	190.2	46021.70	45995.15	162.26
23	284.7	46116.20	45831.15	-1.74
24	270.7	46102.20	45848.79	15.9
25	164.6	45996.10	45845.12	12.23
26	234.2	46065.70	45836.26	3.37
27	233.3	46064.80	45875.1	42.21
29	143.2	45974.69	45834.55	1.66
30	341.2	46172.74	45834.71	1.82
31	310.3	46141.81	45836.58	3.69
32	276.3	46107.79	45829.38	-3.51
33	221.2	46052.71	45828.39	-4.5
34	218.0	46049.50	45838.76	5.87
35	350.0	46181.50	45845.62	12.73

In order to verify binding of compound 22 to Cys164 in the active site, the protein ligand complex was digested and measured with ESI-MS. FabF in complex with the known ligand cerulenin as well as the apo-enzyme were used as control. The samples were digested with the proteases trypsin, chymotrypsin or trypsin followed by chymotrypsin. Peptides of different sequence length were generated. Unfortunately peptides carrying Cys164, could not be detected in ESI-MS measurements. Neither the peptide of the apo-enzyme nor the peptide after incubation with a covalent ligand.
Therefore, a third digestion enzyme, namely thermolysin, was used. Upon digestion attachment of cerulenin to Cys164 as well as Cys119 could be detected. The covalent screening hit (compound 22) could be determined to bind to Cys376. Peptides of the protein preincubated with compound 22 showed a mass addition of +97 to Cys164, Cys119 and Cys376. Based on these measurements binding of compound 22 to Cys164 cannot be confirmed but also not excluded.

Discussion

To date, cerulenin is the only inhibitor of FabF with a covalent inhibition mechanism. To our knowledge neither an attempt to discover new covalent ligands of FabF nor to optimize the ligand cerulenin was done so far. This opens a wide space for the design of new covalent inhibitors. In drug discovery covalent binding mechanisms were not considered for a long period as reactive warheads might lead to interactions with other targets resulting in toxic effects like for instance mutagenicity or carcinogenicity (Baillie, 2016). Due to the fact that the mode of action for drugs discovered long time ago, like aspirin, was determined to follow a covalent mechanism, the interest for covalent ligands in drug discovery emerged. The advantage of covalent drugs is a high biochemical efficiency and therefore the need of lower doses. In addition, it is assumed that the covalent binding mechanism prevents the development of drug resistance from mutation of binding site residues in protein, which is of great interest especially to target multiresistant bacteria (Bauer, 2015).
Using virtual screening, a ligand binding covalently to FabF wild type was identified (compound 22) using MALDI mass spectrometry. Control measurements with the known natural inhibitor compound cerulenin confirmed the reliability of the method. Nevertheless, for FabF preincubated with cerulenin no apo-enzyme could be detected. For compound 22 only a shoulder appeared, indicating that the ligand interactions with the protein need to be optimized. The compound contains an acryl amide group, that is responsible for the covalent attachment to cysteines of FabF. Inhibitors containing this electrophilic warhead are especially reported for kinases. Several compounds are known as inhibitors for the ErbB family of kinases (Singh et al., 2010) mainly for the epidermal growth factor (EGFR) receptor (Planken et al., 2017) or the Bruton's tyrosine kinase (BTK) (Bauer, 2015), indicating that acryl amides are suitable electrophilic warheads for drug design.
Due to the increase of drug approvals for compounds with covalent binding mechanism the reactivity of acryl amide towards nucleophiles was studied (Singh et al., 2010; Mah et al., 2014; Flanagan et al., 2014; Bauer, 2015). It was shown that on the one hand the reactivity towards nonspecific thiols is weak to moderate for both, substituted and terminal acryl amides and on the other hand the selectivity to the target protein (EGFR) is high. Thus, unspecific binding of compound 22 to a surface cysteine of FabF might be less favourable. This assumption is encouraged as other virtual screening hits with both, substituted and terminal acryl amide groups were not binding to FabF (compounds 20, 21, 26, 27, 29, 31, 32, 33, 34). The mass addition of 97 $g \cdot mol^{-1}$ found at Cys164, Cys119 and Cys376 after incubation of FabF wild type with compound 22 and digestion with thermolysin could not be assigned to a fragment of compound 22. Based on these findings, binding of the ligand to these cysteines could also not be excluded as the mass addition was not found in samples of FabF wild type preincubated with cerulenin. Due to the finding of compound 22 binding to Cys376 measurements with FabF C164Q cannot be used to validate binding in the active site. For this purpose Cys376 would need to be exchanged by a none reactive amino acid.

The predicted binding mode of compound 22 suggested similar hydrogen bond interactions as found for the amide in platensimycin. However, the position of nitrogen and carbonyl are switched. Thus, the oxygen is able to form two hydrogen bonds to both Thr306 and Thr308 side chain hydroxy groups. The phenyl ring is forming no interactions to the protein instead of van der Waals interactions (Figure 3.13). However, the ring gives a great potential in optimizing the ligand in order to form hydrogen bonds similar to those found in platensimycin to residues Ala310 or Thr271. A strategy to obtain derivates with varying substituents at the phenyl ring might be the Buchwald-Hartwig cross coupling reaction (Yin and Buchwald, 2000). Compound 22.1 (Table B.2) could be used as amide building block that reacts with several aryl halide derivatives.

3.1.5 Binding of historic hit compounds

In a previous work the ChemSpider database (www.chemspider.com) was screened for compounds containing an aromatic substructure as found in platensimycin with a similar substitution pattern (Baum et al., 2015). Finally, 32 compounds (Table B.3) were purchased and binding to FabF was investigated using crystallographic methods. The structure of FabF w. t. in complex with compound 63 was determined (PDB code 4JPF). Unexpectedly, the binding site was located at an crystallographic interface. Nevertheless biophysical measurements to detect binding with FabF were still outstanding.
Here, BLI was used to determine binding events. Binding of compounds 36 to 67 to FabF C164Q, FabF w. t. and biocytin was measured (Figure 3.14).

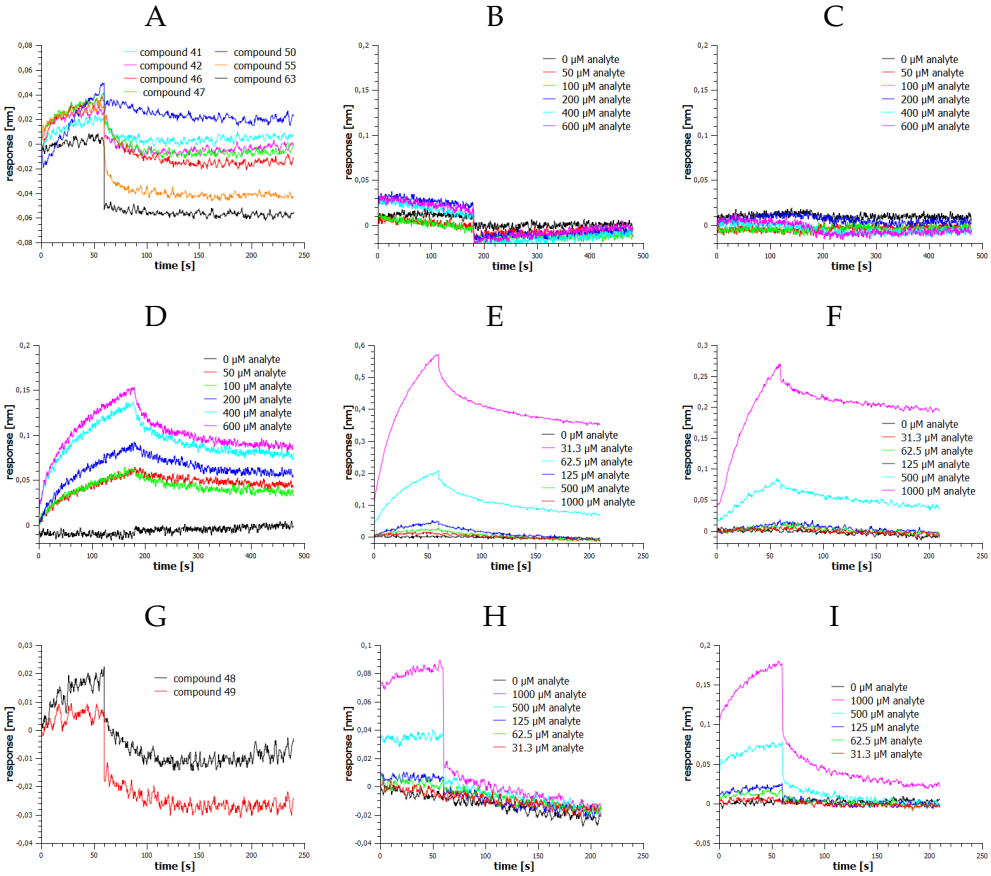

FIGURE 3.14: **Validation of non-covalent virtual screening hits.** Association and dissociation curves of historic hit compounds at a constant concentration of 400 μM (A, G). Concentration series of compound 42 (B), compound 43 (C), compound 44 (H), compound 45 (I), compound 46 (D) and repetition experiment of compound 46 (E). The response were measured with FabF C164Q and substracted with the response of biocytin (A-E, G-I). The response of FabF C164Q substracted with the response of FabF w. t. for compound 46 (F).

Follow-up experiments with a concentration series were carried out for the three most promising compounds. Selection criteria were the shape of association and dissociation curves as well as the level of response. In the follow-up experiments, compounds 42 and 43 had responses close to zero for all concentrations (Figure 3.14, B, C). Association and dissociation curves recorded for compound 46 indicated a binding event (Figure 3.14, D). The measured responses are concentration dependent, except of the lowest and the two highest concentrations. The latter might indicate saturation. A dissociation constant of 28.8± 0.98 μM was calculated. In a repetition experiment, also including a measurement with FabF w. t. the result was not reproducible (Figure 3.14, E, F). In addition, compound 44 and 45, which are structurally related to compound 46 were measured with FabF C164Q and FabF w. t. (Figure 3.14, G, H). The three compounds are naphtoic acids with substitution of hydroxy groups at different positions of the aromatic ring system (Table B.3). Comparing the response at a concentration of 400-500 μM obtained in the screening with the response obtained in the follow-up experiment revealed that all of the three compounds had a different behaviour. This might indicate unspecific binding.

Discussion

A set of 32 historic hit compounds containing aromatic substructures with a similar substitution pattern as found in platensimycin was tested using BLI for binding to FabF C164Q. Unfortunately, none of the compounds could be identified as ligand for FabF. Compound 59 was previously co-crystallised with FabF w. t. (PDB code 4JPF) and bound at a crystallographic interface. This compound resulted in no response in the BLI experiment. Not even unspecific binding to FabF could be measured. Two compounds identified as hits in the primary screening (compound 42 and 43) turned out to be false positives in the follow up experiments, as no association and dissociation could be observed.
Concentration dependency for compound 46 was observed. In spite of that, the association did not reach equilibrium within the time of the experiment (190 s) and dissociation occurred incomplete within 200 seconds, which is unlikely for fragments. The two highest concentrations had the same level of response which might indicate saturation. The compound is a naphthoic acid derivative substituted with two hydroxy groups at position 3 and 5. Two other compounds (44 and 45) are as well derivatives of naphthoic acid substituted with a single hydroxy group at position 3 (compound 45) or 6 (compound 44). To clarify specificity of binding these three compounds were as well measured against FabF wild type. In respect to the exclusion and selection criteria discussed in chapter 3.1.3 all compounds could be excluded as specific binders for both FabF w. t. and FabF C164Q. Finally, these results confirmed the importance of platensimycin's branched ring system, which binds outside the pocket and forms hydrogen bond interactions to Ala310 and Thr271.

Conclusion and future perspectives

Virtual screening approaches to identify new starting points for drug design revealed two scaffolds. The first, a thiazolidinone-4-carboxylic-acid, the second an acryl amide substructure responsible for covalent binding to FabF. Binding of the thiazolidinone-4-carboxylic acid derivatives (compound 6 and 8; Figure 3.10) should be validated using another method than BLI. Other derivatives with a five membered ring at the second position could be purchased to get more knowledge about structure-activity relationships. For compound 22 covalent attachment to Cys164 in the active site has to be confirmed. ESI-MS measurements after digestion of thermolysin might help to verify the binding position. Also, binding of the derivatives (compounds 22.1 -22.7) should be clarified using MALDI and ESI-MS. For both, the covalent and the non-covalent ligands, the binding mode is of great interest for further optimization of the ligands to improve binding affinity. Due to the tremendously disappointing attempts of co-crystallisation and soaking the ligands with *Pseudomonas aeruginosa* FabF (Chapter 3.1.6), a different crystallisation system should be tried. A possible alternative is to use *E. coli* FabF as the binding site is conserved (sequence identity 65.8%; Chapter 1.3.1). Several derivatives of platensimycin have been successfully co-crstallised with this protein. 8 of these structure are published in the PDB (01.03.2018). As soon as the binding mode is determined, the ligands could be optimized and derivatives could be synthesized.

3.1.6 Crystallisation of FabF

Crystallisation of FabF wild type and FabF C164Q

Crystals of FabF w. t. were obtained with reservoir condition III, IV and VI. For the conditions III and IV crystals of good quality, which means uniform crystal growth and a certain thickness and size of the crystal were obtained. Crystals obtained with condition VI were not suitable for X-ray diffraction experiments. Reservoir condition V, which hat resulted to the structure of FabF w. t. (PDB code 4B7V and 4JPF) only resulted in precipitation of the protein. Using reservoir condition I, FabF w. t. precipitated as well. However, reservoir condition I in combination with lauroyl-CoA resulted in the formation of cubic crystals. Crystals of the variant FabF C164Q were obtained with the reservoir condition II, that was also used for the published structure (PDB code 4JB6). All crystallisation approaches were performed with FabF samples without His-tag.
As all ligands of FabF are dissolved in DMSO the influence of the solvent to crystal growth was investigated. It turned out, that a DMSO concentration in the crystallisation drop higher than 1.5% limited the quality of the crystals so that X-ray diffraction experiments were no linger possible.

JCSG-plus and PACT premier screening

The virtual screening hit FC-4 was validated to bind covalently to FabF wild type using MALDI mass spectrometry. Unfortunately, co-crystallisation with FabF wild type using the reservoir conditions listed in table 2.12 led to precipitation. Thus, a crystallisation screen for new crystallisation conditions was carried out using the JCSG-plus^{TM}(MD1-37) and PACT premier^{TM} (MD1-29) screen. Several conditions led to crystal formation (Table 3.4).
Crystals of good quality were formed in 3 reservoir conditions of the JCSG-plus screen: J1-7 (drop 1), J1-15 (drop 1) and J2-47 (drop 2). In the first one long and narrow plates and in the second one plates growing from the same origin and lying on top of each other were formed. The latter led to formation of trapezoid formed plates. The first two reservoir conditions had in common a basic pH (9-9.5), a high molecular PEG (6000-8000) and no salt. The latter had an acidic pH (5.5) with PEG3350 and magnesium chloride as salt. Crystals of good quality were also obtained in the PACT premier screening: P1-35 (drop 1, 2), P2-27 (drop 1, 2), P2-28 (drop 2,3), P2-29 (drop 3), P2-31 (drop 3), P2-34 (drop 1) and P2-46 (drop 3). All of these crystals were drawn-out plates in form of a tie. The reservoir conditions had in common 20% (w/v) PEG3350 and a buffer of bis-tris propane with a pH of 7.5 or 8.5 (P2-46). They differ in their type of salt (NaI, $NaNO_3$, Na-acetate, phosphate).
Three Crystals formed with reservoir condition P2-28 were send to the ESRF synchrotron and X-ray data were collected at the ID30A-1 beamline. Two of them did not diffract, whereas the third one was solved in space group $P12_11$. Electron density for the ligand was not found.

TABLE 3.4: **JCSG-plus and PACT premier screening results.** Reservoir condition of the JCSG-plus screen (upper part) and the PACT premier screen (lower part) that resulted in crystal formation and their supplier ID's. The crystallisation drop consisted of protein:reservoir in a ratio of 2:1 (drop 1) 1:1 (drop 2) and 1:2 (drop 3).

ID	drop	salt	c [M]	buffer	c [M]	pH	precipitant	c (w/v)
J1-5	3	$Mg(HCO_2)_2 \cdot 2\,H_2O$	0.2	-	-	-	PEG3350	20%
J1-7	1, 3	-	-	CHES	0.1	9.5	PEG8000	20%
J1-10	1, 2, 3	$K_2(HCO_2)$	0.2	-	-	-	PEG3350	20%
J1-12	1, 2, 3	KNO_3	0.2	-	-	-	PEG3350	20%
J1-15	1, 2, 3	-	-	BICINE	0.1	9.0	PEG6000	20%
J1-42	1, 2, 3	$MgCl_2 \cdot 6\,H_2O$	0.2	Tris	0.1	8.5	PEG8000	20%
J2-33	1, 2, 3	KSCN	0.1	-	-	-	PEG2000 MME	30%
J2-34	1, 2, 3	KBr	0.15	-	-	-	PEG2000 MME	30%
J2-46	1	CH_3COONH_4	0.2	Bis-Tris	0.1	5.5	PEG3350	25%
J2-47	1, 2	$MgCl_2 \cdot 6\,H_2O$	0.2	Bis-Tris	0.1	5.5	PEG3350	25%
P1-27	3	-	-	PCTP	0.1	6.0	PEG1500	25%
P1-28	2, 3	-	-	PCTP	0.1	7.0	PEG1500	25%
P1-31	1, 2, 3	NaCl	0.2	HEPES	0.1	7.0	PEG6000	20%
P1-32	1, 2, 3	NH_4Cl	0.2	HEPES	0.1	7.0	PEG6000	20%
P1-34	1, 2, 3	$MgCl_2 \cdot 6\,H_2O$	0.2	HEPES	0.1	7.0	PEG6000	20%
P1-35	1	$CaCl_2 \cdot 2\,H_2O$	0.2	HEPES	0.1	7.0	PEG6000	20%
P1-43	1, 2, 3	NaCl	0.2	Tris	0.1	8.0	PEG6000	20%
P1-45	2, 3	LiCl	0.2	Tris	0.1	8.0	PEG6000	20%
P2-6	2, 3	$NaHCO_2$	0.2	-	-	-	PEG3350	20%
P2-7	1, 2, 3	NaCH3COO $\cdot 3\,H_2O$	0.2	-	-	-	PEG3350	20%
P2-13	1, 2, 3	NaF	0.2	Bis-Tris propane	0.1	6.5	PEG3350	20%
P2-14	1, 2, 3	NaBr	0.2	Bis-Tris propane	0.1	6.5	PEG3350	20%
P2-15	2, 3	NaI	0.2	Bis-Tris propane	0.1	6.5	PEG3350	20%
P2-16	3	KSCN	0.2	Bis-Tris propane	0.1	6.5	PEG3350	20%
P2-18	2, 3	$NaHCO_2$	0.2	Bis-Tris propane	0.1	6.5	PEG3350	20%
P2-19	1, 2, 3	NaCH3COO $\cdot 3\,H_2O$	0.2	Bis-Tris propane	0.1	6.5	PEG3350	20%
P2-22	1, 2	$(Na/K)_3PO_4$	0.02	Bis-Tris propane	0.1	6.5	PEG3350	20%
P2-25	1, 2, 3	NaF	0.2	Bis-Tris propane	0.1	7.5	PEG3350	20%
P2-26	1, 2, 3	NaBr	0.2	Bis-Tris propane	0.1	7.5	PEG3350	20%
P2-27	1, 2, 3	NaI	0.2	Bis-Tris propane	0.1	7.5	PEG3350	20%
P2-28	2, 3	KSCN	0.2	Bis-Tris propane	0.1	7.5	PEG3350	20%
P2-29	2, 3	$NaNO_3$	0.2	Bis-Tris propane	0.1	7.5	PEG3350	20%
P2-31	1, 3	NaCH3COO $\cdot 3\,H_2O$	0.2	Bis-Tris propane	0.1	7.5	PEG3350	20%
P2-34	1, 2, 3	$(Na/K)_3PO_4$	0.02	Bis-Tris propane	0.1	7.5	PEG3350	20%
P2-41	2, 3	$NaNO_3$	0.2	Bis-Tris propane	0.1	8.5	PEG3350	20%
P2-46	3	$(Na/K)_3PO_4$	0.02	Bis-Tris propane	0.1	8.5	PEG3350	20%

Co-crystallisation of FabF C164Q with fragment screening hits

The validated fragment hits were co-crystallised with FabF C164Q using reservoir condition II (Table 2.12). Three different concentrations of PEG3350 (25.5%, 26.5%, 27.5%) were used. Nuclei were formed within the first 12 hours and crystal growth stopped after 1 day and 12 hours. The crystal size was around 200-400 μm. Data collection was performed with 16 crystals. These crystals were in the shape of drawn-out plates growing as stars from one origin and covered 10 fragments (compounds 4-G6, 5-D10, 5-C7, 5-D5, 8-B8, 6-G6, 8-C11, 7-G5, 7-A10, 8-E3). The X-ray data were collected at the P13 beamline at the DESY synchrotron.

Soaking and co-crystallisation of FabF with virtual screening hits

Crystals of FabF C164Q and FabF w. t. were obtained using reservoir conditions II, III and IV. These crystals were in form of plates with a size of 200 to 400 μM. After soaking in times of 10 minutes up to 6 hours the crystals were quick dipped into the cryo protectant solution and X-ray data were collected at the ID30A-1 beamline at the ESRF synchrotron or the P13 beamline at the DESY syncrotron. Crystals of soaking experiments covered the following compounds: 3, 5, 22, 23, 25, 39, 48, 49, 50, 61, 63. Also the crystals soaked with the known inhibitors cerulenin and platensimycin and the substrate lauroyl-CoA were send for X-ray data collection.

Structure solution

In total, diffraction data of 67 FabF crystals soaked or co-crystallised with a ligand were collected. 40 crystals of FabF wild type and 27 of FabF C164Q. For the majority of the data sets space group determination using XDS resulted in P222 for both FabF wild type and FabF C164Q. During molecular replacement a significant twinning fraction was detected and due to R-values around 0.3 during refinement the solution seemed to be wrong. Thus, the structure was indexed and integrated in space group P1. A cell content analysis indicated 8 molecules per asymmetric unit. Molecular replacement using four copies of FabF wild type (PDB code 4B7V) as matrix resulted in one solution. The correct space group was determined using CCP4's software tool Zanuda. The suggested space group was $P12_11$ with two dimers in the asymmetric unit for almost all structures. For 4 structures of FabF C164Q Zanuda suggested space group C121. The structures with space group $P12_11$ and those with C121 were refined using phenix.refine and the PDB-REDO server. Water molecules were added using phenix.refine and correct placement was checked manually in COOT leading to a decrease of the R-values into the range of 0.15 to 0.2. The mutation C164Q was also manually inserted in COOT. Coordinates of the ligands were prepared using phenix.eLBOW. The $2F_o$-F_c and the F_o-F_c electron density difference maps were screened for electron density of the ligand using COOT. Unfortunately, no reasonable position of any ligand neither covalent nor non-covalent bond was found.

Discussion

Crystals of good quality for FabF wild type and FabF C164Q were obtained with the previously reported reservoir conditions (Table 2.12). However, co-crystallisation of FabF with both non-covalent and covalent ligands had a great influence on crystal growth. The quality of the crystals suffered from the amount of DMSO. But also DMSO free crystallisation with ligands dissolved in aqueous solutions like lauroyl-CoA and cerulenin or using the DMSO free co-crystallisation approach (Chapter 3.1.6) resulted in non optimal crystal formation for X-ray diffraction experiments. Reservoir condition I only resulted in crystal formation if lauroyl-CoA is present. Nevertheless, electron density of lauroyl was not present indicating that lauroyl-CoA is acting like a salt.
For almost all diffraction data sets obtained in this work crystal twinning was observed during integration and refinement. This crystal property is a hindrance for automatic measurements and crystallisation screenings. The data collection strategy has to be manually adjusted and solving the data sets takes much more time. However, twinning is not an uncommon effect (Parsons, 2003) and solving these data is performed with established strategies nowadays.

Conclusion and future perspectives

Several reservoir conditions resulted in crystals for both FabF wild type and FabF C164Q. Nevertheless the quality of the crystals regarding the requirements for X-ray diffraction experiments is strongly influenced by the concentration of DMSO and the presence of a ligand. Thus, the crystallisation screening using FabF wild type preincubated with the covalent ligand FC-4 resulted in new reservoir condition feasible for co-crystallisation. In the future, more reservoir conditions need to be found for which the presence of ligands do not influence the quality of the crystals. Also, conditions resulting in not twinned crystals should be screened for.

3.2 KPC-2

3.2.1 Virtual screening

Using virtual screening, new starting points for the design of novel antibiotics targeting β-lactamase KPC-2 should be identified. In order to raise the prospects of success, the compounds were filtered in advance of the docking. Thus, a pharmacophore model was necessary. For that purpose, based on the available crystal structures conformational changes near the binding site and the binding mode of known ligands was investigated.
Alignment and superposition of the binding site residues of the 7 available crystal structures of KPC-2 revealed a rigid binding site with only Trp105 (Ambler numbering for class A β-lactamases) adopting two different rotamers, a closed conformation found 6 times and an open one, found two times. In one structure both rotamers were present (PDB code 3RXW). Both rotamers are illustrated in Figure 1.9. Thus, for virtual screening the structure with the highest resolution was selected (*Klebsiella pneumoniae* KPC2 in complex with the covalent inhibitor penam sulfone PSR-3-226 (PDB code 3RXW), 1.26 Å resolution). This structure contained both rotamers of Trp105. For virtual screening, the closed conformation was chosen because it was found in the majority of the structures and it enables the formation of π-π-interactions.
Only little diversity with respect to bound ligands was found in the *Kp* KPC-2 structures. To obtain a more detailed picture on key interactions and to derive a pharmacophore hypothesis, PoSSuM - Search K (Ito et al., 2015) was used to search for similar binding sites containing non-covalent ligands. This resulted in 13 structures, all having tetrazoles or carboxylates bound in the hydrophilic pocket formed by the amino acids corresponding to Thr235, Thr237, Ser130 and Ser70 in *Kp* KPC-2 (Figure 1.9).

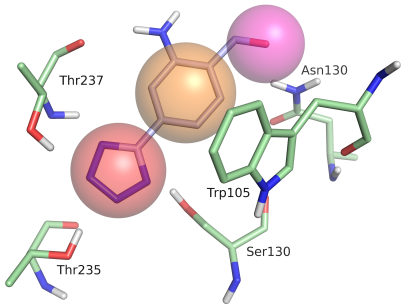

FIGURE 3.15: **Pharmacophore model for KPC-2.** The pharmacophore model of the KPC-2 binding site based on the reference ligand. It contained a hydrogen bond acceptor feature for the interaction with Thr237, Thr235 and Ser130, a hydrogen bond donor feature for the interaction with Asn130 and an aromatic feature to interact with Trp105.

Seven structures are the result of a fragment screening for the *E. coli* CTX-M class A β-lactamase and four are derivatives of the most potent screening hit. The remaining two are the *Serratia fonticola* SFC-1 S70A β-lactamase in a non-covalent complex with meropenem and the *E. coli* Toho-1 R274N:R276N β-lactamase in complex with a boronic acid. Superposition of the binding site residues of *Kp* KPC2 and CTX-M β-lactamase structures gave a rmsd

between 1.09 and 1.19, 0.59 between *Kp* KPC-2 and *S. fonticola* SFC-1 and 1.57 between *Kp* KPC-2 and *E. coli* Toho-1.
All of the ligands in these structures as well as the β-lactamase binding protein found in complex with KPC-2 (PDB code 3E2L, 3E2K) and the covalent ligand of the structure used as receptor, formed a hydrogen-bond to threonines equivalent to Thr235 or Thr237 in KPC-2. Accordingly, a hydrogen bond acceptor at the corresponding ligand position was considered to be crucial for binding. Further, in most of the structures the ligands formed interactions with Trp105. Therefore, this interaction was also included in the pharmacophore hypothesis. Hydrogen-bond interactions to Asp132 were found in four structures (PDB codes 3RXW, 3G32, 3G30, 4EUZ) and included as well. A hierarchical approach was adopted for virtual screening. For docking, DOCK3.6 was used. The docking setup was validated by docking a set of four tetrazole ligands from *E. coli* CTX-M-9 β-lactamase structures 3G2Y (ligand GF4), 3G35 (ligand F13), 4DE0 (ligand (OJB) and 4DE2 (ligand DN3). All binding modes were successfully predicted.Our in-house database of around 5 million purchasable compounds was filtered for lead-like molecules (Brenk et al., 2008). Next, the obtained hits were screened with the above described pharmacophore resulting in 44658 compounds.
Out of these 31122 compounds could be docked into the *Kp* KPC-2 binding site. Filtering these binding poses again with the pharamacophore resulted in 2894 compounds. These were divided into three clusters, depending on the functional group placed in the hydrophilic pocket (tetrazoles, carboxylates, sulfonamides) and inspected by eye. Finally, 31 compounds were selected for hit validation (compounds 68-98; Table B.4).

3.2.2 Hit validation

Virtual screening hits were validated with an enzymatic assay using the chromogenic β-lactamase substrate CENTA^{TM}(100 μM, K_M= 70 μM; Bebrone et al., 2001). The same substrate was used in a competition experiment to determine the inhibitory constant (K_I). Four of the 31 compounds had IC_{50} and K_I values below 1 mM (Table B.4, 3.5). A further six compounds had K_I values below 1 mM but IC_{50} values greater than 1 mM (Table B.4). Compound 78 was found as hit compound in a previous screening for inhibitors of the CTX-M β-lactamase (Chen and Shoichet, 2009; K_I= 21 μM). The K_I was in agreement with the value measured for KPC-2 (30 μM). Compound 77 is structurally related to compound 78. Both ligands share a 5-phenyl-(3-amide)-tetrazole scaffold. Only the ring linked to the amide is varied. The other two hit compounds (compound 76 and 86) only differ in the core. Compound 76 had a benzothiazole core and compound 86 a benzodiazole core.

TABLE 3.5: **Validated virtual screening hits of KPC-2.**

76	77	78	86
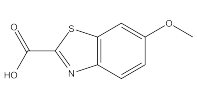	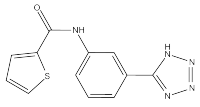	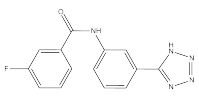	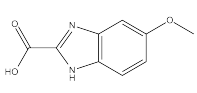
IC_{50}= 0.09 mM	IC_{50}= 0.51 mM	IC_{50}= 0.07 mM	IC_{50}= 0.88 mM

3.2.3 Hit optimisation

In order to improve the binding affinity of compound 78 different substituents placed in the pocket formed by Asn132, Asn170 and Leu166 were explored. To select suitable compounds, in silico synthesis was carried out. We chose to replace the amide linker with a sulfonamide and to diversify the group connected with the linker (Figure 2.4). The sulfonamide was predicted to interact with the side chains of Asp170 and 132. The diversified ring should be oriented towards Leu166 (Figure 3.16).

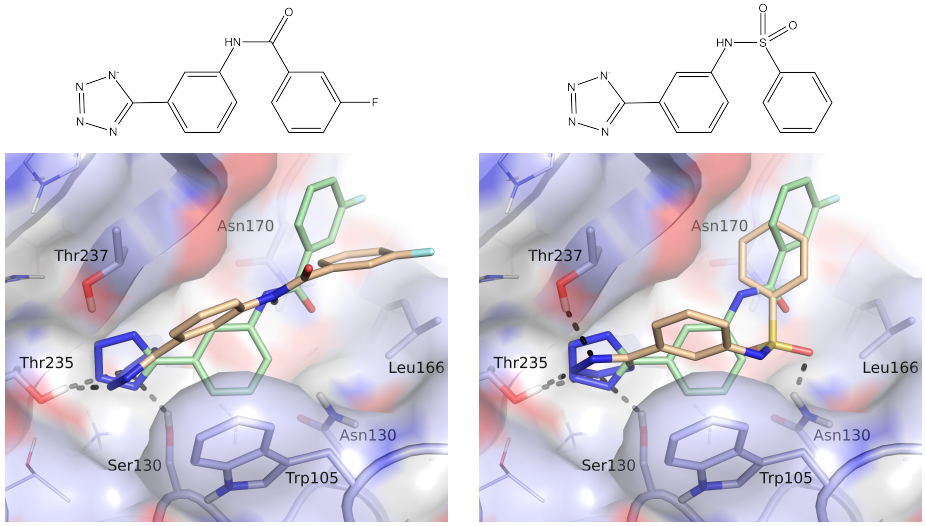

FIGURE 3.16: **Optimisation of compound 78.** Left: Binding mode of compound 78 found in CTX-M-9 β lactamase (PDB code 3G35) (green) and predicted binding mode of compound 78 (beige) in the *Pa* FabF receptor. Right: Predicted binding mode of optimised compound 78.16 (beige) superimposed with binding mode of compound 78 (PDB code 3G35). Putative hydrogen-bond interactions of compound 78 and compound 78.16 are indicated as black dots.

For that purpose, our in-house building blocks library was screened for sulfone halides that were subsequently virtually reacted with the amine part of the molecule (amine 1 in Figure 2.4). The library contained 3572 sulfone halides, resulting in 11123 derivatives of compound 78 after in silico transformation. Docking these compounds in to the *Kp* KPC-2 pocket with subsequent pharmacophore filtering resulted in 1970 poses. To obtain a diverse set, the compounds were clustered based on BCUT descriptors. The compounds in each cluster were ranked by predicated ligand efficiency and the top 5 molecules were inspected by eye. Finally, 10 compounds were shortlisted for synthesis (compounds 78.16-78.25; Table B.4). Beside this synthesis also derivatives of compound 78 were purchased (compounds 78.1-78.15; Table B.4).

3.2.4 Activity of derivatives

Derivatives of compound 78 were purchased, all of them contained the substructure of amine 1 (Figure 2.4). Three of them had an amide, 12 had an sulfonamide linker. The attached group was varying. Compound 78.4 is the sulfonamide equivalent to compound 78. IC_{50} values were measured using the chromogenic β-lactamase reporter substrate nitrocefin (114.28 μM, K_M= 36 μM; Pagès et al., 2016).
Compound 78.4 inhibits KPC-2 by 25% for the highest concentration of 0.2 mM. For six compounds the inhibition was less than 10% for the highest concentration (compound 78.2, 78.7, 78.8, 78.9, 78.12, 78.15). The remaining compounds inhibited KPC-2 by not more than 38% for the highest concentration (Table B.4).

3.2.5 Discussion

Virtual screening

Using virtual screening, 10 ligands binding to KPC-2 with K_I values lower than 1 mM, were identified. Six of them contained a carboxylate moiety (compound 68, 69, 76, 86, 87, 91), four of them the bioisosteric tetrazole group (compound 77, 78, 79, 92). Both groups were predicted to bind into the hydrophilic pocket formed by the amino acids corresponding to Thr235, Thr237, Ser130 and Ser70 (Figure 1.9). The by far most potent ligand 78 is structurally related to compound 77. Both ligands share a phenyl-tetrazole group, which is connected via an amide linker to a fluorophenyl ring (78) or a thiophene ring (77). The K_I value determined for compound 78 was 30 μM, that one of the thiophene derivative 190 μM. Compound 78 was already found as a hit in a previous screening for inhibitors of the CTX-M β-lactamase, confirming the potency as a lead structure for β-lactamase inhibitor design (Chen and Shoichet, 2009). 5-substituted tetrazoles are important derivatives of the tetrazole group in medicinal chemistry (Roh et al., 2012; Ostrovskii et al., 2012). Tetrazoles are bioistoeres of carboxylates having improved pharmacokinetic properties, due to an around 10 times higher lipophilicity and a stronger resistance to metabolic degradation. Beside Chen and Shoichet, 2009 several other groups reported antibacterial activity in association with 5-substituted tetrazoles (Dai et al., 2015; Feinn et al., 2017). Thus, compound 78 was chosen for optimisation.

Hit optimisation

Compound 78 was modified by replacing the amide with a sulfonamide and diversifying the group connected with the linker. The sulfonamide linker is often used in medicinal chemistry. Compounds containing this group are among others associated with antibacterial, anticancer and antiviral biological activity (Supuran et al., 2003; Gioiello et al., 2013). Compared with the amide linker the geometry of the ligand is different due to a change of the sp^2 hybridised carbon atom in the amide and a sp^3 hybridised sulfur atom in the sulfonamide (Elguero et al., 1989). 12 sulfonamide derivatives and three amide derivatives of 78 were purchased

and tested, but the inhibitory constant could not be improved. 10 sulfonamide derivatives were shortlisted for synthesis, which is outstanding. Based on the predicted binding mode, additional hydrogen-bond interactions between the sulfonamide oxygen and the side chain of Asn130 would be possible, and an increased binding affinity would be expected. As the purchased derivatives did not have increased inhibitory activity, the predicted binding modes are likely not representing the native binding mode.

Conclusion and future perspectives

A virtual screening approach served to identify four compounds binding to KPC-2 with inhibitory constants below 400 μM, two of them with the same 5-phenyl-(3-amide)-tetrazole scaffold. Based on the predicted binding mode the identified tetratozole scaffold was optimise in order to improve the hydrogen bond interaction pattern of the ligand. It was shown that the sulfonamide linker is not feasible for improvement of the inhibitory activity. For further improvement other linkers might be tried. Also, the ligands should be co-crystallised with KPC-2 in order to determine the native binding mode. The two other hit compounds (compound 76 and 86) could be optimised as well, based on the predicted binding mode. In addition, the derivatives of 78 developed by Nichols et al., 2012 as CTX-M β-lactamase inhibitors should be tested for inhibitory activity against KPC-2, as well.

3.3 Concluding remarks and future perspectives

In this thesis, enzymes involved in cell membrane and cell wall synthesis of Gram-negative bacteria were chosen as target for the discovery of new starting points for the design of antibiotics. On the one hand the enzyme FabF as part of the fatty acid synthesis cycle to target the formation of the phospholipid bilayer on the other hand the carbapenemase KPC-2 to target the formation of the peptidoglycan layer were chosen.
A challenge in the FabF project was the absence of suitable binding and enzymatic assays in combination with platensimycin, being the only inhibitor available to proof new concepts for assays. This inhibitor is prone to hydrolysis and the high dissociation constant prohibits the use as a control ligand in binding assays. Using biolayer interferometry a binding assay suitable for high throughput screenings was established. In addition, the enzymatic assay of FabF used so far in literature was optimised and a proof of concept confirmed the feasibility. Unfortunately, the contribution of platensimycin's branched ring system to the binding affinity could not be clarified. This knowledge will be a basic building block for future optimisation of ligands. Three ligands could be identified using virtual screening. One with a covalent binding mode, the two others with the same scaffold binding none covalently. Also, a fragment screening served to identify 16 fragments as binding specific to FabF C164Q. In continuing studies the binding modes of these ligands need to be determined. A second assay, using a different method need to be setup to validate the binding.
The binding site of KPC-2 is challenging for virtual screening approaches. The binding site is relatively flat and amino acid side chains to form hydrogen bond interactions are lacking beside the hydrophilic pocket formed by the side chains corresponding to amino acids Ser130, Thr235 and Thr237. In addition, the side chain of Trp105 is flexible and adopts two conformations, which need to be considered. Nevertheless, two scaffolds were identified. The most potent ligand was also found in a virtual screening to find ligands for the CTX-M class A β-lactamase and a K_I in the same order of magnitude could be determined. This reveals the close structural relation between ESBL β-lactamases and carbapenemases. Optimisation of this screening hit to address additional amino acids for hydrogen bond interactions was not successful. The replacement of the amide linker by a sulfonamide did not enhance the binding affinity. In future experiments, other linker might be tried. Also the second scaffold could be optimised.
Finally, for both target proteins two new scaffolds were identified using virtual screening. As major challenge remains the co-crystallisation of the proteins with the ligands. Knowing the binding mode is a big step forward in rational drug design. All ligands identified as hits have a great potential for optimisation and will be a good starting point for the design of new lead-structures to develop new antibiotics.

Appendix A

Media and Buffer

TABLE A.1: Media and buffer

	components	concentration
Autoinduction media	tryptone	10 g/l
	yeast extract	5 g/l
	$MgSO_4$ (1M)	1 ml
	50x5052	20 ml
	20xNPS	50 ml
50x5052	Glycerol	25%
	Glucose	2.5 %
	alpha-Lactose	10%
20xNPS	$(NH_4)_2SO_4$	0.5 M
	KH_2PO_4	1 M
	Na_2HPO_4	1 M
LB-medium	tryptone	10 g/l
	NaCl	10 g/l
	yeast extract	5 g/l
buffer A/B (FabF w. t.), pH 8.0	HEPES	25 mM
	NaCl	500 mM
	Imidazol	20/500 mM
buffer C (FabF w. t.), pH 7.5	HEPES	25 mM
	NaCl	150 mM
buffer A/B (FabF C164Q), pH 7.8	phosphate	50 mM
	NaCl	300 mM
	Glycerol	10 %(v/v)
	Imidazol	20/500 mM
buffer C (FabF C164Q), pH 7.4	phosphate	50 mM
	NaCl	150 mM
	glycerol	10% (v/v)
	DTT	0.5 mM
buffer A/B (TEV), pH 7.8	phosphate	50 mM
	NaCl	150 mM
	glycerol	10% (v/v)
	imidazol	25/500 mM

TABLE A.1: Media and buffer

	components	concentration
buffer C (TEV), pH 7.4	phosphate	50 mM
	NaCl	150 mM
	EDTA	1 mM
	DTT	5 mM
	glycerol	10% (v/v)
buffer A/B (*S.pneumoniae* ACPS), pH 7.8	HEPES	50 mM
	NaCl	150 mM
	Imidazol	0/500 mM
buffer C (*S.pneumoniae* ACPS), pH 7.4	HEPES	50 mM
	$MgCl_2$	10 mM
	DTT	1 mM
	glycerol	50 %
buffer A/B (*E.coli* ACPS), pH 7.8	HEPES	50 mM
	$MgCl_2$	10 mM
	Imidazol	0/500 mM
	glycerol	10% (v/v)
buffer C (*E.coli* ACPS), pH 7.4	HEPES	50 mM
	$MgCl_2$	10 mM
	DTT	1 mM
	glycerol	50 %
Assay-buffer, pH 7.4	phosphate	50 mM
	EDTA	0.5 mM
	TritonX100	0.05%
ITC-buffer, pH 7.4	phosphate	50 mM
	NaCl	150 mM
	Glycerol	10%
	DMSO	0.55%

Appendix B

Virtual Screening Hits

TABLE B.1: **Virtual screening hits of *Pa* FabF (DOCK3.6).** BLI responses were measured at a concentration of 400 μM (1-9) or 500 μM (10-18). The response listed is the response of FabF w.t. substracted from the response of FabF C164Q.

compound	structure	total score [kJ/mol]	LE	BLI - response [nm]
1	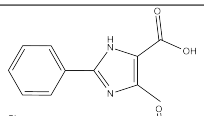	-38.5600	-2.571	0.0222
2	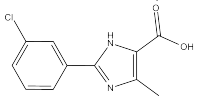	-39.7800	-2.486	-0.0012
3	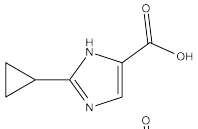	-33.0500	-3.005	0.0028
4	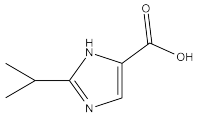	-30.7000	-2.791	0.0047
5	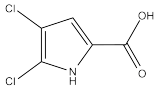	-32.5400	-3.254	0.0045
6	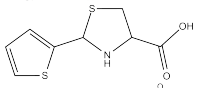	-35.3800	-2.722	0.7557
7	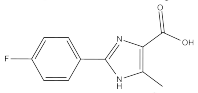	-37.5800	-2.349	0.0107
8	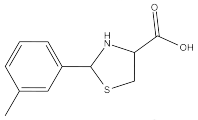	-41.2200	-2.748	0.1421
9	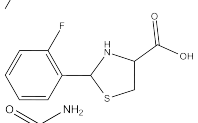	-42.0000	-2.800	-0.0014
10	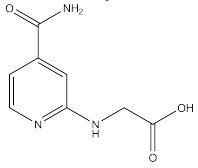	-33.0400	-2.360	0.001

TABLE B.1: **Virtual screening hits of *Pa* FabF (DOCK3.6).** BLI responses were measured at a concentration of 400 μM (1-9) or 500 μM (10-18). The response listed is the response of FabF w.t. substracted from the response of FabF C164Q.

compound	structure	total score [kJ/mol]	LE	BLI - response [nm]
11	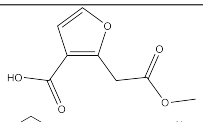	-18.4900	-1.422	-0.005
12	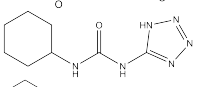	-23.2700	-1.551	0.001
13	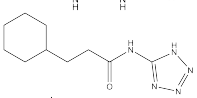	-21.1500	-1.322	0.011
14	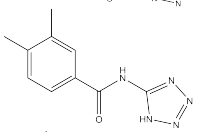	-22.9400	-1.434	-0.025
15	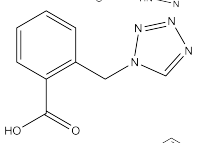	-15.2000	-1.013	0.003
16	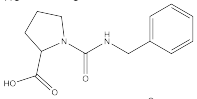	-30.4500	-1.692	0.000
17	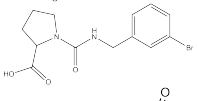	-34.6600	-1.824	-0.002
18	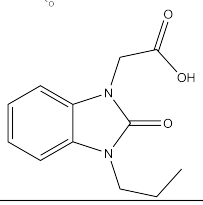	-17.3300	-1.019	-0.001

TABLE B.2: **Covalent virtual screening hits of *Pa* FabF (FlexX).**

compound	structure	total score [kJ/mol]	LE
20	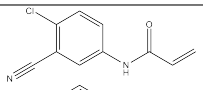	-5.550	-0.396
21	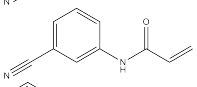	-9.876	-0.760
22	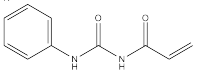	-10.460	-0.747
22.1	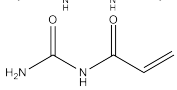	-8.485	-1.061
22.2	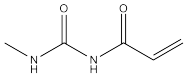	-8.080	-0.898
22.3	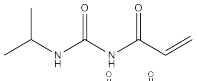	-8.492	-0.772
22.4	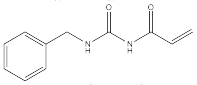	-11.377	0.758
22.5	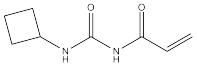	-9.163	-0.764
22.6	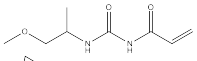	-8.013	-0.616
22.7	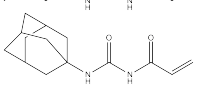	-3.550	-0.197
23	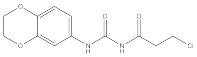	-15.200	-0.8
24	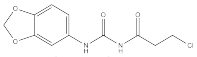	-15.783	-0.877
25	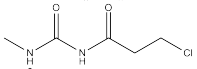	-8.080	-0.808
26	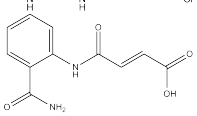	-11.923	-0.701
27	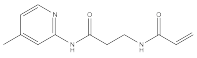	-16.373	-0.963
28			
29	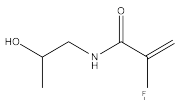	-5.996	-0.560
30	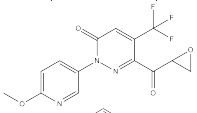	-10.936	-0.456
31	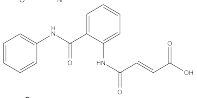	-11.923	-0.518
32	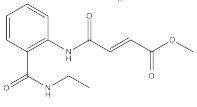	-	-

TABLE B.2: **Covalent virtual screening hits of *Pa* FabF (FlexX).**

compound	structure	total score [kJ/mol]	LE
33	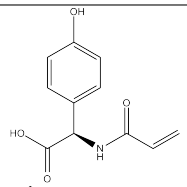	-7.932	-0.496
34	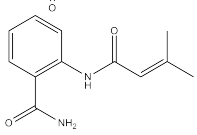	-	-
35	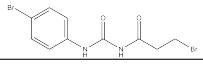	-10.572	-0.661

TABLE B.3: **Historic hit compounds.** BLI response was measured at a concentration of 400 μM. The response listed is the response of biocytin substracted from the response of FabF C164Q.

compound	structure	BLI - response [nm]
36	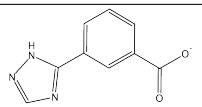	0.0072
37	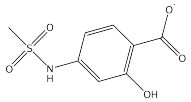	0.0204
38	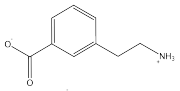	0.0269
39	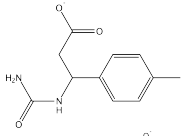	0.0031
40	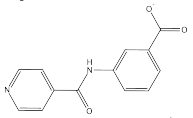	0.0054
41	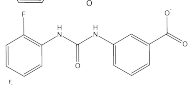	0.0143
42	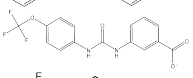	0.0329
43	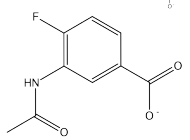	0.0348
44	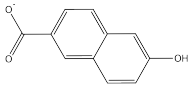	0.0176
45	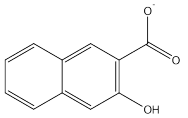	0.0067
46	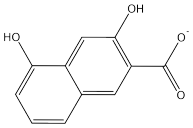	0.0397
47	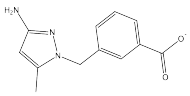	0.0078
48	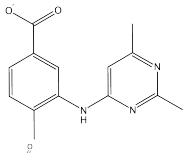	0.0055
49	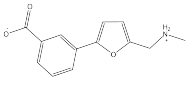	0.0224

TABLE B.3: **Historic hit compounds.** BLI response was measured at a concentration of 400 μM. The response listed is the response of biocytin substracted from the response of FabF C164Q.

compound	structure	BLI - response [nm]
50	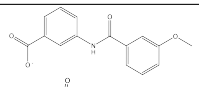	0.0175
51	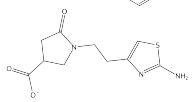	0.0293
52	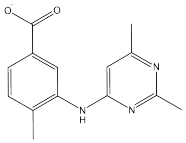	-0.0005
53	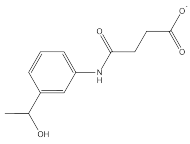	0.0103
54	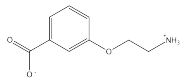	0.0096
55	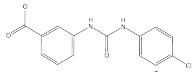	0.0200
56	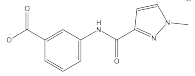	0.0123
57	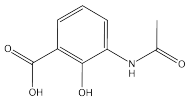	0.0048
58	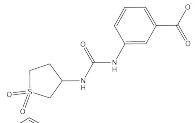	-0.0040
59	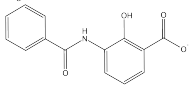	0.0112
60	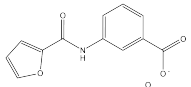	0.0128
61	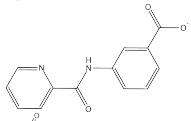	0.0248
62	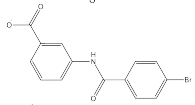	0.0191
63	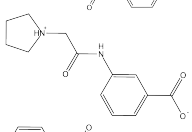	0.0015
64	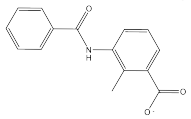	-0.0127

TABLE B.3: **Historic hit compounds.** BLI response was measured at a concentration of 400 μM. The response listed is the response of biocytin substracted from the response of FabF C164Q.

compound	structure	BLI - response [nm]
65	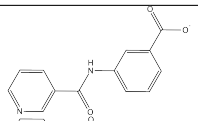	0.0046
66	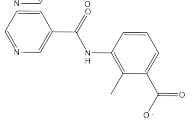	0.0126
67	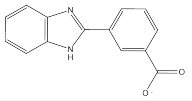	0.0188

TABLE B.4: **Virtual screening hits of KPC-2 (DOCK3.6).** The IC_{50} value was measured with CENTA as reporter substrate for compounds 68 - 98. For the derivatives of compound 78 nitrocefin was used as reportersubstrate. For the latter, if no IC_{50} was measured the percentage of inhibition at the highest concentration is given in parentheses.

compound	structure	total score [kJ/mol]	LE	IC_{50} [mM]	K_I [mM]
68	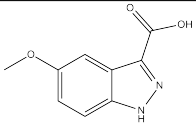	-33.730	-2.409	1.20	0.49
69	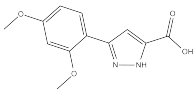	-16.980	-0.943	2.38	0.98
70	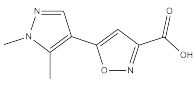	-23.000	-1.533	3.68	1.52
71	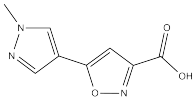	-20.970	-1.498	2.85	1.17
72	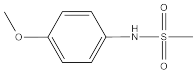	-31.300	-2.408	5.11	2.10
73	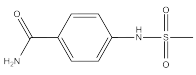	-30.940	-2.210	4.63	1.91
74	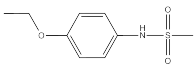	-31.600	-2.257	6.83	2.81

TABLE B.4: **Virtual screening hits of KPC-2 (DOCK3.6).** The IC_{50} value was measured with CENTA as reporter substrate for compounds 68 - 98. For the derivatives of compound 78 nitrocefin was used as reportersubstrate. For the latter, if no IC_{50} was measured the percentage of inhibition at the highest concentration is given in parentheses.

compound	structure	total score [kJ/mol]	LE	IC_{50} [mM]	K_I [mM]
75	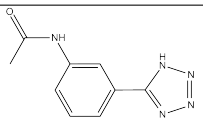	-25.990	-1.856	7.49	3.08
76	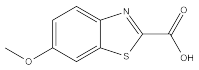	-36.000	-2.571	0.09	0.133
77	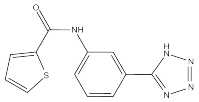	-28.860	-1.519	0.51	0.190
78	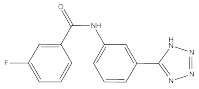	-28.030	-1.335	0.07	0.03
78.1	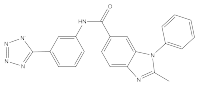	-	-	>1.0 (37)	-
78.2	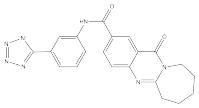	-	-	no inhibition	-
78.3	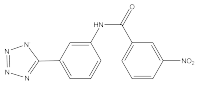	-	-	>0.2 (38)	-
78.4	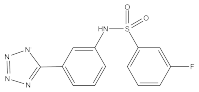	-	-	>0.2 (25)	-
78.5	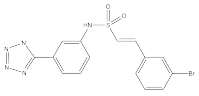	-	-	>1.0 (30)	-
78.6	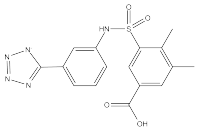	-	-	>1.0 (37)	-
78.7	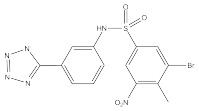	-	-	no inhibition	-
78.8	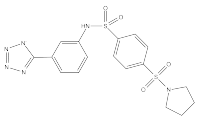	-	-	no inhibition	-

TABLE B.4: **Virtual screening hits of KPC-2 (DOCK3.6).** The IC_{50} value was measured with CENTA as reporter substrate for compounds 68 - 98. For the derivatives of compound 78 nitrocefin was used as reportersubstrate. For the latter, if no IC_{50} was measured the percentage of inhibition at the highest concentration is given in parentheses.

compound	structure	total score [kJ/mol]	LE	IC_{50} [mM]	K_I [mM]
78.9	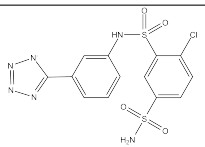	-	-	no inhibition	-
78.10	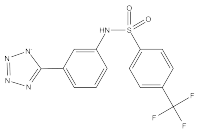	-	-	>500 (20)	-
78.11	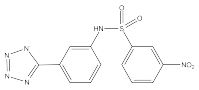	-	-	>0.6 (23)	-
78.12	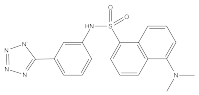	-	-	not dissolvable	-
78.13	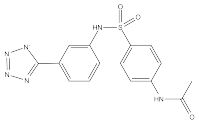	-	-	>0.2 (16)	-
78.14	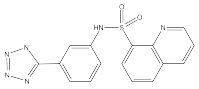	-	-	>0.2 (13)	-
78.15	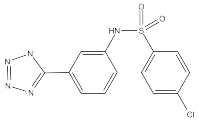	-	-	no inhibition	-
78.16	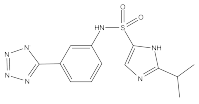	-40.45	-1.76	-	-
78.17	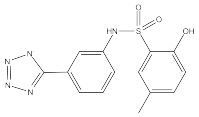	-14.32	-0.62	-	-
78.18	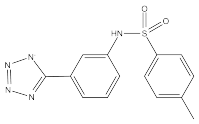	-32.63	-1.48	-	-
78.19	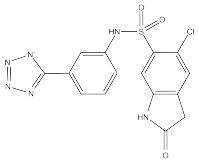	-39.75	-1.53	-	-

TABLE B.4: **Virtual screening hits of KPC-2 (DOCK3.6).** The IC_{50} value was measured with CENTA as reporter substrate for compounds 68 - 98. For the derivatives of compound 78 nitrocefin was used as reportersubstrate. For the latter, if no IC_{50} was measured the percentage of inhibition at the highest concentration is given in parentheses.

compound	structure	total score [kJ/mol]	LE	IC_{50} [mM]	K_I [mM]
78.20	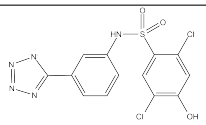	-35.47	-1.48	-	-
78.21	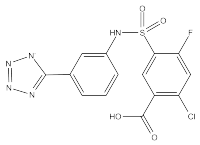	-37.73	-1.45	-	-
78.22	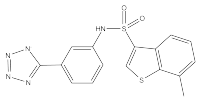	-29.68	-1.19	-	-
78.23	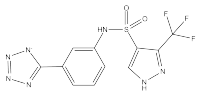	-35.63	-1.48	-	-
78.24	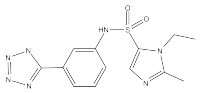	-42.63	-1.85	-	-
78.25	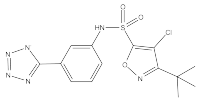	-38.37	-1.53	-	-
79	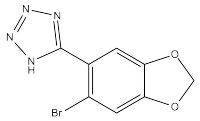	-30.940	-2.063	2.02	0.62
80	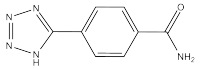	-27.230	-1.945	9.29	3.82
81	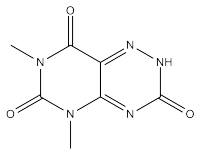	-28.420	-1.895	2.92	1.20
82	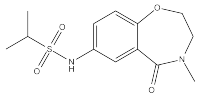	-31.810	-1.591	3.14	1.29
83	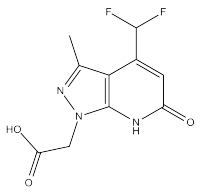	-26.540	-1.474	5.18	2.13

TABLE B.4: **Virtual screening hits of KPC-2 (DOCK3.6).** The IC_{50} value was measured with CENTA as reporter substrate for compounds 68 - 98. For the derivatives of compound 78 nitrocefin was used as reportersubstrate. For the latter, if no IC_{50} was measured the percentage of inhibition at the highest concentration is given in parentheses.

compound	structure	total score [kJ/mol]	LE	IC_{50} [mM]	K_I [mM]
84	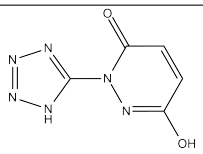	-29.760	-2.289	3.27	1.34
85	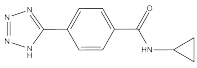	-28.370	-1.669	4.94	2.04
86	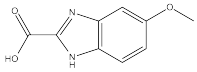	-33.580	-2.399	0.88	0.36
87	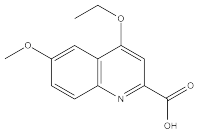	-37.200	-2.067	1.38	0.44
88	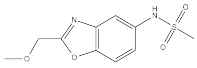	-30.580	-1.799	7.16	2.95
89	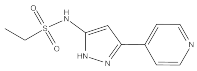	-32.690	-1.923	-	-
90	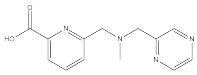	-36.300	-1.911	4.36	1.79
91	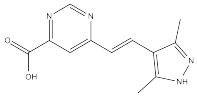	-20.210	-1.123	1.41	0.58
92	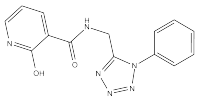	-47.320	-2.151	1.08	0.45
93	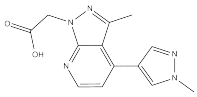	-32.570	-1.629	3.98	1.64
94	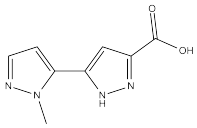	-	-	10.11	4.16
95	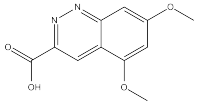	-29.110	-1.712	4.88	2.01
96	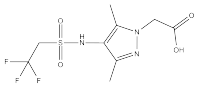	-	-	6.09	2.51

TABLE B.4: **Virtual screening hits of KPC-2 (DOCK3.6).** The IC_{50} value was measured with CENTA as reporter substrate for compounds 68 - 98. For the derivatives of compound 78 nitrocefin was used as reportersubstrate. For the latter, if no IC_{50} was measured the percentage of inhibition at the highest concentration is given in parentheses.

compound	structure	total score [kJ/mol]	LE	IC_{50} [mM]	K_I [mM]
97	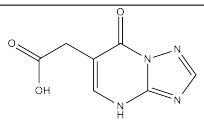	-28.370	-2.026	-	-
98	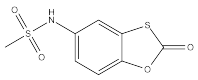	-31.860	-2.124	7.28	3.00

Appendix C

Fragment Screening

TABLE C.1: **Primary fragment screening results.** Responses of FabF C164Q substracted with responses of FabF w. t. (dark gray: FabF C164Q specific hits, light gray: FabF w. t. specific hits.

compound	response	compound	response	compound	response
1-B2 (A-B2)	0.0187	5-B2 (E-B2)	0.0729	9-B2 (I-B2)	-0.0037
1-B3 (A-B3)	-0.0233	5-B3 (E-B3)	0.0027	9-B3 (I-B3)	-0.003
1-B4 (A-B4)	-0.0088	5-B4 (E-B4)	0.0058	9-B4 (I-B4)	0.0298
1-B5 (A-B5)	0.0171	5-B5 (E-B5)	0.0523	9-B5 (I-B5)	0.0014
1-B6 (A-B6)	-0.0168	5-B6 (E-B6)	0.0011	9-B6 (I-B6)	0.0348
1-B7 (A-B7)	-0.0248	5-B7 (E-B7)	0.0717	9-B7 (I-B7)	0.0034
1-B8 (A-B8)	-0.0255	5-B8 (E-B8)	0.0069	9-B8 (I-B8)	0.0017
1-B9 (A-B9)	-0.0301	5-B9 (E-B9)	-0.0073	9-B9 (I-B9)	0.0068
1-B10 (A-B10)	-0.004	5-B10 (E-B10)	-0.0189	9-B10 (I-B10)	0.0343
1-B11 (A-B11)	0.0133	5-B11 (E-B11)	-0.025	9-B11 (I-B11)	0.0356
1-C2 (A-C2)	-0.0251	5-C2 (E-C2)	0.2448	9-C2 (I-C2)	0.0208
1-C3 (A-C3)	-0.0326	5-C3 (E-C3)	0.0023	9-C3 (I-C3)	0.0542
1-C4 (A-C4)	-0.0183	5-C4 (E-C4)	0.0481	9-C4 (I-C4)	0.0206
1-C5 (A-C5)	-0.0118	5-C5 (E-C5)	0.0111	9-C5 (I-C5)	-0.0026
1-C6 (A-C6)	-0.0153	5-C6 (E-C6)	0.0248	9-C6 (I-C6)	0.0225
1-C7 (A-C7)	-0.042	5-C7 (E-C7)	0.1505	9-C7 (I-C7)	0.00
1-C8 (A-C8)	-0.1329	5-C8 (E-C8)	0.0126	9-C8 (I-C8)	0.0004
1-C9 (A-C9)	-0.003	5-C9 (E-C9)	0.0129	9-C9 (I-C9)	0.0018
1-C10 (A-C10)	-0.0008	5-C10 (E-C10)	-0.0226	9-C10 (I-C10)	0.0236
1-C11 (A-C11)	-0.0015	5-C11 (E-C11)	0.0236	9-C11 (I-C11)	0.0271

TABLE C.1: **Primary fragment screening results.** Responses of FabF C164Q substracted with responses of FabF w. t. (dark gray: FabF C164Q specific hits, light gray: FabF w. t. specific hits.

compound	response	compound	response	compound	response
1-D2 (A-D2)	0.0818	5-D2 (E-D2)	0.0509	9-D2 (I-D2)	0.0325
1-D3 (A-D3)	-0.0036	5-D3 (E-D3)	0.0316	9-D3 (I-D3)	0.0062
1-D4 (A-D4)	-0.0453	5-D4 (E-D4)	-0.0054	9-D4 (I-D4)	0.033
1-D5 (A-D5)	0.0066	5-D5 (E-D5)	0.0506	9-D5 (I-D5)	0.0012
1-D6 (A-D6)	-0.0259	5-D6 (E-D6)	0.0127	9-D6 (I-D6)	0.0321
1-D7 (A-D7)	-0.0279	5-D7 (E-D7)	0.0186	9-D7 (I-D7)	0.0017
1-D8 (A-D8)	0.019	5-D8 (E-D8)	0.0101	9-D8 (I-D8)	-0.0009
1-D9 (A-D9)	-0.0074	5-D9 (E-D9)	0.0016	9-D9 (I-D9)	0.0053
1-D10 (A-D10)	-0.0079	5-D10 (E-D10)	0.159	9-D10 (I-D10)	0.0335
1-D11 (A-D11)	-0.0223	5-D11 (E-D11)	-0.0069	9-D11 (I-D11)	0.0342
1-E2 (A-E2)	-0.0215	5-E2 (E-E2)	0.0244		
1-E3 (A-E3)	0.0002	5-E3 (E-E3)	-0.0163		
1-E4 (A-E4)	-0.0091	5-E4 (E-E4)	-0.0103		
1-E5 (A-E5)	-0.0152	5-E5 (E-E5)	0.00		
1-E6 (A-E6)	-0.0079	5-E6 (E-E6)	-0.0039		
1-E7 (A-E7)	-0.0215	5-E7 (E-E7)	-0.0206		
1-E8 (A-E8)	-0.0232	5-E8 (E-E8)	0.0212		
1-E9 (A-E9)	-0.018	5-E9 (E-E9)	0.0326		
1-E10 (A-E10)	-0.0079	5-E10 (E-E10)	-0.0309		
1-E11 (A-E11)	-0.0223	5-E11 (E-E11)	-0.0044		
1-F2 (A-F2)	0.0095	5-F2 (E-F2)	0.0061		
1-F3 (A-F3)	-0.0525	5-F3 (E-F3)	-0.0209		
1-F4 (A-F4)	-0.016	5-F4 (E-F4)	0.0674		
1-F5 (A-F5)	-0.0126	5-F5 (E-F5)	0.0083		
1-F6 (A-F6)	-0.0259	5-F6 (E-F6)	-0.0094		
1-F7 (A-F7)	-0.0257	5-F7 (E-F7)	-0.0117		
1-F8 (A-F8)	0.0186	5-F8 (E-F8)	-0.0095		
1-F9 (A-F9)	-0.0302	5-F9 (E-F9)	-0.0013		

TABLE C.1: **Primary fragment screening results.** Responses of FabF C164Q substracted with responses of FabF w. t. (dark gray: FabF C164Q specific hits, light gray: FabF w. t. specific hits.

compound	response	compound	response	compound	response
1-F10 (A-F10)	-0.0014	5-F10 (E-F10)	0.0563		
1-F11 (A-F11)	-0.0302	5-F11 (E-F11)	0.0087		
1-G2 (A-G2)	0.0046	5-G2 (E-G2)	0.0036		
1-G3 (A-G3)	-0.0595	5-G3 (E-G3)	-0.0009		
1-G4 (A-G4)	-0.0213	5-G4 (E-G4)	-0.006		
1-G5 (A-G5)	-0.0437	5-G5 (E-G5)	0.0085		
1-G6 (A-G6)	-0.0161	5-G6 (E-G6)	0.0669		
1-G7 (A-G7)	-0.0619	5-G7 (E-G7)	-0.0022		
1-G8 (A-G8)	0.0037	5-G8 (E-G8)	0.0819		
1-G9 (A-G9)	-0.0244	5-G9 (E-G9)	-0.0001		
1-G10 (A-G10)	-0.067	5-G10 (E-G10)	-0.0002		
1-G11 (A-G11)	0.006	5-G11 (E-G11)	0.0294		
2-B2 (B-B2)	-0.0207	6-B2 (F-B2)	0.0114	1-H2 (J-B2)	0.002
2-B3 (B-B3)	-0.0172	6-B3 (F-B3)	-0.0059	1-H3 (J-B3)	-0.0235
2-B4 (B-B4)	-0.0004	6-B4 (F-B4)	0.1106	1-H4 (J-B4)	0.0127
2-B5 (B-B5)	-0.0039	6-B5 (F-B5)	-0.009	1-H5 (J-B5)	-0.0057
2-B6 (B-B6)	-0.0098	6-B6 (F-B6)	-0.0151	1-H6 (J-B6)	-0.0051
2-B7 (B-B7)	-0.0086	6-B7 (F-B7)	0.0071	1-H7 (J-B7)	-0.0128
2-B8 (B-B8)	-0.0118	6-B8 (F-B8)	-0.0157	1-H8 (J-B8)	0.0196
2-B9 (B-B9)	-0.0339	6-B9 (F-B9)	-0.0042	1-H9 (J-B9)	-0.008
2-B10 (B-B10)	-0.0225	6-B10 (F-B10)	-0.0089	1-H10 (J-B10)	-0.0068
2-B11 (B-B11)	-0.02	6-B11 (F-B11)	-0.0017	1-H11 (J-B11)	0.0007
2-C2 (B-C2)	0.0093	6-C2 (F-C2)	-0.0272	2-A2 (J-C2)	0.0694
2-C3 (B-C3)	0.0082	6-C3 (F-C3)	-0.0171	2-A3 (J-C3)	0.0011
2-C4 (B-C4)	-0.0179	6-C4 (F-C4)	-0.092	2-A4 (J-C4)	0.0121
2-C5 (B-C5)	-0.0179	6-C5 (F-C5)	0.0526	2-A5 (J-C5)	0.0289
2-C6 (B-C6)	0.002	6-C6 (F-C6)	-0.0172	2-A6 (J-C6)	-0.0042
2-C7 (B-C7)	-0.0358	6-C7 (F-C7)	-0.0049	2-A7 (J-C7)	0.0111

TABLE C.1: **Primary fragment screening results.** Responses of FabF C164Q substracted with responses of FabF w. t. (dark gray: FabF C164Q specific hits, light gray: FabF w. t. specific hits.

compound	response	compound	response	compound	response
2-C8 (B-C8)	0.0089	6-C8 (F-C8)	-0.0263	2-A8 (J-C8)	0.0492
2-C9 (B-C9)	0.0215	6-C9 (F-C9)	-0.028	2-A9 (J-C9)	0.0025
2-C10 (B-C10)	-0.0147	6-C10 (F-C10)	-0.0082	2-A10 (J-C10)	0.014
2-C11 (B-C11)	0.0091	6-C11 (F-C11)	0.0016	2-A11 (J-C11)	0.0112
2-D2 (B-D2)	0.0015	6-D2 (F-D2)	0.0242	2-H2 (J-D2)	0.006
2-D3 (B-D3)	0.0099	6-D3 (F-D3)	0.022	2-H3 (J-D3)	0.0052
2-D4 (B-D4)	-0.0275	6-D4 (F-D4)	0.0018	2-H4 (J-D4)	0.0148
2-D5 (B-D5)	0.0245	6-D5 (F-D5)	0.0006	2-H5 (J-D5)	0.0565
2-D6 (B-D6)	0.0008	6-D6 (F-D6)	0.1134	2-H6 (J-D6)	-0.031
2-D7 (B-D7)	-0.0094	6-D7 (F-D7)	-0.0086	2-H7 (J-D7)	0.0014
2-D8 (B-D8)	-0.0076	6-D8 (F-D8)	-0.0043	2-H8 (J-D8)	0.0093
2-D9 (B-D9)	-0.006	6-D9 (F-D9)	0.042	2-H9 (J-D9)	0.0024
2-D10 (B-D10)	-0.0124	6-D10 (F-D10)	-0.0081	2-H10 (J-D10)	-0.0145
2-D11 (B-D11)	-0.0114	6-D11 (F-D11)	-0.0073	2-H11 (J-D11)	0.01
2-E2 (B-E2)	-0.0082	6-E2 (F-E2)	0.0062	3-A2 (J-E2)	0.0035
2-E3 (B-E3)	0.004	6-E3 (F-E3)	0.0236	3-A3 (J-E3)	0.0085
2-E4 (B-E4)	-0.0178	6-E4 (F-E4)	0.0379	3-A4 (J-E4)	0.0062
2-E5 (B-E5)	0.0139	6-E5 (F-E5)	0.0069	3-A5 (J-E5)	0.0111
2-E6 (B-E6)	-0.032	6-E6 (F-E6)	0.0337	3-A6 (J-E6)	0.0042
2-E7 (B-E7)	-0.0051	6-E7 (F-E7)	0.0049	3-A7 (J-E7)	-0.0072
2-E8 (B-E8)	-0.0112	6-E8 (F-E8)	-0.0111	3-A8 (J-E8)	-0.0124
2-E9 (B-E9)	-0.0142	6-E9 (F-E9)	0.021	3-A9 (J-E9)	-0.0027
2-E10 (B-E10)	-0.0078	6-E10 (F-E10)	-0.0063	3-A10 (J-E10)	-0.0095
2-E11 (B-E11)	-0.0115	6-E11 (F-E11)	0.0597	3-A11 (J-E11)	0.0061
2-F2 (B-F2)	0.0227	6-F2 (F-F2)	0.0297	3-H2 (J-F2)	-0.0108
2-F3 (B-F3)	0.0102	6-F3 (F-F3)	0.0176	3-H3 (J-F3)	-0.0171
2-F4 (B-F4)	-0.006	6-F4 (F-F4)	0.0151	3-H4 (J-F4)	0.0064
2-F5 (B-F5)	-0.0209	6-F5 (F-F5)	0.0188	3-H5 (J-F5)	-0.0131

TABLE C.1: **Primary fragment screening results.** Responses of FabF C164Q substracted with responses of FabF w. t. (dark gray: FabF C164Q specific hits, light gray: FabF w. t. specific hits.

compound	response	compound	response	compound	response
2-F6 (B-F6)	0.0096	6-F6 (F-F6)	0.1738	3-H6 (J-F6)	-0.0197
2-F7 (B-F7)	0.0107	6-F7 (F-F7)	-0.0055	3-H7 (J-F7)	-0.0175
2-F8 (B-F8)	-0.0006	6-F8 (F-F8)	-0.0069	3-H8 (J-F8)	-0.0024
2-F9 (B-F9)	0.4906	6-F9 (F-F9)	-0.004	3-H9 (J-F9)	-0.0028
2-F10 (B-F10)	-0.0105	6-F10 (F-F10)	0.1406	3-H10 (J-F10)	-0.0196
2-F11 (B-F11)	0.0064	6-F11 (F-F11)	-0.0004	3-H11 (J-F11)	-0.0078
2-G2 (B-G2)	-0.0162	6-G2 (F-G2)	-0.0119	1-A2 (J-G2)	-0.0011
2-G3 (B-G3)	0.0021	6-G3 (F-G3)	-0.0051	1-A3 (J-G3)	-0.0213
2-G4 (B-G4)	-0.0472	6-G4 (F-G4)	0.1548	1-A4 (J-G4)	-0.0134
2-G5 (B-G5)	-0.0055	6-G5 (F-G5)	0.1467	1-A5 (J-G5)	-0.0155
2-G6 (B-G6)	0.0012	6-G6 (F-G6)	0.1785	1-A6 (J-G6)	-0.0271
2-G7 (B-G7)	0.0016	6-G7 (F-G7)	-0.0074	1-A7 (J-G7)	-0.0248
2-G8 (B-G8)	0.0122	6-G8 (F-G8)	0.0004	1-A8 (J-G8)	-0.0187
2-G9 (B-G9)	-0.0146	6-G9 (F-G9)	-0.0183	1-A9 (J-G9)	-0.0295
2-G10 (B-G10)	-0.0053	6-G10 (F-G10)	0.0754	1-A10 (J-G10)	-0.0254
2-G11 (B-G11)	0.0189	6-G11 (F-G11)	-0.0056	1-A11 (J-G11)	-0.0207
3-B2 (C-B2)	-0.0017	7-B2 (G-B2)	-0.0015	4-A2 (K-B2)	0.0081
3-B3 (C-B3)	-0.0113	7-B3 (G-B3)	-0.0077	4-A3 (K-B3)	0.0287
3-B4 (C-B4)	-0.0163	7-B4 (G-B4)	-0.0088	4-A4 (K-B4)	0.0069
3-B5 (C-B5)	-0.0719	7-B5 (G-B5)	0.041	4-A5 (K-B5)	0.0103
3-B6 (C-B6)	-0.0192	7-B6 (G-B6)	0.1378	4-A6 (K-B6)	0.0209
3-B7 (C-B7)	-0.0041	7-B7 (G-B7)	0.0042	4-A7 (K-B7)	0.0084
3-B8 (C-B8)	0.0086	7-B8 (G-B8)	0.0026	4-A8 (K-B8)	0.0014
3-B9 (C-B9)	-0.0358	7-B9 (G-B9)	0.5927	4-A9 (K-B9)	0.0134
3-B10 (C-B10)	-0.0131	7-B10 (G-B10)	0.0107	4-A10 (K-B10)	-0.0027
3-B11 (C-B11)	-0.0201	7-B11 (G-B11)	0.0076	4-A11 (K-B11)	0.0009
3-C2 (C-C2)	0.0257	7-C2 (G-C2)	-0.0003	4-H2 (K-C2)	0.0016
3-C3 (C-C3)	0.0585	7-C3 (G-C3)	-0.0015	4-H3 (K-C3)	-0.0271

TABLE C.1: **Primary fragment screening results.** Responses of FabF C164Q substracted with responses of FabF w. t. (dark gray: FabF C164Q specific hits, light gray: FabF w. t. specific hits.

compound	response	compound	response	compound	response
3-C4 (C-C4)	0.02	7-C4 (G-C4)	0.00	4-H4 (K-C4)	0.0191
3-C5 (C-C5)	0.0385	7-C5 (G-C5)	-0.0091	4-H5 (K-C5)	0.0139
3-C6 (C-C6)	-0.0023	7-C6 (G-C6)	0.0042	4-H6 (K-C6)	0.0105
3-C7 (C-C7)	0.0979	7-C7 (G-C7)	0.0212	4-H7 (K-C7)	0.0096
3-C8 (C-C8)	0.0963	7-C8 (G-C8)	0.0452	4-H8 (K-C8)	-0.0118
3-C9 (C-C9)	0.1167	7-C9 (G-C9)	0.0024	4-H9 (K-C9)	0.0115
3-C10 (C-C10)	0.0079	7-C10 (G-C10)	0.0123	4-H10 (K-C10)	0.0099
3-C11 (C-C11)	0.0013	7-C11 (G-C11)	0.0204	4-H11 (K-C11)	0.0043
3-D2 (C-D2)	0.013	7-D2 (G-D2)	0.0338	5-A2 (K-D2)	-0.0185
3-D3 (C-D3)	0.0161	7-D3 (G-D3)	0.0496	5-A3 (K-D3)	0.01
3-D4 (C-D4)	-0.0073	7-D4 (G-D4)	0.0119	5-A4 (K-D4)	0.003
3-D5 (C-D5)	0.0057	7-D5 (G-D5)	0.0741	5-A5 (K-D5)	0.0055
3-D6 (C-D6)	-0.0425	7-D6 (G-D6)	0.041	5-A6 (K-D6)	0.0048
3-D7 (C-D7)	-0.0042	7-D7 (G-D7)	-0.0007	5-A7 (K-D7)	0.0057
3-D8 (C-D8)	-0.0111	7-D8 (G-D8)	0.0395	5-A8 (K-D8)	0.0065
3-D9 (C-D9)	-0.012	7-D9 (G-D9)	0.003	5-A9 (K-D9)	-0.0025
3-D10 (C-D10)	-0.0198	7-D10 (G-D10)	0.01	5-A10 (K-D10)	0.0099
3-D11 (C-D11)	-0.0074	7-D11 (G-D11)	0.0223	5-A11 (K-D11)	0.0359
3-E2 (C-E2)	0.0121	7-E2 (G-E2)	0.0134	5-H2 (K-E2)	0.004
3-E3 (C-E3)	0.00	7-E3 (G-E3)	0.1026	5-H3 (K-E3)	0.0076
3-E4 (C-E4)	0.0149	7-E4 (G-E4)	-0.0091	5-H4 (K-E4)	0.0027
3-E5 (C-E5)	0.0084	7-E5 (G-E5)	-0.007	5-H5 (K-E5)	0.0266
3-E6 (C-E6)	-0.032	7-E6 (G-E6)	0.0093	5-H6 (K-E6)	-0.0059
3-E7 (C-E7)	-0.0094	7-E7 (G-E7)	0.0012	5-H7 (K-E7)	0.0027
3-E8 (C-E8)	0.0437	7-E8 (G-E8)	0.009	5-H8 (K-E8)	0.00
3-E9 (C-E9)	-0.018	7-E9 (G-E9)	0.0096	5-H9 (K-E9)	0.0026
3-E10 (C-E10)	-0.0159	7-E10 (G-E10)	0.0496	5-H10 (K-E10)	-0.0003
3-E11 (C-E11)	-0.0017	7-E11 (G-E11)	0.0059	5-H11 (K-E11)	0.0056

TABLE C.1: **Primary fragment screening results.** Responses of FabF C164Q substracted with responses of FabF w. t. (dark gray: FabF C164Q specific hits, light gray: FabF w. t. specific hits.

compound	response	compound	response	compound	response
3-F2 (C-F2)	0.009	7-F2 (G-F2)	0.0044	6-A2 (K-F2)	0.0131
3-F3 (C-F3)	0.0602	7-F3 (G-F3)	0.009	6-A3 (K-F3)	-0.0052
3-F4 (C-F4)	0.0304	7-F4 (G-F4)	0.007	6-A4 (K-F4)	0.1258
3-F5 (C-F5)	-0.0045	7-F5 (G-F5)	0.0356	6-A5 (K-F5)	-0.0005
3-F6 (C-F6)	-0.0165	7-F6 (G-F6)	0.1298	6-A6 (K-F6)	0.0092
3-F7 (C-F7)	-0.0022	7-F7 (G-F7)	0.0072	6-A7 (K-F7)	0.0006
3-F8 (C-F8)	0.0379	7-F8 (G-F8)	0.0123	6-A8 (K-F8)	-0.0162
3-F9 (C-F9)	0.0165	7-F9 (G-F9)	0.0089	6-A9 (K-F9)	0.0037
3-F10 (C-F10)	-0.0139	7-F10 (G-F10)	0.0236	6-A10 (K-F10)	0.0116
3-F11 (C-F11)	-0.0001	7-F11 (G-F11)	0.3039	6-A11 (K-F11)	0.023
3-G2 (C-G2)	0.014	7-G2 (G-G2)	0.0042	6-H2 (K-G2)	0.0086
3-G3 (C-G3)	-0.0059	7-G3 (G-G3)	0.1172	6-H3 (K-G3)	0.0214
3-G4 (C-G4)	0.0091	7-G4 (G-G4)	0.0145	6-H4 (K-G4)	0.0894
3-G5 (C-G5)	-0.0087	7-G5 (G-G5)	0.1519	6-H5 (K-G5)	0.041
3-G6 (C-G6)	-0.0058	7-G6 (G-G6)	0.0644	6-H6 (K-G6)	0.0069
3-G7 (C-G7)	-0.019	7-G7 (G-G7)	-0.0025	6-H7 (K-G7)	-0.0038
3-G8 (C-G8)	-0.0025	7-G8 (G-G8)	0.0045	6-H8 (K-G8)	0.0099
3-G9 (C-G9)	0.0044	7-G9 (G-G9)	0.0054	6-H9 (K-G9)	0.0475
3-G10 (C-G10)	-0.0075	7-G10 (G-G10)	0.0501	6-H10 (K-G10)	0.0128
3-G11 (C-G11)	0.0016	7-G11 (G-G11)	0.0142	6-H11 (K-G11)	0.0072
4-B2 (D-B2)	0.0181	8-B2 (H-B2)	-0.0275	7-A2 (L-B2)	0.0282
4-B3 (D-B3)	0.0814	8-B3 (H-B3)	-0.031	7-A3 (L-B3)	0.025
4-B4 (D-B4)	0.0268	8-B4 (H-B4)	-0.0218	7-A4 (L-B4)	-0.0176
4-B5 (D-B5)	0.1317	8-B5 (H-B5)	-0.0092	7-A5 (L-B5)	-0.0411
4-B6 (D-B6)	0.0071	8-B6 (H-B6)	0.0059	7-A6 (L-B6)	-0.0528
4-B7 (D-B7)	0.0195	8-B7 (H-B7)	-0.0354	7-A7 (L-B7)	-0.0587
4-B8 (D-B8)	0.0032	8-B8 (H-B8)	0.061	7-A8 (L-B8)	-0.0424
4-B9 (D-B9)	0.0017	8-B9 (H-B9)	-0.0493	7-A9 (L-B9)	0.0231

TABLE C.1: **Primary fragment screening results.** Responses of FabF C164Q substracted with responses of FabF w. t. (dark gray: FabF C164Q specific hits, light gray: FabF w. t. specific hits.

compound	response	compound	response	compound	response
4-B10 (D-B10)	0.0381	8-B10 (H-B10)	-0.0486	7-A10 (L-B10)	0.1073
4-B11 (D-B11)	-0.0061	8-B11 (H-B11)	-0.0023	7-A11 (L-B11)	0.0955
4-C2 (D-C2)	0.0045	8-C2 (H-C2)	0.1132	7-H2 (L-C2)	0.0243
4-C3 (D-C3)	-0.0014	8-C3 (H-C3)	0.0215	7-H3 (L-C3)	0.0142
4-C4 (D-C4)	-0.001	8-C4 (H-C4)	0.0096	7-H4 (L-C4)	-0.0115
4-C5 (D-C5)	0.0053	8-C5 (H-C5)	-0.0087	7-H5 (L-C5)	-0.0426
4-C6 (D-C6)	0.0135	8-C6 (H-C6)	0.0102	7-H6 (L-C6)	0.0285
4-C7 (D-C7)	0.2523	8-C7 (H-C7)	-0.0035	7-H7 (L-C7)	-0.0297
4-C8 (D-C8)	0.0134	8-C8 (H-C8)	0.0254	7-H8 (L-C8)	0.0042
4-C9 (D-C9)	0.1833	8-C9 (H-C9)	0.1968	7-H9 (L-C9)	0.016
4-C10 (D-C10)	0.0072	8-C10 (H-C10)	0.0003	7-H10 (L-C10)	0.3018
4-C11 (D-C11)	0.0027	8-C11 (H-C11)	0.069	7-H11 (L-C11)	0.0845
4-D2 (D-D2)	0.0126	8-D2 (H-D2)	-0.0006	8-A2 (L-D2)	-0.0111
4-D3 (D-D3)	0.0021	8-D3 (H-D3)	-0.0333	8-A3 (L-D3)	0.0099
4-D4 (D-D4)	-0.0067	8-D4 (H-D4)	-0.0073	8-A4 (L-D4)	0.0016
4-D5 (D-D5)	0.0078	8-D5 (H-D5)	-0.0175	8-A5 (L-D5)	-0.0315
4-D6 (D-D6)	0.0083	8-D6 (H-D6)	0.0221	8-A6 (L-D6)	0.0032
4-D7 (D-D7)	0.0051	8-D7 (H-D7)	-0.0403	8-A7 (L-D7)	-0.0041
4-D8 (D-D8)	-0.0096	8-D8 (H-D8)	0.021	8-A8 (L-D8)	-0.0057
4-D9 (D-D9)	0.005	8-D9 (H-D9)	-0.0299	8-A9 (L-D9)	-0.0364
4-D10 (D-D10)	-0.0113	8-D10 (H-D10)	0.0087	8-A10 (L-D10)	0.0242
4-D11 (D-D11)	-0.0135	8-D11 (H-D11)	0.0292	8-A11 (L-D11)	0.0523
4-E2 (D-E2)	0.0143	8-E2 (H-E2)	0.0085	8-H2 (L-E2)	0.0173
4-E3 (D-E3)	-0.0092	8-E3 (H-E3)	0.0792	8-H3 (L-E3)	-0.1375
4-E4 (D-E4)	0.0279	8-E4 (H-E4)	0.0486	8-H4 (L-E4)	0.0386
4-E5 (D-E5)	-0.011	8-E5 (H-E5)	0.0359	8-H5 (L-E5)	0.0535
4-E6 (D-E6)	0.0025	8-E6 (H-E6)	0.0846	8-H6 (L-E6)	0.023
4-E7 (D-E7)	0.0025	8-E7 (H-E7)	0.0045	8-H7 (L-E7)	0.0049

TABLE C.1: **Primary fragment screening results.** Responses of FabF C164Q substracted with responses of FabF w. t. (dark gray: FabF C164Q specific hits, light gray: FabF w. t. specific hits.

compound	response	compound	response	compound	response
4-E8 (D-E8)	0.0656	8-E8 (H-E8)	0.0055	8-H8 (L-E8)	0.0066
4-E9 (D-E9)	-0.1435	8-E9 (H-E9)	-0.0085	8-H9 (L-E9)	-0.0178
4-E10 (D-E10)	-0.0073	8-E10 (H-E10)	0.0059	8-H10 (L-E10)	0.147
4-E11 (D-E11)	-0.0114	8-E11 (H-E11)	0.0049	8-H11 (L-E11)	0.0017
4-F2 (D-F2)	-0.0044	8-F2 (H-F2)	-0.0052	9-A2 (L-F2)	0.0289
4-F3 (D-F3)	0.0647	8-F3 (H-F3)	0.0789	9-A3 (L-F3)	0.0007
4-F4 (D-F4)	-0.0046	8-F4 (H-F4)	-0.0285	9-A4 (L-F4)	0.027
4-F5 (D-F5)	-0.0072	8-F5 (H-F5)	-0.0172	9-A5 (L-F5)	-0.0061
4-F6 (D-F6)	-0.0095	8-F6 (H-F6)	0.0007	9-A6 (L-F6)	0.0267
4-F7 (D-F7)	-0.0029	8-F7 (H-F7)	-0.0199	9-A7 (L-F7)	-0.0005
4-F8 (D-F8)	0.0373	8-F8 (H-F8)	-0.0392	9-A8 (L-F8)	-0.0027
4-F9 (D-F9)	-0.0088	8-F9 (H-F9)	0.0094	9-A9 (L-F9)	-0.0011
4-F10 (D-F10)	-0.0075	8-F10 (H-F10)	-0.0395	9-A10 (L-F10)	0.0362
4-F11 (D-F11)	-0.0114	8-F11 (H-F11)	0.0117	9-A11 (L-F11)	0.04
4-G2 (D-G2)	-0.0041	8-G2 (H-G2)	-0.0063	9-H2 (L-G2)	0.0034
4-G3 (D-G3)	-0.005	8-G3 (H-G3)	0.0666	9-H3 (L-G3)	-0.0032
4-G4 (D-G4)	0.0019	8-G4 (H-G4)	-0.0264	9-H4 (L-G4)	0.0122
4-G5 (D-G5)	0.0162	8-G5 (H-G5)	-0.0158	9-H5 (L-G5)	-0.0055
4-G6 (D-G6)	0.0733	8-G6 (H-G6)	-0.0017	9-H6 (L-G6)	0.0121
4-G7 (D-G7)	-0.0071	8-G7 (H-G7)	-0.0284	9-H7 (L-G7)	-0.0022
4-G8 (D-G8)	0.0011	8-G8 (H-G8)	0.0185	9-H8 (L-G8)	-0.0023
4-G9 (D-G9)	0.0091	8-G9 (H-G9)	-0.0161	9-H9 (L-G9)	-0.0026
4-G10 (D-G10)	-0.0186	8-G10 (H-G10)	0.041	9-H10 (L-G10)	0.0202
4-G11 (D-G11)	-0.0025	8-G11 (H-G11)	0.0808	9-H11 (L-G11)	0.0179

TABLE C.2: Validation of primary FabF C164Q specific screening hits. Responses of FabF C164Q substracted with responses of FabF wild type.

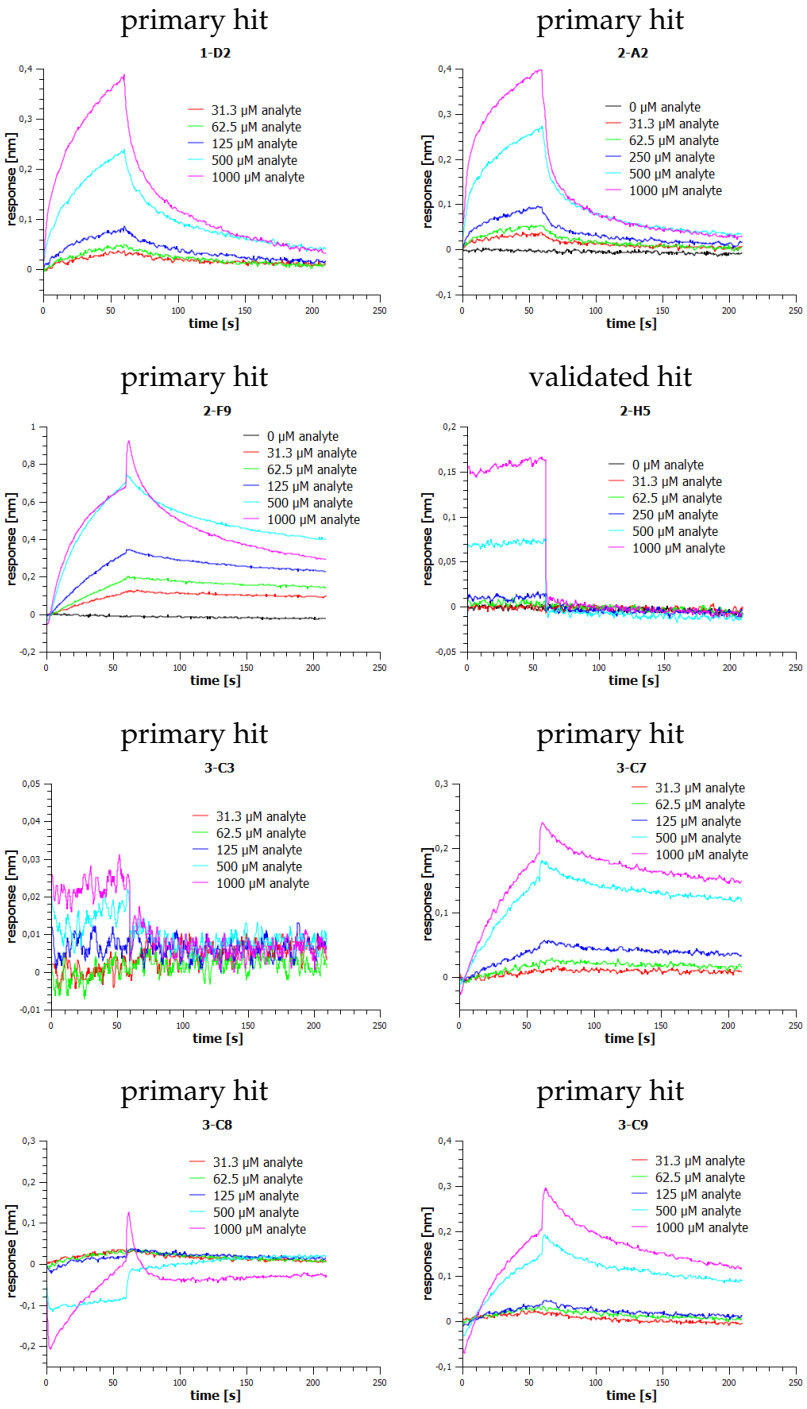

primary hit

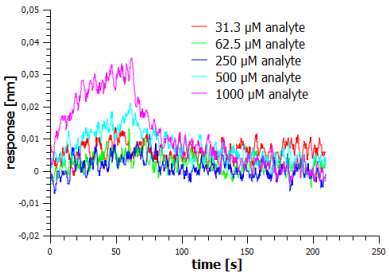

primary hit

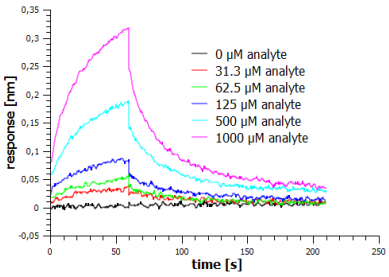

validated hit

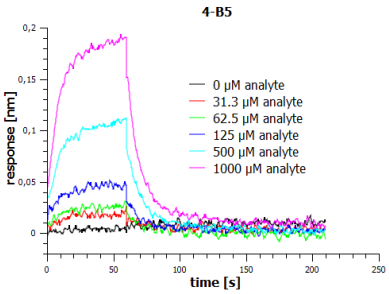

primary hit

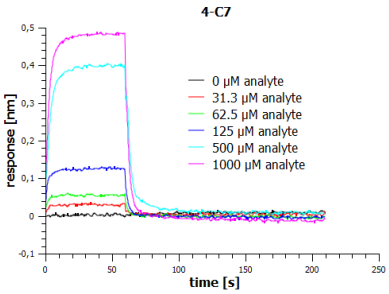

primary hit

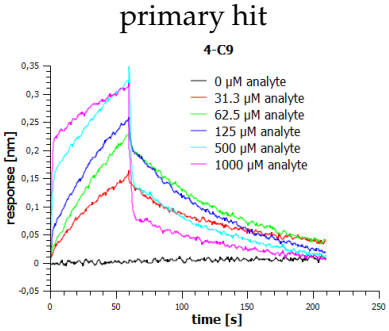

primary hit

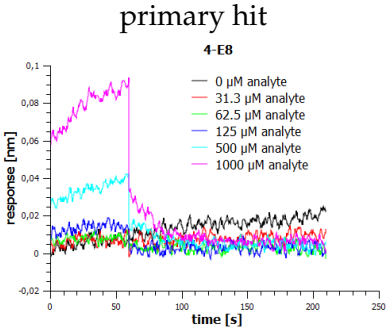

primary hit

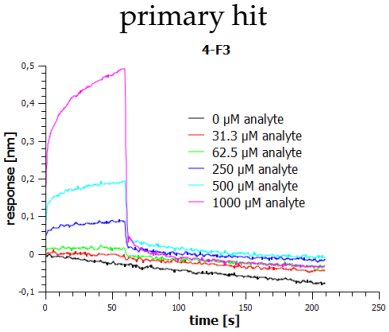

validated hit

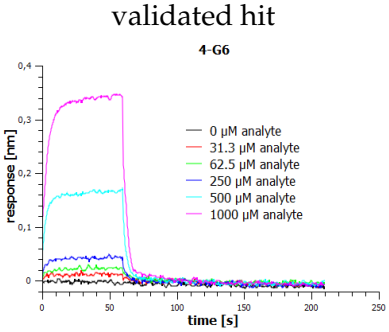

primary hit

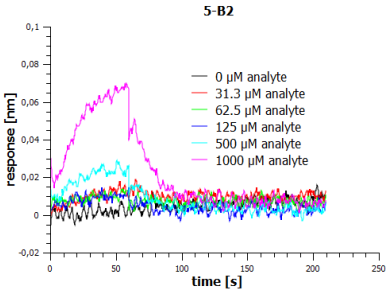

primary hit

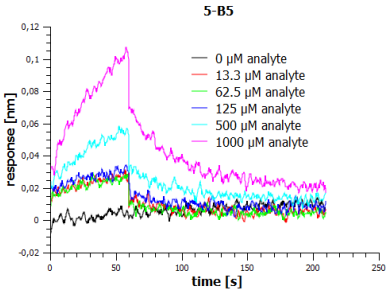

primary hit

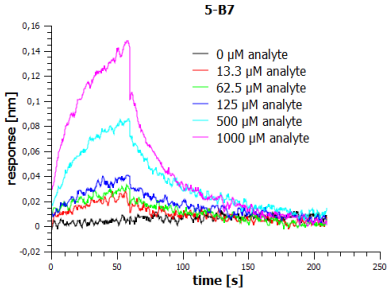

primary hit

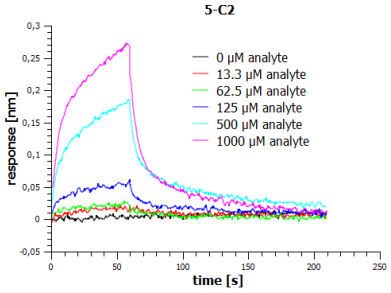

validated hit

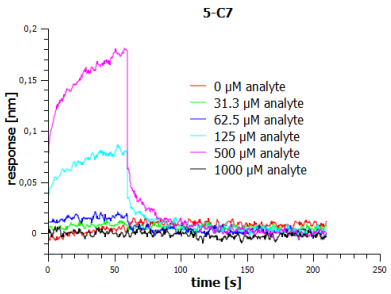

primary hit

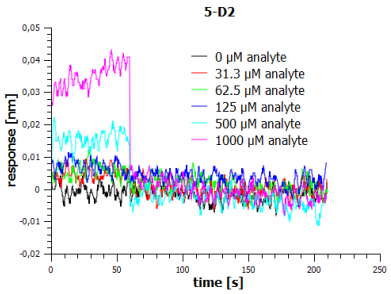

primary hit

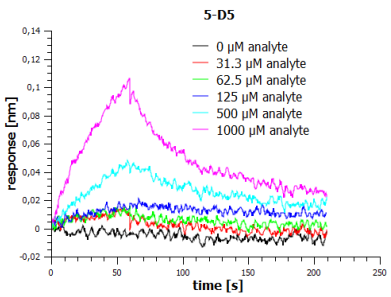

validated hit

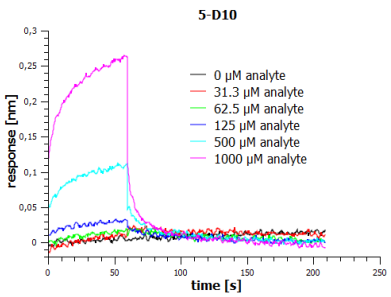

primary hit

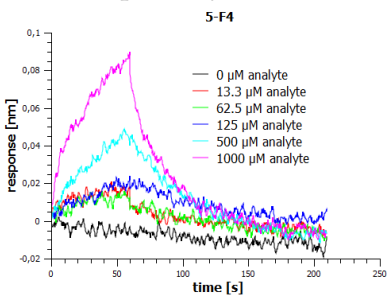

primary hit

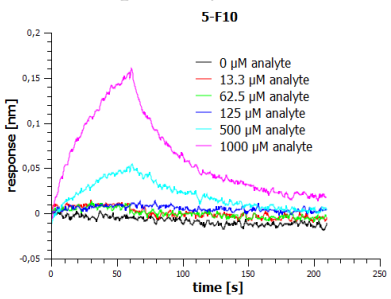

primary hit

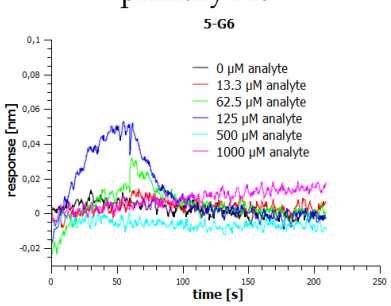

primary hit

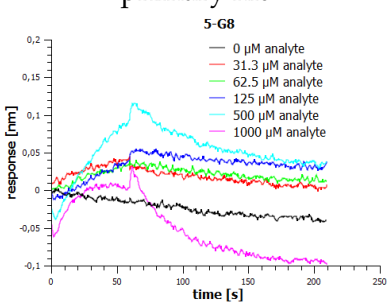

primary hit

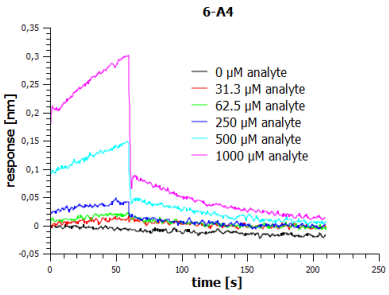

primary hit

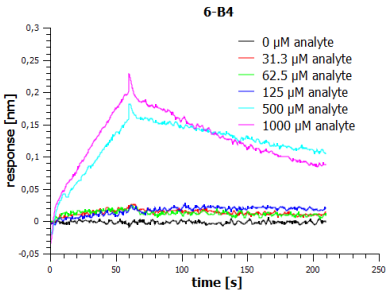

validated hit

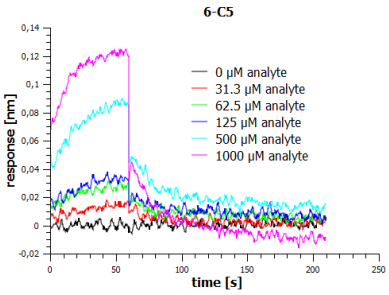

primary hit

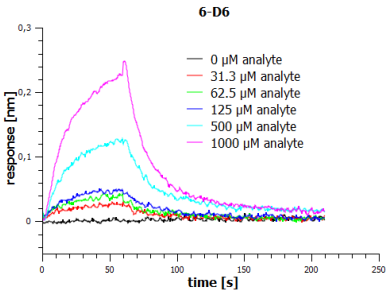

primary hit

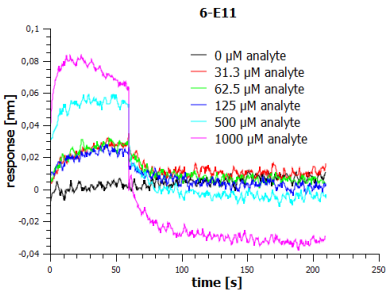

primary hit

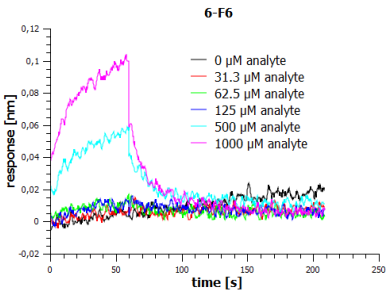

primary hit

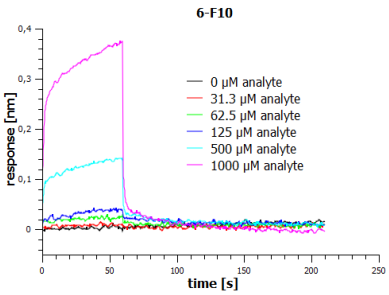

primary hit

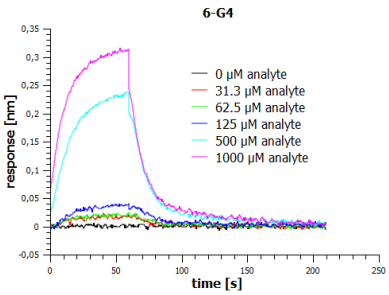

primary hit

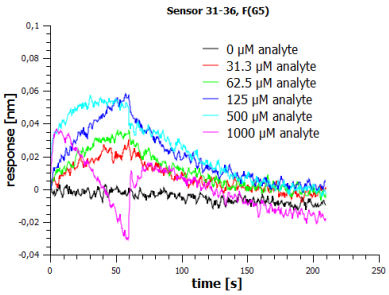

validated hit

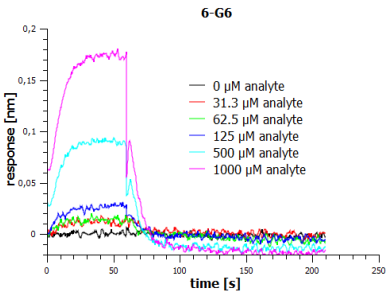

validated hit

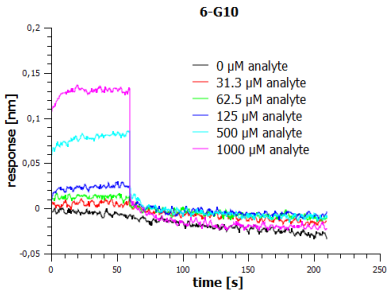

primary hit

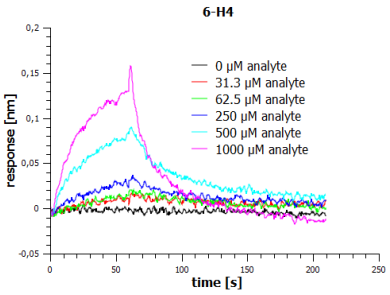

primary hit

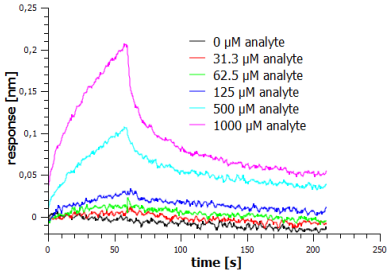

primary hit

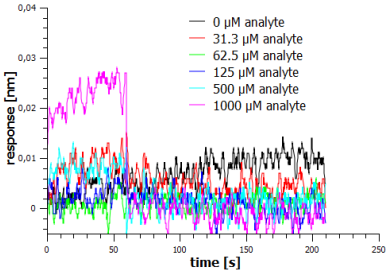

primary hit

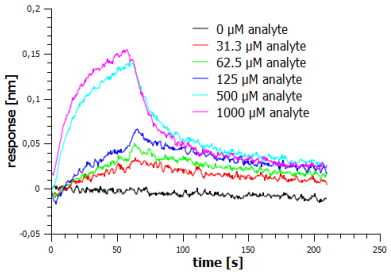

primary hit

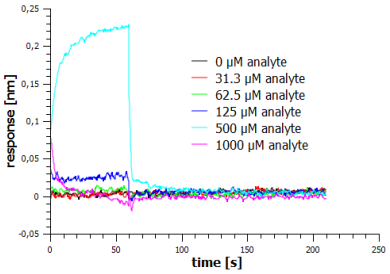

primary hit

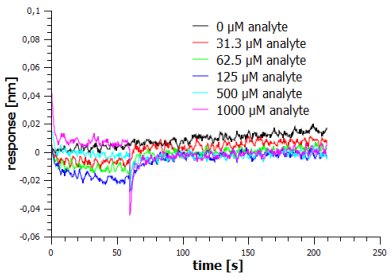

primary hit

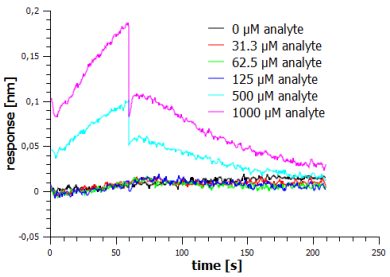

primary hit

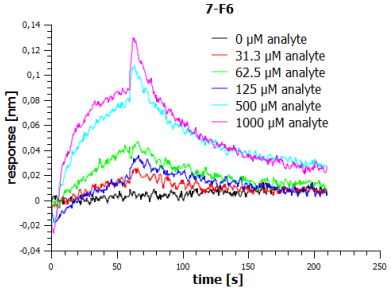

primary hit

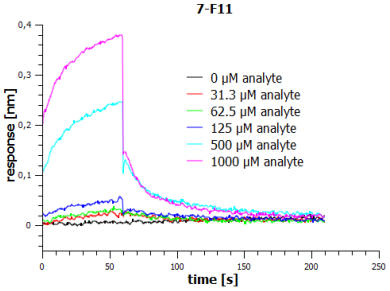

validated hit

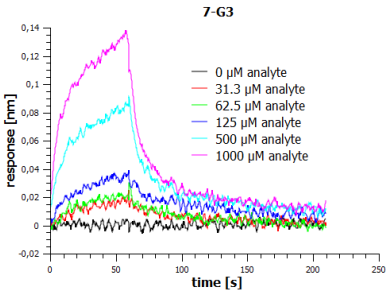

validated hit

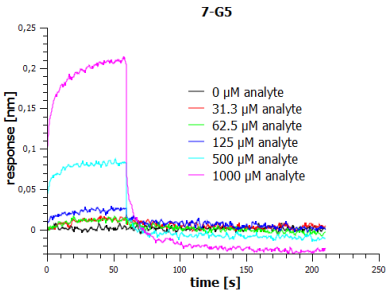

primary hit

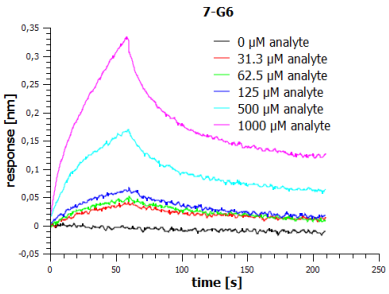

primary hit

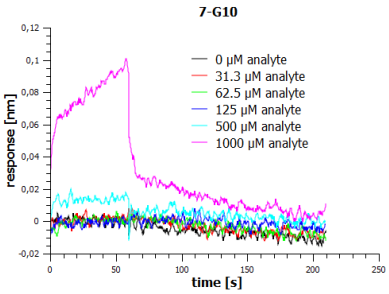

primary hit

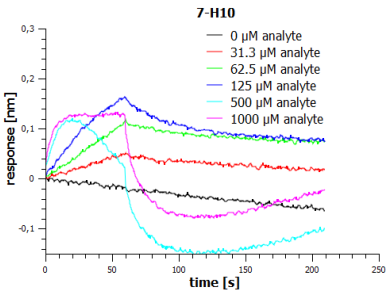

primary hit

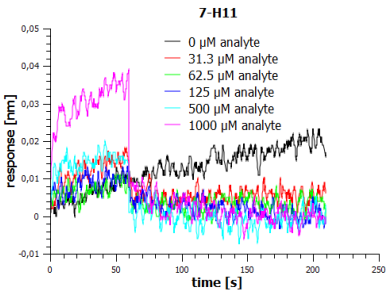

validated hit

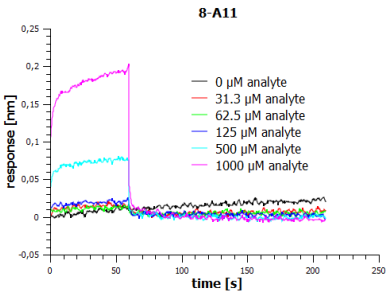

validated hit

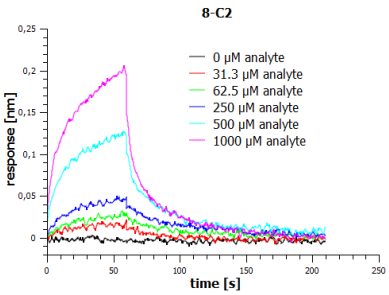

primary hit

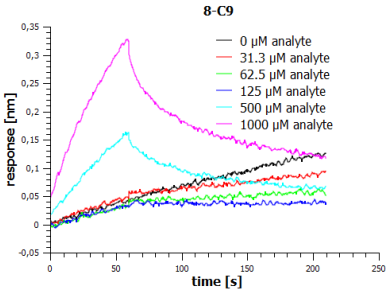

validated hit

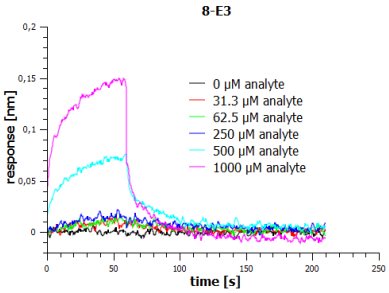

primary hit

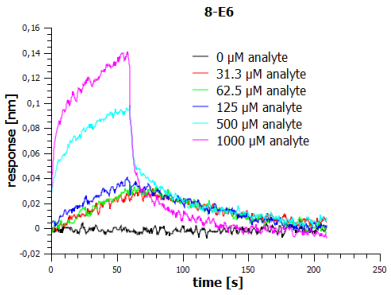

validated hit

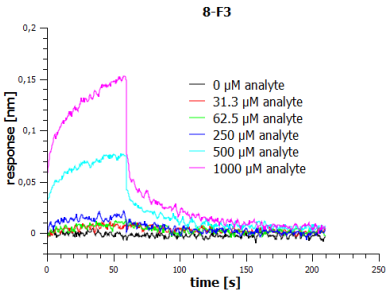

validated hit

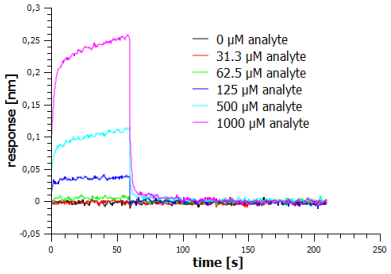

primary hit

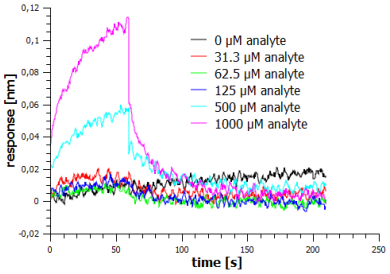

primary hit

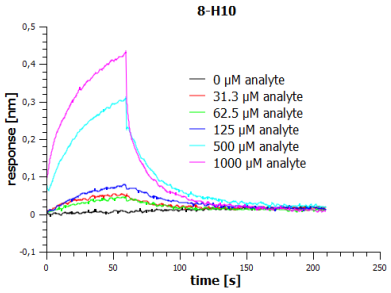

primary hit

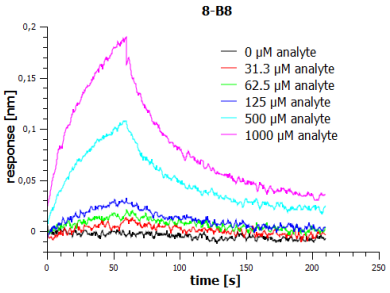

primary hit

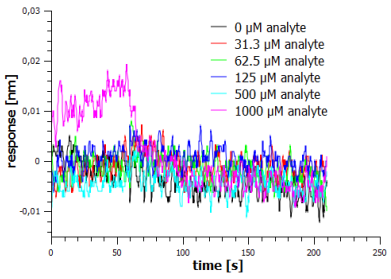

primary hit

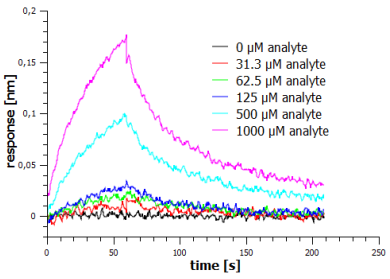

validated hit

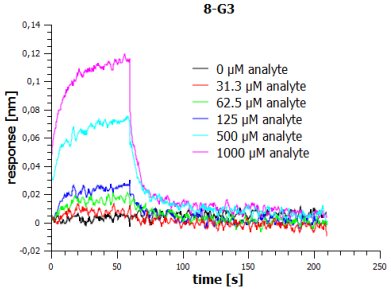

TABLE C.3: **Structures of FabF w. t. specific fragment screening hits.**

1-C8	1-F3	1-G3	1-G7
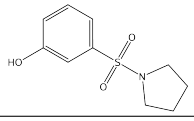	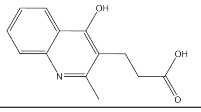	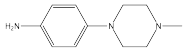	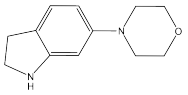
1-G10	3-B5	4-E9	6-C4
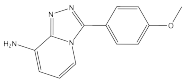	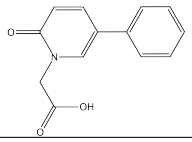	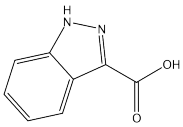	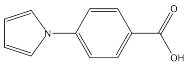
7-A6	7-A7	8-H3	
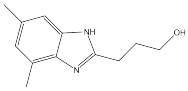	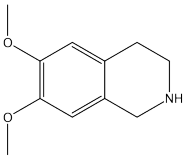	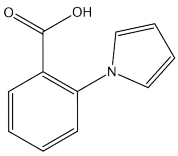	

Appendix D

Structure Validation

compound 1
solubility: 200 mM in DMSO
^{1}H-NMR (600 MHz, DMSO): not consistent with structure.
ESI-MS (*m/z*): $[M+H]^+$ calcd for $C_{11}H_{11}N_2O_2^+$ 203.1; found 203.1; $[M+Na]^+$ calcd for $C_{11}H_{10}N_2O_2Na^+$ 225.1; found 225.2.

compound 2
solubility: 200 mM in DMSO
^{1}H-NMR (600 MHz, DMSO): δ 8.54 - 7.88 (m, 3H), 7.55 - 7.49 (m, 1H), 7.48 - 7.45 (m, 1H).

compound 3
solubility: 200 mM in DMSO
^{1}H-NMR (600 MHz, DMSO): δ 8.35 - 7.97 (m, 2H), 2.18 (t, *J*=8.2 Hz, 1H), 1.21 - 1.11 (m, 4H).

compound 4
solubility: 200 mM in DMSO
^{1}H-NMR (600 MHz, DMSO): not consistent with structure.

compound 5
solubility: 200 mM in DMSO
^{1}H-NMR (600 MHz, DMSO): δ 6.81 (s, 1H).

compound 6
solubility: 100 mM in DMSO
^{1}H-NMR (600 MHz, DMSO): not consistent with structure.

compound 7
solubility: 200 mM in DMSO
^{1}H-NMR (600 MHz, DMSO): not consistent with structure.

compound 8
solubility: 100 mM in DMSO
^{1}H-NMR (600 MHz, DMSO): δ 7.74 - 7.66 (m, 1H), 7.48 - 6.89 (m, 4H), 2.38 - 2.34 (m, 2H), 2.08 - 1.97 (m, 4H).

compound 9
solubility: 200 mM in DMSO
^{1}H-NMR (600 MHz, DMSO): not consistent with structure.

compound 10
solubility: 200 mM in DMSO
^{1}H-NMR (600 MHz, DMSO): δ 8.03 (d, *J*=5.4 Hz, 1H), 7.98 (s, 1H), 7.47 (s, 1H), 7.19 - 6.90 (m, 2H), 6.88 (dd, *J*=1.1, 5.4 Hz, 1H), 3.93 (d, *J*=5.8 Hz, 2H).

compound 11
solubility: 200 mM in DMSO
^{1}H-NMR (600 MHz, DMSO): not consistent with structure.

compound 12
solubility: 200 mM in DMSO
^{1}H-NMR (600 MHz, DMSO): δ 10.14 - 10.08 (m, 1H), 6.62 - 6.51 (m, 1H), 3.54 - 3.49 (m, 1H), 1.84 - 1.78 (m, 2H), 1.65 (dd, *J*=4.0, 9.1 Hz, 2H), 1.57 - 1.50 (m, 1H), 1.36 - 1.07 (m, 5H).

compound 13
solubility: 100 mM in DMSO
^{1}H-NMR (600 MHz, DMSO): δ 11.95 - 11.85 (m, 1H), 1.72 - 1.53 (m, 5H), 1.53 - 1.42 (m, 3H), 1.27 - 1.04 (m, 3H), 0.90 - 0.82 (m, 2H).

compound 14
solubility: 200 mM in DMSO
^{1}H-NMR (600 MHz, DMSO): δ 12.31 - 12.26 (m, 1H), 7.92 (s, 1H), 7.84 (d, *J*=7.6 Hz, 1H), 7.33 (d, *J*=8.0 Hz, 1H), 2.32 - 2.20 (m, 6H).

compound 15
solubility: 200 mM in DMSO
^{1}H-NMR (600 MHz, DMSO): δ 9.38 (s, 1H), 7.99 (d, *J*=7.6 Hz, 1H), 7.61 (dd, *J*=7.6, 7.6 Hz, 1H), 7.52 (dd, *J*=7.6, 7.6 Hz, 1H), 7.19 (d, *J*=7.6 Hz, 1H), 6.04 (s, 2H).

compound 16
solubility: 200 mM in DMSO
^{1}H-NMR (600 MHz, DMSO): δ 7.34 (dd, *J*=7.4, 7.4 Hz, 2H), 7.31 - 7.20 (m, 3H), 4.57 - 4.48 (m, 2H), 4.29 - 4.25 (m, 1H), 3.54 - 3.48 (m, 1H), 2.16 - 2.10 (m, 1H), 2.06 - 1.73 (m, 3H), 1.63 (ddd, *J*=7.7, 10.3, 19.5 Hz, 1H).

compound 19
solubility: not dissolvable in DMSO.

compound 20
solubility: 200 mM in DMSO
^{1}H-NMR (600 MHz, DMSO): δ 10.59 (s, 1H), 8.27 (d, *J*=2.2 Hz, 1H), 7.89 (dd, *J*=2.5, 9.1 Hz, 1H), 7.72 (d, *J*=8.7 Hz, 1H), 6.42 (dd, *J*=9.8, 17.1 Hz, 1H), 6.35 - 6.30 (m, 1H), 5.85 (dd, *J*=1.6, 10.0 Hz, 1H).

compound 21
solubility: 200 mM in DMSO
^{1}H-NMR (600 MHz, DMSO): δ 10.49 (s, 1H), 8.18 (s, 1H), 7.88 - 7.85 (m, 1H), 7.67 - 7.50 (m, 2H), 6.43 (dd, *J*=10.2, 17.1 Hz, 1H), 6.32 (dd, *J*=1.8, 17.1 Hz, 1H), 5.83 (dd, *J*=1.6, 10.0 Hz, 1H).

compound 22
solubility: 200 mM in DMSO
^{1}H-NMR (600 MHz, DMSO): δ 10.94 (s, 1H), 10.72 (s, 1H), 7.57 - 7.53 (m, 2H), 7.36 (t, *J*=7.8 Hz, 2H), 7.11 (t, *J*=7.3 Hz, 1H), 6.51 - 6.44 (m, 2H), 5.97 (dd, *J*=2.5, 9.1 Hz, 1H).
ESI-MS (*m/z*): $[M+H]^+$ calcd for $C_{10}H_{11}N_2O_2^+$ 191.1; found 191.0; $[M+Na]^+$ calcd for $C_{10}H_{10}N_2O_2Na^+$ 213.1; found 213.0.

compound 22.1
solubility: 200 mM in DMSO
^{1}H-NMR (600 MHz, DMSO): δ 10.37 - 10.32 (m, 1H), 7.85 (s, 1H), 7.32 (s, 1H), 6.45 - 6.29 (m, 2H), 5.86 (dd, *J*=2.2, 9.8 Hz, 1H).
ESI-MS (*m/z*): $[M+H]^+$ calcd for $C_4H_7N_2O_2^+$ 115.0; found 115.1; $[M+Na]^+$ calcd for $C_4H_6N_2O_2Na^+$ 137.0; found 137.0.

compound 22.2
solubility: 200 mM in DMSO
^{1}H-NMR (600 MHz, DMSO): δ 10.48 (s, 1H), 8.31 (s, 1H), 6.44 - 6.29 (m, 2H), 5.86 (dd, *J*=2.0, 9.6 Hz, 1H), 2.74 - 2.72 (m, 3H).
ESI-MS (*m/z*): $[M+H]^+$ calcd for $C_5H_9N_2O_2^+$ 129.1; found 129.1; $[M+Na]^+$ calcd for $C_5H_8N_2O_2Na^+$ 151.1; found 151.0.

compound 22.3
solubility: 200 mM in DMSO
^{1}H-NMR (600 MHz, DMSO): δ 10.47 (s, 1H), 8.34 - 8.32 (m, 1H), 6.45 - 6.30 (m, 2H), 5.87 (dd, *J*=1.8, 9.8 Hz, 1H), 3.88 - 3.81 (m, 1H), 1.15 - 1.13 (m, 6H).
ESI-MS (*m/z*): $[M+H]^+$ calcd for $C_7H_{13}N_2O_2^+$ 157.1; found 157.0; $[M+Na]^+$ calcd for $C_7H_{12}N_2O_2Na^+$ 179.1; found 179.0.

compound 22.4
solubility: 200 mM in DMSO
^{1}H-NMR (600 MHz, DMSO): δ 10.59 (s, 1H), 8.87 (t, *J*=6.2 Hz, 1H), 7.35 (dd, *J*=7.6, 7.6 Hz, 2H), 7.32 - 7.22 (m, 3H), 6.46 - 6.31 (m, 2H), 5.88 (dd, *J*=1.8, 10.2 Hz, 1H), 4.41 (d, *J*=5.8 Hz, 2H).
ESI-MS (*m/z*): $[M+H]^+$ calcd for $C_{11}H_{13}N_2O_2^+$ 205.1; found 205.1; $[M+Na]^+$ calcd for $C_{11}H_{12}N_2O_2Na^+$ 227.1; found 227.1.

compound 22.5
solubility: 200 mM in DMSO
^{1}H-NMR (600 MHz, DMSO): δ 10.49 (s, 1H), 8.61 (d, *J*=6.9 Hz, 1H), 6.44 - 6.30 (m, 2H), 5.87 (dd, *J*=2.2, 9.4 Hz, 1H), 4.22 - 4.17 (m, 1H), 2.25 - 2.10 (m, 2H), 1.96 - 1.87 (m, 2H), 1.69 - 1.58 (m, 2H).
ESI-MS (*m/z*): $[M+H]^+$ calcd for $C_8H_{13}N_2O_2^+$ 169.1; found 169.1; $[M+Na]^+$ calcd for $C_8H_{12}N_2O_2Na^+$ 191.1; found 191.0.

compound 22.6
solubility: 200 mM in DMSO
^{1}H-NMR (600 MHz, DMSO): δ 10.50 (s, 1H), 8.51 (d, *J*=7.3 Hz, 1H), 6.44 - 6.30 (m, 2H), 5.87 (dd, *J*=2.0, 9.6 Hz, 1H), 3.97 - 3.91 (m, 1H), 1.12 (d, *J*=6.5 Hz, 3H).
ESI-MS (*m/z*): $[M+H]^+$ calcd for $C_8H_{15}N_2O_3^+$ 187.1; found 187.1; $[M+Na]^+$ calcd for $C_8H_{14}N_2O_3Na^+$ 209.1; found 209.1.

compound 22.7
ESI-MS (*m/z*): $[M+H]^+$ calcd for $C_{14}H_{21}N_2O_2^+$ 249.1; found 249.2; $[M+Na]^+$ calcd for $C_{14}H_{20}N_2O_2Na^+$ 271.1; found 271.2.

compound 23
solubility: 200 mM in DMSO
^{1}H-NMR (600 MHz, DMSO): not consistent with structure.

compound 24
solubility: 200 mM in DMSO
^{1}H-NMR (600 MHz, DMSO): not consistent with structure.

compound 25
solubility: 200 mM in DMSO
^{1}H-NMR (600 MHz, DMSO): δ 10.39 (s, 1H), 8.16 (s, 1H), 3.81 (t, *J*=6.2 Hz, 2H), 2.72 - 2.70 (m, 3H).

compound 26
solubility: 200 mM in DMSO
^{1}H-NMR (600 MHz, DMSO): not consistent with structure.

compound 27
solubility: 200 mM in DMSO
^{1}H-NMR (600 MHz, DMSO): δ 10.42 - 10.39 (m, 1H), 8.32 - 8.03 (m, 2H), 6.93 (d, *J*=5.1 Hz, 1H), 6.22 (dd, *J*=10.2, 17.1 Hz, 1H), 6.07 (dd, *J*=1.8, 17.1 Hz, 1H), 5.56 (dd, *J*=1.8, 10.2 Hz, 1H), 3.52 - 3.50 (m, 2H), 2.34 - 2.25 (m, 5H).
ESI-MS (*m/z*): $[M+H]^+$ calcd for $C_{12}H_{16}N_3O_2^+$ 234.1; found 234.2; $[M+Na]^+$ calcd for $C_{12}H_{15}N_3O_2Na^+$ 256.1; found 256.1.

compound 28
solubility: not dissolvable in DMSO.

compound 29
solubility: 200 mM in DMSO
^{1}H-NMR (600 MHz, DMSO): δ 7.80 (dd, *J*=6.4, 6.4 Hz, 1H), 5.66 (s, 1H), 5.32 (d, *J*=1.1 Hz, 1H), 4.68 (d, *J*=4.7 Hz, 1H), 3.73 - 3.65 (m, 1H), 3.07 - 3.03 (m, 2H), 1.86 (s, 3H), 1.01 (d, *J*=6.2 Hz, 3H).

compound 30
solubility: 200 mM in DMSO
^{1}H-NMR (600 MHz, DMSO): not consistent with structure.

compound 31
solubility: 200 mM in DMSO
^{1}H-NMR (600 MHz, DMSO): not consistent with structure.

compound 32
solubility: 200 mM in DMSO
^{1}H-NMR (600 MHz, DMSO): not consistent with structure.

compound 33
solubility: 200 mM in DMSO
^{1}H-NMR (600 MHz, DMSO): δ 9.49 (s, 1H), 8.68 (d, *J*=6.9 Hz, 1H), 7.20 (d, *J*=8.7 Hz, 2H), 6.76 (d, *J*=8.7 Hz, 2H), 6.42 (dd, *J*=10.2, 17.1 Hz, 1H), 6.12 (dd, *J*=1.8, 17.1 Hz, 1H), 5.61 (dd, *J*=1.8, 10.2 Hz, 1H), 5.26 (d, *J*=7.3 Hz, 1H).

compound 34
solubility: 200 mM in DMSO
^{1}H-NMR (600 MHz, DMSO): δ 11.63 (s, 1H), 8.53 (d, *J*=8.4 Hz, 1H), 8.25 (s, 1H), 7.80 - 7.78 (m, 1H), 7.69 (s, 1H), 7.50 - 7.46 (m, 1H), 7.10 (dd, *J*=7.4, 7.4 Hz, 1H), 5.77 (s, 1H), 2.14 (s, 3H), 1.89 (s, 3H).

compound 35
solubility: 200 mM in DMSO
^{1}H-NMR (600 MHz, DMSO): not consistent with structure.

compound 4-B5
solubility: 200 mM in DMSO
^{1}H-NMR (850 MHz, DMSO): δ 10.48 (s, 1H), 7.74 (d, *J*=1.8 Hz, 1H), 7.41 (d, *J*=8.0 Hz, 1H), 7.37 (dd, *J*=8.0, 8.0 Hz, 1H), 7.16 (d, *J*=7.8 Hz, 1H), 3.92 (s, 2H).

compound 4-G6
solubility: 200 mM in DMSO
^{1}H-NMR (850 MHz, DMSO): δ 10.06 (s, 1H), 9.41 (s, 1H), 8.02 - 8.01 (m, 1H), 7.85 (d, *J*=4.9 Hz, 1H), 7.28 (s, 1H), 7.23 - 7.21 (m, 1H), 7.15 - 7.09 (m, 2H), 6.52 - 6.50 (m, 1H).

compound 5-B2
solubility: 200 mM in DMSO
^{1}H-NMR (850 MHz, DMSO): δ 7.17 - 7.09 (m, 2H), 6.87 - 6.82 (m, 2H), 4.78 (s, 2H), 3.52 - 3.38 (m, 4H), 2.19 (s, 3H), 1.61 - 1.58 (m, 2H), 1.52 - 1.51 (m, 2H), 1.44 - 1.42 (m, 2H).

compound 5-C7
solubility: 200 mM in DMSO
^{1}H-NMR (850 MHz, DMSO): δ 8.41 (s, 1H), 7.26 - 7.23 (m, 2H), 7.00 - 6.98 (m, 2H), 6.82 (t, textitJ=7.3 Hz, 1H), 6.78 (s, 1H), 3.76 (t, *J*=5.1 Hz, 4H), 3.21 (t, *J*=5.2 Hz, 4H), 2.28 (s, 3H).

compound 5-D5
solubility: 200 mM in DMSO
^{1}H-NMR (850 MHz, DMSO): δ 7.46 (dd, *J*=2.2, 2.2 Hz, 2H), 6.39 (dd, *J*=2.2, 2.2 Hz, 2H), 2.71 (s, 3H).

compound 5-D10
solubility: 200 mM in DMSO
^{1}H-NMR (850 MHz, DMSO): δ 8.36 (d, *J*=7.0 Hz, 1H), 7.75 (d, *J*=8.8 Hz, 2H), 7.61 (d, *J*=8.8 Hz, 1H), 7.50 (s, 1H), 7.12 (d, *J*=8.8 Hz, 2H), 6.80 (dd, *J*=6.2, 9.1 Hz, 1H), 6.70 - 6.67 (m, 1H), 3.85 (s, 3H).

compound 6-G6
solubility: 200 mM in DMSO
^{1}H-NMR (850 MHz, DMSO): δ 8.36 (d, *J*=6.5 Hz, 1H), 8.21 (s, 1H), 7.27 (d, *J*=1.8 Hz, 1H), 7.10 - 7.04 (m, 2H), 7.03 (d, *J*=6.7 Hz, 1H), 6.77 (dd, *J*=6.7, 6.7 Hz, 1H), 6.52 - 6.50 (m, 1H), 5.13 (s, 2H), 2.55 - 2.48 (m, 3H).

compound 7-A10
solubility: 200 mM in DMSO
^{1}H-NMR (850 MHz, DMSO): δ 10.55 (s, 1H), 8.78 - 8.76 (m, 1H), 8.32 (s, 1H), 7.78 (d, *J*=8.0 Hz, 1H), 7.63 - 7.60 (m, 1H), 6.64 (d, *J*=1.8 Hz, 1H), 5.96 - 5.90 (m, 2H), 4.43 (d, *J*=5.4 Hz, 2H).

compound 7-G5
solubility: 200 mM in DMSO
^{1}H-NMR (850 MHz, DMSO): δ 7.76 (s, 1H), 7.66 (d, *J*=7.8 Hz, 2H), 7.39 (d, *J*=7.8 Hz, 2H), 7.36 (s, 1H), 5.04 (t, *J*=5.7 Hz, 1H), 4.48 (d, *J*=5.7 Hz, 2H), 2.40 (s, 3H).

compound 8-B8
solubility: 200 mM in DMSO
^{1}H-NMR (850 MHz, DMSO): δ 8.27 - 8.23 (m, 3H), 8.05 (d, *J*=3.1 Hz, 1H), 7.97 (d, *J*=3.1 Hz, 1H), 7.91 - 7.89 (m, 1H), 7.66 - 7.64 (m, 1H), 7.62 - 7.58 (m, 2H), 4.30 (s, 2H).

compound 8-C2
solubility: 200 mM in DMSO
^{1}H-NMR (850 MHz, DMSO): not consistent with structure.

compound 8-C11
solubility: 200 mM in DMSO
^{1}H-NMR (850 MHz, DMSO): not consistent with structure.

compound 8-E3
solubility: 200 mM in DMSO
^{1}H-NMR (850 MHz, DMSO): δ 7.29 (dd, *J*=7.5, 7.5 Hz, 2H), 7.25 (d, *J*=6.7 Hz, 2H), 7.21 (t, *J*=7.3 Hz, 1H), 7.14 (dd, *J*=7.7, 7.7 Hz, 1H), 6.84 (d, *J*=7.3 Hz, 1H), 6.74 (d, *J*=8.0 Hz, 1H), 5.36 (s, 2H), 4.17 (s, 2H), 3.75 (t, *J*=7.4 Hz, 2H), 2.92 (t, *J*=7.4 Hz, 2H).

compound 8-F3
solubility: 200 mM in DMSO
^{1}H-NMR (850 MHz, DMSO): δ 7.53 - 7.47 (m, 3H), 7.40 (dd, *J*=7.5, 7.5 Hz, 2H), 7.33 (t, *J*=7.4 Hz, 1H), 7.08 (d, *J*=7.8 Hz, 1H), 6.48 (dd, *J*=4.9, 7.8 Hz, 1H), 5.63 (s, 2H), 5.12 (s, 2H).

compound 8-G3
solubility: 200 mM in DMSO
^{1}H-NMR (850 MHz, DMSO): δ 9.14 (s, 1H), 7.74 - 7.74 (m, 1H), 6.85 (d, *J*=8.0 Hz, 1H), 6.78 (d, *J*=1.6 Hz, 1H), 6.71 (dd, *J*=1.6, 8.0 Hz, 1H), 5.99 (s, 2H), 5.18 (d, *J* =3.6 Hz, 1H), 2.28 (s, 3H), 2.09 (s, 3H).

Bibliography

Afonine, Pavel V, Ralf W Grosse Kunstleve, Nathaniel Echols, Jeffrey J Headd, Nigel W Moriarty, et al. (2012). "Towards automated crystallographic structure refinement with phenix.refine". In: *Acta Crystallographica Section D: Biological Crystallography* 68.4, pp. 352–367.

Ambler, R P (1980). "The structure of β-lactamases". In: *Philosophical Transactions of the Royal Society of London* 289.1036, pp. 321–331.

Amino, Yusuke, Yoshinobu Takino, Megumi Kaneko, Fumie Ookura, Mai Yamamoto, et al. (2016). "Synthesis, Characterization, and Evaluation of Thiazolidine Derivatives of Cysteine for Suppressing Eumelanin Production". In: *Chemical & Pharmaceutical Bulletin* 64.12, pp. 1681–1691.

Andres, Charles J, Joanne J Bronson, Stanley V D'Andrea, Milind S Deshpande, Paul J Falk, et al. (2000). "4-Thiazolidinones: Novel inhibitors of the bacterial enzyme MurB". In: *Bioorganic and Medicinal Chemistry Letters* 10.8, pp. 715–717.

Antunes, Dinler A, Didier Devaurs, and Lydia E Kavraki (2015). "Understanding the challenges of protein flexibility in drug design." In: *Expert Opinion on Drug Discovery* 10.12, pp. 1301–1313.

Baillie, Thomas A (2016). "Targeted Covalent Inhibitors for Drug Design". In: *Angewandte Chemie - International Edition* 55, pp. 13408–13421.

Banerjee, A, E Dubnau, A Quemard, V Balasubramanian, Kyung Sun Um, et al. (1994). "inhA, a gene encoding a target for isoniazid and thionamide in Mycobacterium tuberculosis". In: *Science* 263.5144, pp. 227–230.

Bauer, Renato A (2015). "Covalent inhibitors in drug discovery: From accidental discoveries to avoided liabilities and designed therapies". In: *Drug Discovery Today* 20.9, pp. 1061–1073.

Baum, B, L S Lecker, M Zoltner, E Jaenicke, R Schnell, et al. (2015). "Structures of *Pseudomonas aeruginosa* β-ketoacyl- (acyl - carrier - protein) synthase II (FabF) and a C164Q mutant provide templates for antibacterial drug discovery and identify a buried potassium ion and a ligand-binding site that is an artefact of the crystal form". In: *Acta Crystallographica Section F: Structural Biology Communications* 71, pp. 1020–1026.

Bebrone, Carine, Catherine Moali, Florence Mahy, Sandrine Rival, Jean D Docquier, et al. (2001). "CENTA as a chromogenic substrate for studying β-lactamases". In: *Antimicrobial Agents and Chemotherapy* 45.6, pp. 1868–1871.

Bello, Martiniano, Marlet Martínez Archundia, and José Correa Basurto (2013). "Automated docking for novel drug discovery." In: *Expert opinion on drug discovery* 8.7, pp. 821–34.

Berman, Helen M, John Westbrook, Zukang Feng, Gary Gilliland, T N Bhat, et al. (2000). "The Protein Data Bank". In: *Nucleic acids research* 28.1, pp. 235–242.

Bjelton, Lilian and Gun Brit Fransson (1990). "Availability of Cysteine and of L-2-Oxo-Thiazolidine-4-Carboxylic Acid as a Source of Cysteine in

Intravenous Nutrition". In: *Journal of Parenteral and Enteral Nutrition* 14.2, pp. 177–182.

Böhm, Hans Joachim (1994). "The development of a simple empirical scoring function to estimate the binding constant for a protein-ligand complex of known three-dimensional structure". In: *Journal of Computer Aided Molecular Design* 8.3, pp. 243–256.

Borgaro, Janine G, Andrew Chang, Carl A MacHutta, Xujie Zhang, and Peter J Tonge (2011). "Substrate recognition by β-ketoacyl-ACP synthases". In: *Biochemistry* 50.49, pp. 10678–10686.

Brenk, Ruth, John J Irwin, and Brian Shoichet (2005). "Here Be Dragons: Docking and Screening in an Uncharted Region of Chemical Space". In: *Journal of Biomolecular Screening* 10.7, pp. 667–674.

Brenk, Ruth, Alessandro Schipani, Daniel James, Agata Krasowski, Ian Hugh Gilbert, et al. (2008). "Lessons learnt from assembling screening libraries for drug discovery for neglected diseases". In: *ChemMedChem* 3.3, pp. 435–444.

Brünger, Axel T (1992). "Free R value: a novel statistical quantity for assessing the accuracy of crystal structures". In: *Nature* 355, pp. 472–475.

Cantón, R, M Akóva, Y Carmeli, C G Giske, Y Glupczynski, et al. (2012). "Rapid evolution and spread of carbapenemases among *Enterobacteriaceae* in Europe". In: *Clinical Microbiology and Infection* 18.5, pp. 413–431.

Chayen, Naomi E (2004). "Turning protein crystallisation from an art into a science". In: *Current Opinion in Structural Biology* 14.5, pp. 577–583.

Chen, Yu and Brian K Shoichet (2009). "Molecular docking and ligand specificity in fragment-based inhibitor discovery". In: *Nature Chemical Biology* 5.5, pp. 358–364.

Christopeit, Tony, Ke-Wu Yang, Shao-Kang Yang, and Hanna-Kirsti S Leiros (2016). "The structure of the metallo-β-lactamase VIM-2 in complex with a triazolylthioacetamide inhibitor research communications". In: *Acta Crystallographica Section F: Structural Biology Communications* 72, pp. 813–819.

Coleman, Ken (2011). "Diazabicyclooctanes (DBOs): a potent new class of non-β-lactam β-lactamase inhibitors". In: *Current Opinion in Microbiology* 14.5, pp. 550–555.

Congreve, Miles, Robin Carr, Chris Murray, and Harren Jhoti (2003). "A 'Rule of Three' for fragment-based lead discovery?" In: *Drug Discovery Today* 8.19, pp. 876–877.

Cornell, Wendy D, Piotr Cieplak, Christopher I Bayly, and Peter A Kollman (1993). "Application of RESP Charges To Calculate Conformational Energies, Hydrogen Bond Energies, and Free Energies of Solvation". In: *Journal of the American Chemical Society* 115.21, pp. 9620–9631.

Credico, Barbara Di, Gianna Reginato, Luca Gonsalvi, Maurizio Peruzzini, and Andrea Rossin (2011). "Selective synthesis of 2-substituted 4-carboxy oxazoles, thiazoles and thiazolidines from serine or cysteine amino acids". In: *Tetrahedron* 67.1, pp. 267–274.

Da Silva, Ivanildo Mangueira, João Da Silva Filho, Priscila Brandão Gomes Da Silva Santiago, Micalyne Soares Do Egito, Carlos André De Souza, et al. (2014). "Synthesis and antimicrobial activities of 5-arylidene-thiazolidine-2,4- dione derivatives". In: *BioMed Research International* 5, pp. 1–8.

Dai, Ling-Ling, Hui-Zhen Zhang, Sangaraiah Nagarajan, Syed Rasheed, and Cheng-He Zhou (2015). "Synthesis of tetrazole compounds as a

novel type of potential antimicrobial agents and their synergistic effects with clinical drugs and interactions with calf thymus DNA". In: *Medicinal Chemistry Communications* 6.1, pp. 147–154.

Danley, Dennis E (2006). "Crystallization to obtain protein-ligand complexes for structure-aided drug design". In: *Acta Crystallographica Section D: Biological Crystallography* 62.6, pp. 569–575.

Diederichs, Kay (2010). "Quantifying instrument errors in macromolecular X - Ray data sets". In: *Acta Crystallographica Section D: Biological Crystallography* 66.6, pp. 733–740.

Doran, James L, Brenda K Leskiw, Sven Aippersbach, and Susan E Jensen (1990). "Isolation and Characterization of a β-Lactamase Inhibitory Protein from *Streptomyces clavuligerus* and Cloning and Analysis of the Corresponding Gene". In: *Journal of Bacteriology* 172.9, pp. 4909–4918.

Doyle, Sharon A (2005). "Screening for the expression of soluble recombinant protein in Escherichia coli." In: *Methods in molecular biology* 310.1, pp. 115–121.

Drekonja, Dimitri M, Susan E Beekmann, Sean Elliott, Deepa Mukundan, Hari Polenakovik, et al. (2014). "Challenges in the Management of Infections due to Carbapenem-Resistant *Enterobacteriaceae*". In: *Infection Control and Hospital Epidemiology* 35.4, pp. 437–439.

Du, Xing, Yi Li, Yuan-Ling Xia, Shi-Meng Ai, Jing Liang, et al. (2016). "Insights into Protein–Ligand Interactions: Mechanisms, Models, and Methods". In: *International Journal of Molecular Sciences* 17.2, p. 144.

Edwards, Patricia, Janet Sabo Nelsen, James G Metz, and Katayoon Dehesh (1997). "Cloning of the fabF gene in an expression vector and in vitro characterization of recombinant fabF and fabB encoded enzymes from *Escherichia coli*". In: *FEBS Letters* 402.1, pp. 62–66.

Elguero, Jose, Pilar Goya, and Isabel Rozas (1989). "An Ab Initio Comparative Study of the Electronic Properties of Sulfonamides and Amides". In: *Journal of Molecular Structure (Theochem)* 184, pp. 115–129.

Elinder, Malin, Matthis Geitmann, Thomas Gossas, Per Källblad, Johan Winquist, et al. (2011). "Experimental validation of a fragment library for lead discovery using SPR biosensor technology." In: *Journal of Biomolecular Screening* 16.1, pp. 15–25.

Emsley, P, B Lohkamp, WG Scott, and K Cowtan (2010). "Features and development of Coot". In: *Acta Crystallographica Section D: Biological Crystallography* D66, pp. 486–501.

Evans, Philip (2006). "Scaling and assessment of data quality". In: *Acta Crystallographica Section D: Biological Crystallography* 62.1, pp. 72–82.

Farley, Christopher and Douglas H Juers (2014). "Efficient cryoprotection of macromolecular crystals using vapor diffusion of volatile alcohols". In: *Journal of Structural Biology* 188, pp. 102–106.

Feinn, Liana, Joshua Dudley, Adiel Coca, and L Roberts Elizabeth (2017). "Antimicrobial Evaluation of 5-Substituted Aryl 1H-Tetrazoles". In: *Medicinal Chemistry* 13.4, pp. 359–364.

Feldwisch-Drentrup, Hinnerk (2017). "Patientin verstirbt mit Resistenz gegen 26 Antibiotika". In: *Deutsche Apotheker Zeitung*.

Feng, Zhiyang, Debjani Chakraborty, Scott B S B Dewell, B V B Boojala Vijay B Reddy, and Sean F S F Brady (2012). "Environmental DNA encoded antibiotics fasa-mycin A and B inhibit FabF in type II fatty-acid biosynthesis." In: *Journal of the American Chemical Society* 134.6, pp. 2981–2987.

Fisher, Martin, Ramkrishna Basak, Arnout P Kalverda, Colin W G Fishwick, W Bruce Turnbull, and Adam Nelson (2014). "Discovery of novel FabF ligands inspired by platensimycin by integrating structure based design with diversity oriented synthetic accessibility". In: *Organic & Biomolecular Chemistry* 12.3, pp. 486–494.

Flanagan, Mark E, Joseph A Abramite, Dennis P Anderson, Ann Aulabaugh, Upendra P Dahal, et al. (2014). "Chemical and computational methods for the characterization of covalent reactive groups for the pro-spective design of irreversible inhibitors". In: *Journal of Medicinal Chemistry* 57.23, pp. 10072–10079.

French, G L (2010). "The continuing crisis in antibiotic resistance". In: *International Journal of Antimicrobial Agents* 36, S3–S7.

Friesner, Richard A, Jay L Banks, Robert B Murphy, Thomas A Halgren, Jasna J Klicic, et al. (2004). "Glide: A New Approach for Rapid, Accurate Docking and Scoring. 1. Method and Assessment of Docking Accuracy". In: *Journal of Medicinal Chemistry* 47.7, pp. 1739–1749.

García-Ruiz, Juan Manuel (2003). "Nucleation of protein crystals". In: *Journal of Structural Biology* 142, pp. 22–31.

Garwin, Jeffrey L, Amy L Klages, and John E Cronan (1980). "Structural, Enzymatic, and Genetic Studies of β-Ketoacyl-Acyl Carrier Protein Synthases I and II of *Escherichia coli*". In: *Journal of Biological Chemistry* 255.24, pp. 11949–11956.

Gellatly, Shaan L and Robert E W Hancock (2013). "*Pseudomonas aeruginosa*: New insights into pathogenesis and host defenses". In: *Pathogens and Disease* 67.3, pp. 159–173.

Giannetti, Anthony M, Bruce D Koch, and Michelle F Browner (2008). "Surface Plasmon Resonance Based Assay for the Detection and Characterization of Promiscuous Inhibitors". In: *Journal of Medicinal Chemistry* 51.3, pp. 574–580.

Gioiello, Antimo, Emiliano Rosatelli, Michela Teofrasti, Paolo Filipponi, and Roberto Pellicciari (2013). "Building a Sulfonamide Library by Eco-Friendly Flow Synthesis". In: *Amerian Chemical Society Combinatorial Science* 15.5, pp. 235–239.

Goncalves, Victor, James A Brannigan, Emmanuelle Thinon, Tayo O Olaleye, Remigiusz Serwa, et al. (2012). "A fluorescence-based assay for N-myristoyl-transferase activity". In: *Analytical Biochemistry* 421, pp. 342–344.

Grzegorek, Katharina (2015). "Nach der Keimkrise ist vor der Keimkrise". In: *Aerzte Zeitung*.

Gududuru, Veeresa, Eunju Hurh, James T Dalton, and Duane D Miller (2005). "Discovery of 2 - arylthiazolidine - 4 - carboxylic acid amides as a new class of cytotoxic agents for prostate cancer". In: *Journal of Medicinal Chemistry* 48.7, pp. 2584–2588.

Guedes, Isabella A, Camila S de Magalhaes, and Laurent E Dardenne (2014). "Receptor-ligand molecular docking". In: *Biophysical Reviews* 6.1, pp. 75–87.

Hanes, Melinda S, Kevin M Jude, James M Berger, Robert A Bonomo, and Tracy M Handel (2009). "Structural and Biochemical Characterization of the Interaction between KPC-2 β -Lactamase and β -Lactamase Inhibitor Protein". In: *Biochemistry* 48, pp. 9185–9193.

Hawkins, G D, Giesen D J, Lynch G C, Chambers C C, and Rossi I (2003). "AMSOL-version 7.0". In: 7.0.

Heath, Richard J and Charles O Rock (2002). "The Claisen Condensation in Biology". In: *Naturl Product Reports* 19, pp. 581–596.

Hoflack, J, P J DeClerq, and S Cauberghs (1989). "SCA: Systematic conformational analysis". In: *Quantum Chemical Program Exchange* QCPE program QCMP079, Indiana University, Bloomington, IN, USA.

Hopkins, A L, C R Groom, and A Alex (2004). "Ligand efficiency : a useful metric for lead selection". In: *Drug Discovery Today* 9.10, pp. 430–431.

Huang, Sheng-You, Sam Z Grinter, and Xiaoqin Zou (2010). "Scoring functions and their evaluation methods for protein-ligand docking: recent advances and future directions." In: *Physical Chemistry Chemical Physics* 12.40, pp. 12899–908.

Huovinen, Pentti, Saara Huovinen, and George A Jacoby (1988). "Sequence of PSE-2 β-Lactamase". In: *Antimicrobial Agents and Chemotherapy* 32.1, pp. 134–136.

Ito, Jun Ichi, Kazuyoshi Ikeda, Kazunori Yamada, Kenji Mizuguchi, and Kentaro Tomii (2015). "PoSSuM v.2.0: Data update and a new function for investigating ligand analogs and target proteins of small-molecule drugs". In: *Nucleic Acids Research* 43.D1, pp. D392–D398.

Iversen, Bjørn G, Trond Jacobsen, Hanne-merete Eriksen, Geir Bukholm, Kjetil K Melby, and Karin Nyga (2007). "An Outbreak of *Pseudomonas aeruginosa* Infection Caused by Contaminated Mouth Swabs". In: *Clinical Infectious Diseases* 44, pp. 794–801.

Jaurin, Bengtake and Thomas Grundström (1981). "AmpC cephalosporinase of *Escherichia coli* K-12 has a different evolutionary origin from that of β-lactamases of the penicillinase type". In: *Proceedings of the National Academy of Sciences* 78.8, pp. 4897–4901.

Joosten, Robbie P, Fei Long, Garib N Murshudov, and Anastassis Perrakis (2014). "The PDB_REDO server for macromolecular structure model optimization". In: *IUCrJ* 1.4, pp. 213–220.

Kabsch, Wolfgang (2010). "XDS". In: *Acta Crystallographica Section D: Biological Crystallography* 66.2, pp. 125–132.

Kantardjieff, Katherine A and Bernhard Rupp (2003). "Matthews coefficient probabilities: Improved estimates for unit cell contents of proteins, DNA, and protein-nucleic acid complex crystals". In: *Protein Science* 12.9, pp. 1865–1871.

Karplus, P and K Diederichs (2012). "Linking Crystallographic Model and Data Quaility". In: *Science* 336.6084, pp. 1030–1033.

Karplus, P Andrew and Kay Diederichs (2015). "Assessing and maximizing data quality in macromolecular crystallography". In: *Current Opinion in Structural Biology* 34, pp. 60–68.

Kass, Leon R (1968). "The antibacterial activity of 3-Decynoyl-N-acetylcysteamine". In: *Journal of Biological Chemistry* 243.12, pp. 3223–3228.

Ke, W, C R Bethel, K M Papp-Wallace, S R R Pagadala, M l Nottingham, et al. (2012). "Crystal Structures of KPC-2 β-Lactamase in Complex with 3-Nitrophenyl Boronic Acid and the Penam Sulfone PSR-3-226". In: *Antimicrobial Agents and Chemotherapy* 56.5, pp. 2713–2718.

Keseru, Gyorgy M, Daniel Andrew Erlanson, Gyorgy G Ferenczy, Michael M Hann, Christopher W Murray, and Stephen D. Pickett (2016). "Design principles for fragment libraries – Maximizing the value of learnings

from Pharma fragment based drug discovery (FBDD) programs for use in academia". In: *Journal of Medicinal Chemistry* 59.18, pp. 8189–8206.

Kitchen, D, H Decornez, J Furr, and J Bajorath (2004). "Docking and scoring in virtual screening for drug discovery: methods and applications". In: *Nature Reviews Drug Discovery* 3.11, pp. 935–949.

Klebe, G and T Mietzner (1994). "A fast and efficient method to generate biologically relevant conformations". In: *Jouranl of Computer-Aided Molecular Design* 8, pp. 583–606.

Klebe, Gerhard (2009). *Wirkstoffdesign*. Vol. 2nd edition. Heidelberg, Germany: Spektrum Akademischer Verlag, pp. 371–379.

Kodali, Srinivas, Andrew Galgoci, Katherine Young, Ronald Painter, Lynn L Silver, et al. (2005). "Determination of selectivity and efficacy of fatty acid synthesis inhibitors". In: *Journal of Biological Chemistry* 280.2, pp. 1669–1677.

Kong, Kok Fai, Lisa Schneper, and Kalai Mathee (2010). "β-lactam antibiotics: From antibiosis to resistance and bacteriology". In: *Apmis* 118.1, pp. 1–36.

Kramer, Bernd, Matthias Rarey, and Thomas Lengauer (1999). "Evaluation of the FLEX X Incremental Construction Algorithm for Protein – Ligand Docking". In: *PROTEINS: Structure, Function, and Genetics* 37.6, pp. 228–241.

Krishnan, Nikhil P, Nhu Q Nguyen, and Krisztina M Papp-Wallace (2015). "Inhibition of Klebsiella β -Lactamases (SHV-1 and KPC-2) by Avibactam : A Structural Study". In: *PLoS ONE* 10.9, pp. 1–13.

Kumaraswamy, Sriram and Renee Tobias (2015). *Label-free kinetic analysis of an antibody-antigen interaction using biolayer interferometry.* Vol. 1278, pp. 165–182.

Kuntz, I D, K Chen, K A Sharp, and P A Kollman (1999). "The maximal affinity of ligands". In: *Proceedings of the National Academy of Sciences* 96, pp. 9997–10002.

Kuntz, Irwin D, Jeffrey M Blaney, Stuart J Oatley, Robert Langridge, and Thomas E Ferrin (1982). "A Geometric Approach to Macromolecule-Ligand Interactions". In: *Journal of molecular biology* 161, pp. 269–288.

Labute, Paul (2009). "Protonate3D: Assignment of ionization states and hydrogen coordinates to macromolecular structures". In: *Proteins: Structure, Function and Bioinformatics* 75.1, pp. 187–205.

Lebedev, Andrey A and Michail N Isupov (2014). "Space-group and origin ambiguity in macromolecular structures with pseudo-symmetry and its treatment with the program Zanuda". In: *Acta Crystallographica Section D: Biological Crystallography* 70.9, pp. 2430–2443.

Lecker, Laura Sabina Maria and Bill Hunter (2012). "Assessment of Bacterial Enzymes as Potential Targets for Early Stage Drug Discovery". Bachelor Thesis. University Carolo-Wilhemina zu Braunschweig & University of Dundee, pp. 1–66.

Li, Jiabo, Tianhai Zhu, Gregory D Hawkins, Paul Winget, Daniel A Liotard, et al. (1999). "Extension of the platform of applicability of the SM5.42R universal solvation model". In: *Theoretical Chemistry Accounts* 103, pp. 9–63.

Linnanmaa, Seppo, David Harwood, and Larry S Davis (1988). "Pose Determination of a Three-Dimensional Object Using Triangle Pairs". In: *IEEE Transactions on Pattern Analysis and Machine Intelligence* 10.5, pp. 634–647.

Liu, Weizhi, Cong Han, Lihong Hu, Kaixian Chen, Xu Shen, and Hualiang Jiang (2006). "Characterization and inhibitor discovery of one novel malonyl-CoA: Acyl carrier protein transacylase (MCAT) from *Helicobacter pylori*". In: *FEBS Letters* 580, pp. 697–702.

Liu, Yu, Fanbo Jing, Yingying Xu, Yuanchao Xie, Fangyuan Shi, et al. (2011). "Design, synthesis and biological activity of thiazolidine-4-carboxylic acid derivatives as novel influenza neuraminidase inhibitors". In: *Bioorganic and Medicinal Chemistry* 19.7, pp. 2342–2348.

Lorber, David M and Brian K Shoichet (2005). "Hierarchical Docking of Databases of Multiple Ligand Conformations". In: *Current Topics in Medicinal Chemistry* 5.8, pp. 739–749.

Machutta, Carl A, Gopal R Bommineni, Sylvia R Luckner, Kanishk Kapilashrami, Bela Ruzsicska, et al. (2010). "Slow onset inhibition of bacterial β-keto-acyl-(acyl carrier protein) synthases by thiolactomycin". In: *Journal of Biological Chemistry* 285.9, pp. 6161–6169.

Madigan, M T, J M Martinko, D A Stahl, and D P Clark (2012). *Brock - The Biology of Microorganisms*. Vol. 13th edition. Pearson. Harlow, England: Pearson Education Limited, p. 781.

Mah, Robert, Jason R Thomas, and Cynthia M Shafer (2014). "Drug discovery considerations in the development of covalent inhibitors". In: *Bioorganic and Medicinal Chemistry Letters* 24.1, pp. 33–39.

Marcella, Aaron M and Adam W Barb (2016). "A rapid fluorometric assay for the S-malonyltransacylase FabD and other sulfhydryl utilizing enzymes". In: *Journal of Biological Methods* 3.4, p. 53.

Matthews, B W (1968). "Solvent Content of Protein Crystals". In: *Journal of Molecular Biology* 33, pp. 491–497.

— (1974). "Determination of Molecular Weight from Protein Crystals". In: *Journal of Molecular Biology* 82, pp. 513–526.

McCoy, Airlie J, Ralf W Grosse-Kunstleve, Paul D Adams, Martyn D Winn, Laurent C Storoni, and Randy J Read (2007). "Phaser crystallographic software". In: *Journal of Applied Crystallography* 40.4, pp. 658–674.

McPherson, Alexander (1990). "Current approaches to macromolecular crystallization". In: *European Journal of Biochemistry* 189, pp. 1–23.

— (2004). "Introduction to protein crystallization". In: *Methods* 34, pp. 254–265.

Mégraud, Francis (2012). "The challenge of *Helicobacter pylori* resistance to antibiotics: The comeback of bismuth-based quadruple therapy". In: *Therapeutic Advances in Gastroenterology* 5.2, pp. 103–109.

Meng, Elaine C, Brian K Shoichet, and Irwin D Kuntz (1992). "Automated Docking with Grid-Based Energy Evaluation". In: *Journal of Computational Chemistry* 13.4, pp. 505–524.

Michels, Tillmann and D Rudolf (2012). "Acid-Mediated Prevention of Aspartimide Formation in Solid Phase Peptide Synthesis". In: *Organic Letters* 14.20, pp. 5218–5221.

Moriarty, Nigel W, Ralf W Grosse-Kunstleve, and Paul D Adams (2009). "Electronic ligand builder and optimization workbench (eLBOW): A tool for ligand coordinate and restraint generation". In: *Acta Crystallographica Section D: Biological Crystallography* 65.10, pp. 1074–1080.

Morisaki, Masuo and Konrad Bloch (1971). "Inhibition of β-Hydroxy-decanoyl Thioester Dehydrase by Some Allenic Acids and Their Thioesters". In: *Bioorganic Chemistry* 1, pp. 188–193.

Mysinger, Michael M and Brian K Shoichet (2010). "Rapid context-dependent ligand desolvation in molecular docking". In: *Journal of Chemical Information and Modeling* 50.9, pp. 1561–1573.

Nespolo, Massimo (2015). "Tips and traps on crystal twinning: How to fully describe your twin". In: *Crystal Research and Technology* 50.5, pp. 362–371.

Nguyen, Nhu Q, Nikhil P Krishnan, Laura J Rojas, Fabio Prati, Emilia Caselli, et al. (2016). "Crystal Structures of KPC-2 and SHV-1 β-Lactamases in Complex with the Boronic Acid Transition State Analog S02030". In: *Antimicrobial Agents and Chemotherapy* 60.3, pp. 1760–1766.

Nicholls, A and B Honig (1991). "A rapid finite difference algorithm, utilizing successive over relaxation to solve the Poisson Boltzmann equation." In: *Journal of Computational Chemistry* 12.4, pp. 435–445.

Nichols, D A, P Jaishankar, W Larson, E Smith, G Liu, et al. (2012). "Structure-based design of potent and ligand-efficient inhibitors of CTX-M class A β-lactamase". In: *Journal of Medicinal Chemistry* 55.5, pp. 2163–2172.

Novoradovsky, Alexey, Vivian Zhang, Madhushree Gosh, Holly Hogrefe, Joseph A Sorge, and Terry Gaasterland (2005). "Computational Principles of Primer Design for Site Directed Mutagenesis". In: *Nanotechnology conference; NSTI nanotech 2005*. Vol. 1, pp. 532–535.

Ondeyka, John G, Deborah L Zink, Katherine Young, Ronald Painter, Srinivas Kodali, et al. (2006). "Discovery of Bacterial Fatty Acid Synthase Inhibitors from a Phoma Species as Antimicrobial Agents Using a New Antisense-Based Strategy". In: *Journal of Natural Products* 69, pp. 377–380.

Ostrovskii, V A, R E Trifonov, and E A Popova (2012). "Medicinal chemistry of tetrazoles". In: *Russian Chemical Bulletin* 61.4, pp. 768–780.

Padayatti, Pius S, Anjaneyulu Sheri, Monica A Totir, Marion S Helfand, Marianne P Carey, et al. (2006). "Rational Design of a β-Lactamase Inhibitor Achieved via Stabilization of the trans-Enamine Intermediate : 1.28 Å Crystal Structure of wt SHV-1 Complex with a Penam Sulfone". In: *Journal of American Chemical Society* 128, pp. 13235–13242.

Pagès, Jean Marie, Sabine Peslier, Thomas A Keating, Jean Philippe Lavigne, and Wright W Nichols (2016). "Role of the outer membrane and porins in susceptibility of β-lactamase-producing Enterobacteriaceae to ceftazi-dime-avibactam". In: *Antimicrobial Agents and Chemotherapy* 60.3, pp. 1349–1359.

Papp-Wallace, Krisztina M, Magdalena Taracila, Christopher J Wallace, Kristine M Hujer, Christopher R Bethel, et al. (2010). "Elucidating the role of Trp105 in the KPC-2 β-lactamase". In: *Protein Science* 19, pp. 1714–1727.

Papp-Wallace, Krisztina M, Andrea Endimiani, Magdalena A Taracila, and Robert A Bonomo (2011). "Carbapenems : Past , Present , and Future". In: *Antimicrobial Agents and Chemotherapy* 55.11, pp. 4943–4960.

Parsons, Simon (2003). "Introduction to twinning". In: *Acta Crystallographica Section* 59, pp. 1995–2003.

Pearlman, Robert S and K M Smith (1998). "Novel software tools for chemical diversity". In: *Perspectives in Drug Discovery and Design* 9, pp. 339–353.

Pemberton, Orville A, Xiujun Zhang, and Yu Chen (2017). "Molecular Basis of Substrate Recognition and Product Release by the *Klebsiella pneumoniae* Carbapenemase (KPC-2)". In: *Journal of Medicinal Chemistry* 60, pp. 3525–3530.

Planken, Simon, Douglas C Behenna, Sajiv K Nair, Theodore O Johnson, Asako Nagata, et al. (2017). "Discovery of N-((3R,4R)-4-Fluoro-1-(6-((3-methoxy- 1- methyl- 1H- pyrazol- 4-yl) amino) -9-methyl- 9H- purin- 2-yl) pyrrolidine-3-yl)acrylamide (PF-06747775) through Structure-Based Drug Design: A High Affinity Irreversible Inhibitor Targeting Oncogenic EGFR Mutants with Selectivity over Wild-Type EGFR". In: *Journal of Medicinal Chemistry* 60.7, pp. 3002–3019.

Powers, Rachel A, Hollister C Swanson, Magdalena A Taracila, Nicholas W Florek, Chiara Romagnoli, et al. (2014). "Biochemical and Structural Analysis of Inhibitors Targeting the ADC-7 Cephalosporinase of *Acinetobacter baumannii*". In: *Biochemistry* 53, pp. 7670–7679.

Price, Allen C, Keum Hwa Choi, Richard J Heath, Zhenmei Li, Stephen W White, and Charles O Rock (2001). "Inhibition of β-ketoacyl-acyl carrier protein synthases by thiolactomycin and cerulenin: Structure and mechanism". In: *Journal of Biological Chemistry* 276.9, pp. 6551–6559.

Rarey, Matthias, Bernd Kramer, Thomas Lengauer, and Gerhard Klebe (1996). "A fast flexible docking method using an incremental construction algorithm." In: *Journal of molecular biology* 261.3, pp. 470–489.

Rich, Rebecca L and David G Myszka (2008). "Survey of the year 2007 commercial optical biosensor literature". In: *Journal of Molecular Recognition* 21.6, pp. 355–400.

Robinson, David (2016). *Integration of the Octet RED 384 Platform for Fragment Based Drug Discovery*. Copenhagen, Denmark: Protein Analysis Workshop and User Meeting.

Rodkey, Elizabeth A, Marisa L Winkler, Christopher R Bethel, Sundar Ram Reddy Pagadala, John D Buynak, et al. (2014). "Penam Sulfones and β-Lactamase Inhibition : SA2-13 and the Importance of the C2 Side Chain Length and Composition". In: *PLoS ONE* 9.1, pp. 1–11.

Roh, Jaroslav, Kateřina Vávrová, and Alexandr Hrabálek (2012). "Synthesis and functionalization of 5-substituted tetrazoles". In: *European Journal of Organic Chemistry* 31, pp. 6101–6118.

Sastry Madhavi, G, Matvey Adzhigirey, Tyler Day, Ramakrishna Annabhimoju, and Woody Sherman (2013). "Protein and ligand preparation: Parameters, protocols, and influence on virtual screening enrichments". In: *Journal of Computer-Aided Molecular Design* 27.3, pp. 221–234.

Schaeffer, Merrill L, Gautam Agnihotri, Craig Volker, Howard Kallender, Patrick J Brennan, and John T Lonsdale (2001). "Purification and Biochemical Characterization of the *Mycobacterium tuberculosis* β-Ketoacyl-acyl Carrier Protein Synthases KasA and KasB". In: *Journal of Biological Chemistry* 276.50, pp. 47029–47037.

Sharma, S K, M Kapoor, T N C Ramya, S Kumar, G Kumar, et al. (2003). "Identification, Characterization, and Inhibition of Plasmodium falciparum β-Hydroxyacyl-Acyl Carrier Protein Dehydratase (FabZ)". In: *Journal of Biological Chemistry* 278.46, pp. 45661–45671.

Shoichet, Brian K, Dale L Bodian, and Irwin D Kuntzt (1992). "Molecular Docking Using Shape Descriptors". In: *Journal of Computational Chemistry* 13.3, pp. 380–397.

Singh, Juswinder, Russell C Petter, and Arthur F Kluge (2010). "Targeted covalent drugs of the kinase family". In: *Current Opinion in Chemical Biology* 14.4, pp. 475–480.

Sivaraman, Sharada, Jacque Zwahlen, Alasdair F Bell, Lizbeth Hedstrom, and Peter J Tonge (2003). "Structure-activity studies of the inhibition of FabI, the enoyl reductase from *Escherichia coli*, by Triclosan: Kinetic analysis of mutant FabIs". In: *Biochemistry* 42.15, pp. 4406–4413.

Skvortsov, A N, V M Uvarov, D A de Vekki, E P Studentsov, and N K Skvortsov (2010). "Conformational analysis, spectral and catalytic properties of 1,3-thiazolidines, ligands for acetophenone hydrosilylation with diphenylsilane". In: *Russian Journal Of General Chemistry* 80.10, pp. 2007–2021.

Stewart, Michael J, Sapan Parikh, Guoping Xiao, Peter J Tonge, and Caroline Kisker (1999). "Structural Basis and Mechanism of Enoyl Reductase Inhibition by Triclosan". In: *Journal of Molecular Biology* 290, pp. 859–865.

Stols, Lucy, Minyi Gu, Lynda Dieckman, Rosemarie Raffen, Frank R Collart, and Mark I Donnelly (2002). "A new vector for high- throughput, ligation- independent cloning encoding a tobacco etch virus protease cleavage site." In: *Protein Expression and Purification* 25, pp. 8–15.

Supuran, Claudiu T, Angela Casini, and Andrea Scozzafava (2003). "Protease Inhibitors of the Sulfonamide Type: Anticancer, Antiinflammatory, and Antiviral Agents". In: *Medicinal Research Reviews* 23.5, pp. 535–558.

Tondi, Donatella, Simon Cross, Alberto Venturelli, MP Costi, G Cruciani, and F Spyrakis (2016). "Decoding the structural basis for carbapenem hydrolysis by class A β-lactamases : fishing for a pharmacophore". In: *Current Drug Targets* 17.9, pp. 983–1005.

Verma, Amit and Shailendra K. Saraf (2008). "4-Thiazolidinone - A biologically active scaffold". In: *European Journal of Medicinal Chemistry* 43.5, pp. 897–905.

Walther-Rasmussen, Jan and Niels Høiby (2007). "Class A carbapenemases". In: *Journal of Antimicrobial Chemotherapy* 60.6, pp. 470–482.

Wang, Jun, Stephen M Soisson, Katherine Young, Wesley Shoop, Srinivas Kodali, et al. (2006). "Platensimycin is a selective FabF inhibitor with potent antibiotic properties". In: *Nature* 441.18, pp. 358–361.

Wang, Jun, Srinivas Kodali, Sang Ho Lee, Andrew Galgoci, Ronald Painter, et al. (2007). "Discovery of platencin, a dual FabF and FabH inhibitor with in vivo antibiotic properties". In: *Procedings of the National Academy of Sciences* 104.18, pp. 7612–7616.

Wartchow, Charles A, Frank Podlaski, Shirley Li, Karen Rowan, Xiaolei Zhang, et al. (2011). "Biosensor-based small molecule fragment screening with biolayer interferometry". In: *Journal of Computer-Aided Molecular Design* 25.7, pp. 669–676.

Weiner, Scott J, Peter A Kollman, David A Case, U Chandra Singh, Caterina Ghio, et al. (1984). "A New Force Field for Molecular Mechanical Simulation of Nucleic Acids and Proteins". In: *Journal of American Chemical Society* 106.3, pp. 765–784.

Weininger, David (1988). "SMILES, a Chemical Language and Information System. 1. Introduction to Methodology and Encoding Rules". In: *Journal of Chemical Information and Computer Sciences* 28, pp. 31–36.

White, Stephen W, Jie Zheng, Yong-mei Zhang, and Charles O Rock (2005). "The structural biology of type II fatty acid biosynthesis". In: *Annual Review of Biochemistry* 74, pp. 791–831.

WHO (2017). *Global priority list of antibiotic-resistant bacteria to guide research, discovery, and development of new antibiotics*.

Yin, Jingjun and Stephen L Buchwald (2000). "Palladium-catalyzed intermolecular coupling of aryl halides and amides". In: *Organic Letters* 2.8, pp. 1101–1104.

Zhang, Yong Mei, Jason Hurlbert, Stephen W. White, and Charles O. Rock (2006). "Roles of the active site water, histidine 303, and phenylalanine 396 in the catalytic mechanism of the elongation condensing enzyme of *Streptococcus pneumoniae*". In: *Journal of Biological Chemistry* 281.25, pp. 17390–17399.

Zheng, Zhong, Joshua B Parsons, Rajendra Tangallapally, Weixing Zhang, Charles O Rock, and Richard E Lee (2014). "Discovery of novel bacterial elongation condensing enzyme inhibitors by virtual screening". In: *Bioorganic and Medicinal Chemistry Letters* 24.11, pp. 2585–2588.